

**SENSITIVITY STUDY FOR THE SIMULATION OF TORNADO/NOR'WESTER
DURING PRE-MONSOON SEASON OVER BANGLADESH USING HIGH
RESOLUTION WRF-ARW MODEL**

**M. Sc. Thesis
BY
BUSRAT JAHAN**



**DEPARTMENT OF PHYSICS
KHULNA UNIVERSITY OF ENGINEERING & TECHNOLOGY
KHULNA-9203, BANGLADESH**

AUGUST 2016

**SENSITIVITY STUDY FOR THE SIMULATION OF TORNADO/NOR'WESTER
DURING PRE-MONSOON SEASON OVER BANGLADESH USING HIGH
RESOLUTION WRF-ARW MODEL**

M. Sc. Thesis

BY

BUSRAT JAHAN

ROLL NO: 1555503

SESSION: JANUARY-2015

A thesis submitted in partial fulfillment of the requirements for the degree of Master of Science in the Department of Physics, Khulna University of Engineering & Technology, Khulna-9203.



**DEPARTMENT OF PHYSICS
KHULNA UNIVERSITY OF ENGINEERING & TECHNOLOGY
KHULNA-9203, BANGLADESH**

AUGUST 2016

DECLARATION

This is to certify that the thesis work entitled "*Sensitivity study for the simulation of Tornado/Nor'wester during pre-monsoon season over Bangladesh using high resolution WRF-ARW model*" has been carried out by Busrat Jahan in the Department of Physics, Khulna University of Engineering & Technology, Khulna, Bangladesh. The above thesis work or any part of this work has not been submitted anywhere for the award of any degree or diploma.

Signature of Supervisor


04.09.16

(Professor Dr. Md. Mahbub Alam)

Signature of Candidate



Busrat Jahan

Approval

This is to certify that the thesis work submitted by *Busrat Jahan* entitled “*Sensitivity study for the simulation of Tornado/Nor’wester during Pre-monsoon season over Bangladesh using High Resolution WRF-ARW Model*” has been approved by the board of examiners for the partial fulfillment of the requirements for the degree of *M. Sc.* in the Department of *Physics*, Khulna University of Engineering & Technology, Khulna, Bangladesh on 26 August 2016.

BOARD OF EXAMINERS

1. Prof. Dr. Md. Mahbub Alam
Department of Physics
Khulna University of Engineering & Technology


.....
Chairman & Supervisor


2. Head
Department of Physics
Khulna University of Engineering & Technology


.....
Member

3. Prof. Dr. Shibendra Shekher Sikder
Department of Physics
Khulna University of Engineering & Technology


.....
Member

4. Prof. Dr. Md. Abdullah Elias Akhter
Department of Physics
Khulna University of Engineering & Technology


.....
Member

5. Dr. Samarendra Karmakar
Director (Rtd.)
SAARC Meteorological Research Centre (SMRC)
63 Jafrabad, 2nd floor, Dhaka-1206


.....
Member (External)

**DEDICATED
TO MY
BELOVED PARENTS**

Acknowledgements

With my great manner it is a pleasure for me to express my deepest sense of gratitude and indebtedness to my reverend supervisor Dr. Md. Mahbub Alam, Professor, Department of Physics, Khulna University of Engineering & Technology, Khulna, for his kind guidance and supervision and for his constant encouragement throughout the research work. His inspiration and friendly cooperation has accelerated my works.

I am indebted to Professor Dr. Shibendra Shekher Sikder, Head, Department of Physics, Khulna University of Engineering & Technology for his strong support in various ways during the entire period of my study in this department. I express my heartfelt gratitude and thanks to Professor Dr. Md. Abdullah Elias Akhter and Professor Dr. Jolly Sultana Department of Physics, Khulna University of Engineering and Technology. Many thanks for their inspiration and advices from the beginning of my study. I gratefully acknowledge Mr. Md. Kamrul Hasan Reza, Mr. Sujit Kumar Shil, Md. Alamgir Hossain, Assistant Professor & Mr. Sumon Halder, Sumon Deb Nath, Lecturer, Department of Physics, KUET for their cooperation regarding writing the thesis.

My personal thankful greetings are to my good friends and well wishers for their help and cooperation. There are numerous people who could not be mentioned individually but their interesting discussions have prompted much thought on various aspects, I would also like to thank them.

I would like to express my heart full thanks to my parents, husband, sisters and nearest relatives for their inspiration, encouragement and multifaceted supports to carry out this thesis work.

I am grateful to the KUET authority for approval of the project in the 33rd meeting of CASR, agenda no. 33/5/10 and providing me the relevant facilities to complete this research work. The Author is grateful to National Centre for Atmospheric Research (NCAR), USA for making the WRF (WRF-ARW) model available to modeling community. The Grid Analysis and Display System software (GrADS) was used for analytical purposes and displaying Figs. Bangladesh Meteorological Department (BMD) is acknowledging for providing necessary data over Bangladesh.

Finally, I want to express my gratitude to almighty Creator for his mercy.

Busrat Jahan

CONTENTS

	Page No.
Title Page	i
Declaration Page	iii
Acknowledgement	v
Contents	vi
List of Figures	ix
List of Tables	xi
Nomenclature	xv
Abstract	xvi
Chapter I: Introduction	1
Chapter II: Review of Literature	7
2.1 Pre-monsoon Rainfall	8
2.2 Pre-monsoon Temperature	8
2.3 Convective Inhibition (CIN)	9
2.4 Level of free convection (LFC)	9
2.5 Lifted condensation Level (LCL)	10
2.6 Latent Heat (LH) Flux	10
2.7 Classification of local severe storms	11
2.8 Nor'wester	11
2.9 Thunderstorm	12
2.9.1 Single-cell Thunderstorm	12
2.9.2 Multi-cell clusters	13
2.9.3 Squall line thunderstorms	14
2.9.4 Super cell thunderstorm	14
2.10 Tornado	16
2.10.1 Life Cycle of Tornado	16
2.10.2 Damage by a Tornado	17
2.10.3 Favorable conditions for tornado genesis	17
2.11 Climatological aspects of nor'wester	18
2.12 Weather Research & Forecasting (WRF) Model	18
2.12.1 Microphysics schemes in WRF-ARW Model	19
2.12.1.1 Kessler Scheme	19
2.12.1.2 Lin <i>et al.</i> Scheme	20
2.12.1.3 WRF Single-Moment 6-class (WSM6) Scheme	20
2.12.1.4 Thompson Scheme	21
2.12.1.5 Stony Brook University (SBU) Microphysics	21

2.12.1.6	WRF double-Moment 6-class (WDM6) Scheme	21
2.12.2	Cumulus Parameterization	22
2.12.2.1	Kain-Fritsch (KF) Scheme	22
2.12.2.2	Betts-Miller-Janjic (BMJ) Scheme	23
2.12.3	Planetary Boundary Layer (PBL) Parameterizations	24
2.12.3.1	Yonsei University (YSU) scheme	24
2.12.4	Map Projection	25
2.12.4.1	Mercator Projection	25
2.12.5	Arakawa Staggered C-Grid	26
Chapter III:	Methodology	27
3.1	Methodology of Stability Index	27
3.1.1	Cross Total Index (CT)	27
3.1.2	Vertical total Index (VT)	27
3.1.3	Total Totals Index (TT)	27
3.1.4	K-Index (KI)	28
3.1.5	Convective Available Potential Energy (CAPE)	28
3.1.6	Convective Inhibition (CIN)	29
3.2	Model Setup	29
3.3	Model Domain and Configuration	30
3.4	Data and Methodology	31
Chapter IV:	Results & Discussion	33
4.1	Nor'wester of 07 April 2012	33
4.1.1	Sea Level Pressure (SLP)	33
4.1.2	Maximum Wind Speed (MWS) at 10 m Level	35
4.1.3	Temperature at 2m Level	38
4.1.4	Vertical Velocity	39
4.1.5	Vorticity	40
4.1.6	Relative Humidity (RH)	41
4.1.7	Maximum Reflectivity (MR)	43
4.1.8	Cross Total Index (CT)	44
4.1.9	Vertical Totals Index (VT)	45
4.1.10	Total Totals Index (TT)	47
4.1.11	K Index (KI)	48
4.1.12	Maximum Convective Available Potential Energy (MCAPE)	49
4.1.13	Minimum Convective Inhibition (MCIN)	51
4.1.14	Latent Heat (LH) Flux	53
4.1.15	Lifted Condensation Level (LCL)	54

4.1.16	Level of Free Convection (LFC)	55
4.1.17	Rain Water Mixing Ratio (RWMR)	55
4.1.18	Cloud Water Mixing Ratio (CWMR)	56
4.2	Nor'wester of 28 April 2012	57
4.2.1	Sea Level Pressure (SLP)	58
4.2.2	Maximum Wind Speed (MWS) at 10 m Level	58
4.2.3	Temperature at 2m Level	61
4.2.4	Vertical Velocity	62
4.2.5	Vorticity	63
4.2.6	Relative Humidity (RH)	64
4.2.7	Maximum Reflectivity (MR)	65
4.2.8	Cross Total Index (CT)	66
4.2.9	Vertical Totals Index (VT)	67
4.2.10	Total Totals Index (TT)	69
4.2.11	K Index (KI)	70
4.2.12	Maximum Convective Available Potential Energy (MCAPE)	71
4.2.13	Minimum Convective Inhibition (MCIN)	71
4.2.14	Latent Heat (LH) Flux	73
4.2.15	Lifted Condensation Level (LCL)	75
4.2.16	Level of Free Convection (LFC)	75
4.2.17	Rain Water Mixing Ratio (RWMR)	76
4.2.18	Cloud Water Mixing Ratio (CWMR)	76
4.3	Nor'wester of 27 April 2014	78
4.3.1	Sea Level Pressure (SLP)	78
4.3.2	Maximum Wind Speed (MWS) at 10 m Level	79
4.3.3	Temperature at 2m Level	81
4.3.4	Vertical Velocity	82
4.3.5	Vorticity	82
4.3.6	Relative Humidity (RH)	83
4.3.7	Maximum Reflectivity (MR)	84
4.3.8	Cross Total Index (CT)	85
4.3.9	Vertical Totals Index (VT)	88
4.3.10	Total Totals Index (TT)	88
4.3.11	K Index (KI)	89
4.3.12	Maximum Convective Available Potential Energy (MCAPE)	90
4.3.13	Minimum Convective Inhibition (MCIN)	93
4.3.14	Latent Heat (LH) Flux	93

4.3.15	Lifted Condensation Level (LCL)	94
4.3.16	Level of Free Convection (LFC)	94
4.3.17	Rain Water Mixing Ratio (RWMR)	95
4.3.18	Cloud Water Mixing Ratio (CWMR)	96
4.4	Nor'wester of 15 May 2014	97
4.4.1	Sea Level Pressure (SLP)	98
4.4.2	Maximum Wind Speed (MWS) at 10 m Level	99
4.4.3	Temperature at 2m Level	102
4.4.4	Vertical Velocity	102
4.4.5	Vorticity	103
4.4.6	Relative Humidity (RH) at 2m Level	104
4.4.7	Maximum Reflectivity (MR)	105
4.4.8	Cross Total Index (CT)	106
4.4.9	Vertical Totals Index (VT)	107
4.4.10	Total Totals Index (TT)	107
4.4.11	K Index (KI)	110
4.4.12	Maximum Convective Available Potential Energy (MCAPE)	113
4.4.13	Minimum Convective Inhibition (MCIN)	113
4.4.14	Latent Heat (LH) Flux	114
4.4.15	Lifted Condensation Level (LCL)	115
4.4.16	Level of Free Convection (LFC)	115
4.4.17	Rain Water Mixing Ratio (RWMR)	116
4.4.18	Cloud Water Mixing Ratio (CWMR)	117
	Chapter V: Conclusions	118
	References	121

List of Figures

Fig. No.	Description	Page
Fig. 1.1:	Single cell thunderstorm	13
Fig. 1.2:	Multi-cell thunderstorm	13
Fig. 1.3:	Squall line thunderstorm	14
Fig. 1.4:	Super cell thunderstorm	15
Fig. 1.5:	Life cycle of a thunderstorm	15
Fig. 3.1:	WRF Model Domain for simulating Nor'wester/Tornado in Bangladesh	30
Fig. 4.1.1:	Model simulated squall line for different MP schemes coupling with (a-f) KF and (g-l) BMJ schemes on 7 April 2012.	34
Fig. 4.1.2:	Time variation (5 minute interval) of SLP at (a-b) Chittagong and (c-d) Dhaka and comparison of observed and model simulated 3-hourly SLP at (e-f) Chittagong and Dhaka using six different MP schemes coupling with KF and BMJ schemes respectively on 7 April 2012.	35
Fig. 4.1.3:	Time variation (5 minute interval) of MWS at 10m level at (a-b) Chittagong and (c-d) Dhaka and comparison of observed and model simulated 3-hourly MWS at (e-f) Chittagong and Dhaka using six different MP schemes coupling with KF and BMJ schemes respectively on 7 April 2012.	36
Fig. 4.1.4:	Time variation (5 minute interval) of temperature at 2m level at (a-b) Chittagong and (c-d) Dhaka and comparison of observed and model simulated 3-hourly temperature at (e-f) Chittagong and Dhaka using six different MP schemes coupling with KF and BMJ schemes respectively on 7 April 2012.	38
Fig. 4.1.5:	Model simulated maximum vertical velocity (shaded) and vorticity (contour, $\times 10^{-5}/s$) using Kessler, Lin <i>et al.</i> , WSM6, Thomson, SBU and WDM6 schemes coupling with (a-f) KF and (g-l) BMJ schemes on 7 April 2012.	40
Fig. 4.1.6:	Time variation of RH at 2m level at (a-b) Chittagong and (c-d) Dhaka on 7 April 2012 using six different MP schemes coupling with KF and BMJ schemes.	42

Fig. 4.1.7: WRF Model simulated reflectivity (shaded) and relative humidity (contour) along the line of maximum vertical velocity using Kessler, Lin <i>et al.</i> , WSM6, Thomson, SBU and WDM6 schemes coupling with (a-f) KF and (g-l) BMJ schemes on 7 April 2012.	42
Fig. 4.1.8: Time variation of reflectivity at (a-b) Chittagong and (c-d) Dhaka on 7 April 2012 using six different MP schemes coupling with KF and BMJ schemes.	43
Fig. 4.1.9: Time variation of CT at (a-b) Chittagong and (c-d) Dhaka on 7 April 2012 using six different MP schemes coupling with KF and BMJ schemes.	45
Fig. 4.1.10: Time variation of VT at (a-b) Chittagong and (c-d) Dhaka on 7 April 2012 using six different MP schemes coupling with KF and BMJ schemes.	46
Fig. 4.1.11: Time variation of TT at (a-b) Chittagong and (c-d) Dhaka on 7 April 2012 using six different MP schemes coupling with KF and BMJ schemes.	47
Fig. 4.1.12: Time variation of K Index at (a-b) Chittagong and (c-d) Dhaka on 7 April 2012 using six different MP schemes coupling with KF and BMJ schemes.	48
Fig. 4.1.13: Time variation of (a-b) MCAPE, (c-d) MCIN, (e-f) LH flux, (g-h) LCL and (i-j) LFC using six MP schemes coupling with KF and BMJ schemes at Chittagong on 7 April 2012.	50
Fig. 4.1.14: Time variation of (a-b) MCAPE, (c-d) MCIN, (e-f) LH flux, (g-h) LCL and (i-j) LFC using six different MP schemes coupling with KF and BMJ schemes at Dhaka on 7 April 2012.	52
Fig. 4.1.15: WRF Model simulated CWMR (shaded) and RWMR (contour) along the line of maximum vertical velocity using Kessler, Lin <i>et al.</i> , WSM6, Thomson, SBU and WDM6 schemes coupling with (a-f) KF and (g-l) BMJ schemes on 7 April 2012.	56
Fig. 4.2.1: Model simulated squall line/nor'wester for different MP schemes coupling with (a-f) KF and (g-l) BMJ schemes on 28 April 2012.	57
Fig. 4.2.2: Time variation of (a-b) SLP, (c-d) MWS at 10m, (e-f) Temperature at 2m, (g-h) RH at 2m and (i-j) MR using six different MP schemes coupling with KF and BMJ schemes at Chittagong on 28 April 2012.	59
Fig. 4.2.3: Time variation of (a-b) SLP, (c-d) MWS at 10m, (e-f) Temperature at 2m, and (g-h) RH at 2m using six different MP schemes coupling with KF and BMJ schemes at Dhaka on 28 April 2012.	60

- Fig. 4.2.4: WRF Model simulated maximum vertical velocity (shaded) and vorticity (contour, $\times 10^{-5}/s$) along the line of maximum vertical velocity using Kessler, Lin *et al.*, WSM6, Thomson, SBU and WDM6 schemes coupling with (a-f) KF and (g-l) BMJ schemes at 28 April 2012. 63
- Fig. 4.2.5: WRF Model simulated reflectivity (shaded) and relative humidity (contour) along the line of maximum vertical velocity using Kessler, Lin *et al.*, WSM6, Thomson, SBU and WDM6 schemes coupling with (a-f) KF and (g-l) BMJ schemes on 28 April 2012. 64
- Fig. 4.2.6: Time variation of (a-b) CT, (c-d) VT, (e-f) TT and (g-h) K-Index using six different MP schemes coupling with KF and BMJ schemes at Chittagong on 28 April 2012. 67
- Fig. 4.2.7: Time variation of (a-b) CT, (c-d) VT, (e-f) TT and (g-h) K-Index using six different MP schemes coupling with KF and BMJ schemes at Dhaka on 28 April 2012. 68
- Fig. 4.2.8: Time variation of (a-b) CAPE, (c-d) CIN, (e-f) LH Flux, (g-h) LCL and (i-j) LFC using six different MP schemes coupling with KF and BMJ schemes at Chittagong on 28 April 2012. 72
- Fig. 4.2.9: Time variation of (a-b) CAPE, (c-d) CIN, (e-f) LH flux, (g-h) LCL and (i-j) LFC using six different MP schemes coupling with KF and BMJ schemes at Dhaka on 28 April 2012. 74
- Fig. 4.2.10: WRF Model simulated CWMR (shaded) and RWMR (contour) along the line of maximum vertical velocity using Kessler, Lin *et al.*, WSM6, Thomson, SBU and WDM6 schemes coupling with (a-f) KF and (g-l) BMJ schemes at 28 April 2012. 77
- Fig. 4.3.1: Time variation of (a-b) SLP, (c-d) MWS at 10m, (e-f) Temperature at 2m, and (g-h) RH at 2m using six different MP schemes coupling with KF and BMJ schemes at Sylhet on 27 April 2014. 79
- Fig. 4.3.2: Time variation of (a-b) SLP, (c-d) MWS at 10m, (e-f) Temperature at 2m, (g-h) RH at 2m and (i-j) MR using six different MP schemes coupling with KF and BMJ schemes at Khulna on 27 April 2014. 80
- Fig. 4.3.3: WRF Model simulated maximum vertical velocity (shaded) and vorticity (contour, $\times 10^{-5}/s$) along the line of maximum vertical velocity using Kessler, Lin *et al.*, WSM6, Thomson, SBU and WDM6 schemes coupling with (a-f) KF and (g-l) BMJ schemes on 27 April 2014. 83

- Fig. 4.3.4: WRF Model simulated reflectivity (shaded) and RH (contour) along the line of maximum vertical velocity using Kessler, Lin *et al.*, WSM6, Thomson, SBU and WDM6 schemes coupling with (a-f) KF and (g-l) BMJ schemes on 27 April 2014. 85
- Fig. 4.3.5: Time variation of (a-b) CT, (c-d) VT, (e-f) TT and (g-h) K-Index using six different MP schemes coupling with KF and BMJ schemes at Sylhet on 27 April 2014. 86
- Fig. 4.3.6: Time variation of (a-b) CT, (c-d) VT, (e-f) TT and (g-h) K-Index using six different MP schemes coupling with KF and BMJ schemes at Khulna on 27 April 2014. 87
- Fig. 4.3.7: Time variation of (a-b) MCAPE, (c-d) MCIN, (e-f) LH Flux, (g-h) LCL and (i-j) LFC using six different MP schemes coupling with KF and BMJ schemes at Sylhet on 27 April 2014. 91
- Fig. 4.3.8: Time variation of (a-b) MCAPE, (c-d) MCIN, (e-f) LH Flux, (g-h) LCL and (i-j) LFC using six different MP schemes coupling with KF and BMJ schemes at Khulna on 27 April 2014. 92
- Fig. 4.3.9: Model simulated CWMR (shaded) and RWMR (contour) along the line of maximum vertical velocity using Kessler, Lin *et al.*, WSM6, Thomson, SBU and WDM6 schemes coupling with (a-f) KF and (g-l) BMJ schemes on 27 April 2014. 95
- Fig. 4.4.1: Model simulated squall line for different MP schemes coupling with (a-f) KF and (g-l) BMJ schemes on 15 May 2014. 97
- Fig. 4.4.2: Time variation of (a-b) SLP, (c-d) MWS at 10m, (e-f) Temperature at 2m, (g-h) RH at 2m and (i-j) Maximum reflectivity using six different MP schemes coupling with KF and BMJ schemes at Barisal on 15 May 2014. 100
- Fig. 4.4.3: Time variation of (a-b) SLP, (c-d) MWS at 10m, (e-f) Temperature at 2m, and (g-h) RH at 2m using six different MP schemes coupling with KF and BMJ schemes at Chittagong on 15 May 2014. 101
- Fig. 4.4.4: WRF Model simulated maximum vertical velocity (shaded) and vorticity (contour, $\times 10^{-5}/s$) along the line of maximum vertical velocity using Kessler, Lin *et al.*, WSM6, Thomson, SBU and WDM6 schemes coupling with (a-f) KF and (g-l) BMJ schemes on 15 May 2014. 103

- Fig. 4.4.5: WRF Model simulated reflectivity (shaded) and RH (contour) along the line of maximum vertical velocity using Kessler, Lin *et al.*, WSM6, Thomson, SBU and WDM6 schemes coupling with (a-f) KF and (g-l) BMJ schemes at 15 May 2014. 105
- Fig. 4.4.6: Time variation of (a-b) CT, (c-d) VT, (e-f) TT and (g-h) K-Index using six different MP schemes coupling with KF and BMJ schemes at Barisal on 15 May 2014. 108
- Fig. 4.4.7: Time variation of (a-b) CT, (c-d) VT, (e-f) TT and (g-h) K-Index using six different MP schemes coupling with KF and BMJ schemes at Chittagong on 15 May 2014. 109
- Fig. 4.4.8: Time variation of (a-b) CAPE, (c-d) CIN, (e-f) LH flux, (g-h) LCL and (i-j) LFC using six different MP schemes coupling with KF and BMJ schemes at Barisal on 15 May 2014. 111
- Fig. 4.4.9: Time variation of (a-b) CAPE, (c-d) CIN, (e-f) LH Flux, (g-h) LCL and (i-j) LFC using six different MP schemes coupling with KF and BMJ schemes at Chittagong on 15 May 2014. 112
- Fig. 4.4.10: WRF Model simulated CWMR (shaded) and RWMR (contour) along the line of maximum vertical velocity using Kessler, Lin *et al.*, WSM6, Thomson, SBU and WDM6 schemes coupling with (a-f) KF and (g-l) BMJ schemes on 15 May 2014. 117

List of Table

Table	Name of the Table	Page
Table 1:	Observed and studied Squall line/Nor'wester in Bangladesh	30
Table 2:	WRF Model and Domain Configurations	31

Nomenclature

ARW	:	Advanced Research WRF
BMD	:	Bangladesh Meteorological Department
BMJ	:	Betts-Miller-Janjic
CP	:	Cumulus Parameterization
FNL	:	Final Reanalysis
GrADS	:	Grid Analysis and Display System
KF	:	Kain-Fritch
BMJ	:	Betts-Miller-Janjic
LBC	:	Lateral boundary conditions
MAE	:	Mean absolute error
MP	:	Microphysics
NCAR	:	National Center for Atmospheric Research
NCEP	:	National Centre for Environment Prediction
PBL	:	Planetary Boundary Layer
UTC	:	Universal Time Co-ordinate
WRF	:	Weather Research and Forecasting
YSU	:	Yonsei University Scheme
KS	:	Kessler
WSM6	:	WRF Single-moment 6-class
TH	:	Thomson
WDM6	:	WRF Double-moment 6-class
SBU	:	Stony Brook University
SLP	:	Sea Level Pressure
RH	:	Relative Humidity
MR	:	Maximum Reflectivity
NWP	:	Numerical weather prediction
AFWA	:	Air Force Weather Agency
FAA	:	Federal Aviation Administration
LLJ	:	Low level jet
RWMR	:	Rain Water Mixing Ratio
CWMR	:	Cloud Water Mixing Ratio
LFC	:	Level of Free Convection
MWS	:	Maximum Wind Speed
LCL	:	Lifted Condensation Level
MCAPE	:	Maximum Convective Available Potential Energy
MCIN	:	Minimum Convective Inhibition
CT	:	Cross Total Index
VT	:	Vertical Totals Index
TT	:	Total Totals Index
KI	:	K Index

Abstract

Comprehensive sensitivity analyses on physical parameterization schemes of Weather Research and Forecasting (WRF-ARW V3.5.1) Model have been carried out for the simulation of squall/nor'wester on 07 April 2012, 28 April 2012, 27 April 2014 and 15 May 2014 over Bangladesh. Final Reanalysis (FNL) data ($1^{\circ} \times 1^{\circ}$) from National Centre for Environment Prediction (NCEP), is used as initial and lateral boundary conditions which is updated at six hourly interval i.e. the model is initialized with 0000, 0600, 1200 and 1800 UTC initial fields of corresponding dates. The NCEP FNL data is interpolated to the model horizontal and vertical grids. The model is configured in a single domain, having 3 km horizontal grid spacing with 173×225 grids in the east-west and north-south directions and 15 vertical levels. By using Grads software, the different meteorological parameters, stability indices and energies are obtained, which are related to Nor'wester/squall line. The six different MP schemes used in this research are Kessler, Lin *et al.*, WSM6, Thompson, SBU and WDM6. The meteorological parameters, which have been analyzed, are Wind Speed at 10m Level, Temperature at 2m Level, Sea Level Pressure (SLP), Relative Humidity (RH), Maximum Reflectivity, Latent Heat, MCAPE, MCIN, Total Total Index (TT), Vertical Total Index (VT), Cross Total Index (CT), K Index (KI), Lifting Condensation Level (LCL) and Level of Free Convection (LFC) at Dhaka, Chittagong, Sylhet, Khulna and Barisal stations. Significant changes are found by all the MPs coupling with CPs in all the parameters during the time of occurrence of squall/gusty wind. Significant changes are found in all the parameters for all MPs coupling with CPs at Dhaka after 0500 UTC and at Chittagong after 0900 UTC of 7 April 2012, which is delayed almost one and half hours. BMJ has simulated reflectivity at a particular time but KF simulated reflectivity wide range of time over Dhaka and Chittagong on 7 April 2012. Significant changes are found by all the MPs coupling with CPs in all the parameters during the time of occurrence of squall at Barisal and Chittagong on 15 May 2014.

Chapter I

Introduction

Bangladesh is located in the tropical monsoon region and its climate is characterized by high temperature, heavy rainfall, often excessive humidity, and fairly marked seasonal variations. The most striking feature of its climate is the reversal of the wind circulation between summer and winter, which is an integral part of the circulation system of the South Asian subcontinent. From the climatic point of view, three distinct seasons can be recognized in Bangladesh - the cool dry season from November through February, the pre-monsoon hot season from March through May, and the rainy monsoon season which lasts from June through October. The month of March may also be considered as the spring season, and the period from mid-October through mid-November may be called the autumn season.

Climate the average condition of the atmosphere near the earth's surface over a long period of time, taking into account temperature, precipitation, humidity, wind, cloud, barometric pressure, etc. Geographical location and physical settings govern the climate of any country. Bangladesh extends from 20°34'N to 26°38'N latitude and from 88°01'E to 92°41'E longitude. Except the hilly southeast, most of the country is a low-lying plain land. It is surrounded by the Assam Hills in the east, the Meghalaya Plateau in the north, the lofty Himalayas lying farther to the north. To its south lies the Bay of Bengal, and to the west lie the plain land of West Bengal and the vast tract of the Gangetic Plain.

Severe thunderstorms, locally known as Nor'westers or Kalbaishakhi, are among the most common natural meteorological phenomena in Bangladesh, Bhutan, southwestern parts of Nepal and northeastern parts of India that occur, especially during the pre-monsoon season (March to May). These systems are embedded within squall lines accompanied by lightning, thunder, tornadoes, hailstorms and heavy rains. Generally, squall line has spatial extent of about few hundred kilometers and travel several hundred kilometers causing large number of loss of lives and severe damages to properties within shortest possible time. The system develops mainly due to merging of mid-tropospheric cold dry northwesterly winds and low-level southerly warm moist winds from the Bay of Bengal. Genesis of these systems takes place over Chhotanagpur plateau area of India due to strong heating in warm sunny days and then travel southeastwards and get intensified after meeting with low-level moist air from the

Bay of Bengal. The southerly low level jet (LLJ) from the Bay of Bengal is very frequent during the pre-monsoon season due to the thermal low produced over land. The LLJ gets established east of the thermal low. The zone of wind discontinuity that forms due to these wind flow regimes and the heat low acts as a triggering mechanism for the generation of local severe thunderstorms. On many occasions, there is an outburst of Nor'wester when a passing westerly trough at 500 hPa is superimposed over the LLJ (Chen and Yu 1988; Chen *et al.* 2005, 2006). The thunderstorms may also originate in-situ in Bangladesh or regenerate from the downstream propagation of the storms originated over the Sub-Himalayan West Bengal, Sikkim, Assam valley and the plateau of the Meghalaya. Usually, these thunderstorms have the spatial extent of a few kilometers and life span less than an hour. However, multi-cell thunderstorms developed due to organized intense convection may have life spans of several hours and may travel over a few hundred kilometers. These thunderstorms reach severity when continental air meets warm moist air from ocean. The lifecycle of these air mass thunderstorms are categorized into three phases on the basis of growth of the thunderclouds. Cumulus stage marks the first stage of growth with the updraft persisting throughout the cell. In the mature stage, there is the presence of both the updraft and the downdraft. The presence of upper level shear adds severity to the storm since it differentiates the zone of the updraft from the zone of downdraft stage. It also extends the lifetime of the cell. The third stage is the dissipating stage marked only by the downdraft throughout the cell. Thunderstorms are typical mesoscale systems dominated by intense convection. The understanding of these weather events is challenging to the atmospheric scientists.

Tornado is a rare weather phenomenon involving a violently rotating column of air which is in contact with a cumulonimbus cloud or, in rare cases, a cumulus cloud base and the surface of the Earth. Tornadoes come in many sizes, but are typically in the form of a visible condensation funnel, whose narrow end touches the ground and is often encircled by a cloud of debris. Litta *et al.* (2010, 2012) simulated severe thunderstorms, which produced tornadoes close to Ludhiana Airport, the northwest region of India on 15 August 2007 and over Orissa on 31 March 2009 using WRF NMM model. The model-simulated meteorological parameters are consistent with each other and all are in good agreement with the observation in terms of the region of occurrence of the intense convective activity. Akter and Ishikawa (2014) studied synoptic features and environmental conditions of Brahmanbaria tornado by using the Japanese 55-year Reanalysis (JRA-55) data (50-km horizontal resolution) and multi-

functional transport satellite images. The results were encouraging in terms of time and the place of occurrence of the event. The use of good resolution, reliable and homogeneous data may produce better prediction of severe storm in this area. Chevuturi *et al.* (2014) showed in a study that the moisture incursion from the Arabian Sea (AS) and the Bay of Bengal (BoB) along with the release of convective available potential energy (CAPE) in the lower levels leads to development of the lower instability over India. On the other hand, the western disturbances in the subtropical westerly jet cause baroclinic instability in the mid/upper troposphere. Both the sources of instability are able to attain condition favorable for rare hail formation. Finch and Dewan (2003) and Das *et al.* (2014, 2015) have shown that many parts of Bangladesh, particularly Brahmanbaria, Tangail, Mymensingh and Dhaka are vulnerable to tornadoes during pre-monsoon season. Litta *et al.* (2012) studied on the simulation of tornado over Orissa on March 31, 2009 using WRF–NMM model. The model-simulated meteorological parameters are consistent with each other and all are in good agreement with the observation in terms of the region of occurrence of the intense convective activity. Richard *et al.* (2013) studied the formation, evolution and decay of the tornado, which was estimated to have been of at least F2 intensity, highlighting a process that can significantly increase the damage of a wildfire event on an Australian pyro-tornadogenesis event. They studied the formation, evolution and decay of the tornado, which was estimated to have been of at least F2 intensity, highlighting a process that can significantly increase the damage of a wildfire event.

Application of WRF model in research and forecasting of severe category thunderstorms including tornadoes during pre-monsoon season is very less in Bangladesh. However, very little work has been done regarding synoptic situations, environmental conditions, and composite characteristics of severe thunderstorms including tornadoes during pre-monsoon season over Bangladesh using WRF model by Das *et al.* (2009) and Basnayake *et al.* (2010), FSU model by Prasad (2006) and MM5 model by Ahasan *et al.* (2008).

Many studies have been conducted to understand the frequency and occurrence of severe thunderstorms over India (Rao and Raman, 1961; Raman & Raghaven, 1961; Krishnamurthy, 1969; Manohar *et al.*, 1999; Kandalgaokar *et al.*, 2002). Few studies (Koteswaran, 1958; Josep, 1982) have been made to understand the formation and propagation of thunderstorms over the region. Simulation of thunderstorms by numerical models has been one of the greatest achievements by the scientists with the advent of high-powered computers. In

addition, tremendous efforts have been deployed by the scientists to understand the dynamics and physical processes of this nonlinear system (Orlanski, 1975). Limited studies have been conducted on numerical simulation of convective clouds and mesoscale convective systems such as cloudburst over the Indian region (Selvam *et al.*, 1991; Das *et al.*, 2006; Mukhopadhyay *et al.*, 2005). Several studies have also been conducted over Bangladesh region to understand frequency and spatial distribution of Nor'wester during pre-monsoon seasons (Chowdury and Karmakar, 1986; Das *et al.*, 1994; Karmakar, 2001; Karmakar and Alam, 2005, 2006, 2007; Prasad, 2006). It is documented that the peak period of occurrence of this phenomenon is in May, having maximum events over Sylhet, Mymensingh and Dhaka regions compared to the least events over northwestern and southwestern parts of Bangladesh. Prasad (2006) conducted a comprehensive study on Nor'wester using ECMWF reanalysis (ERA-40) data. He emphasized that some favorable conditions are to be met in developing these systems over the region. those are an elongated trough extending from North India to Bangladesh, low level pole ward moist flow from the Bay of Bengal, high moisture tongue containing magnitude of about 16-20/ kg intruding from the head BoB into Bangladesh, existence of subtropical jet stream with strong vertical wind shear in the low to mid-tropospheric level over Bangladesh region, presence of a well marked elongated convergence zone in the lower levels extending from the east coast of India to northeast India across Bangladesh, a region of warm air advection at 850 hPa and cold air advection at 300 hPa and intrusion of a plume of high CAPE and low CINE from the BoB into Bangladesh. The massive convective updraft was maintained by strong positive buoyancy, which has maximum at about the 10-km level, probably aided by latent heat of freezing. In Asia, pre-monsoon precipitation systems showed more intense convection in terms of higher echo tops and higher lightning possibility (Kodama *et al.*, 2005). They simulated about 30 Nor'wester events that occurred in 15 days of the season using WRF-ARW model. Composite characteristics of the Nor'wester developed during the season were calculated and TRMM and Dhaka radar data were analyzed to observe some synoptic features of the systems. Cumulus convection modifies the large-scale temperature and moisture fields through detrainment and cumulus-induced subsidence in the environment. The detrainment causes large-scale cooling and moistening, and the cumulus-induced subsidence causes large-scale warming and drying (Arakawa and Schubert, 1974). The Advanced Research Weather Research and Forecasting model (ARW-WRF) is the new-generation model for both weather

research and forecasting (Skamarock *et al.*, 2008), and is also widely used for regional climate research (Leung *et al.*, 2006; Bukovsky and Karoly, 2009; Awan *et al.*, 2011).

The WRF model has been used for the simulation of thunderstorm at Machilipatnam over the east coast of India and a cyclonic circulation over Kerala (Vaidya, 2007) and for simulation of the extreme rainfall event of 26 July 2005 over Mumbai (Vaidya and Kulkarni, 2007; Deb *et al.*, 2008). In United States this model is used for the prediction of warm season rainfall forecasts over the central US (Gallus and Bresch, 2006). A real-time forecast over Taiwan was carried out by studying a mesoscale convective system (MCS) during May 2004 using MM5/WRF mesoscale models. It has been found that the timing of the MCS was slightly better captured by the WRF model than the MM5 model.

The Indian mesosphere–stratosphere–troposphere (MST) radar measurements during the passage of 60 convective systems, the strongest updrafts have been seen in deep convection category in the middle-upper troposphere with value as high as 15–20 m s⁻¹ (Uma and Rao, 2009). The downdrafts are relatively weaker of the order of 5–8 m s⁻¹ and do not vary much with altitude. Robert (2009) has found that the updraft of the cell was 10 km wide, 17 km deep, had updrafts of 10–20 m s⁻¹ throughout its mid to upper levels, and contained a cyclonic vorticity maximum of different types of microphysical schemes and processes on cumulus parameterization were investigated by many Authors (Ferrier *et al.*, 1995; Wu *et al.*, 1999; Tao *et al.*, 2003). Tao *et al.* (1990) showed that the dominant microphysical processes were quite different between the convective and stratiform regions and between the mature and decaying stages.

In the present study, we have simulated and analyzed of different meteorological parameters associated with different squall lines/Nor'westers those formed in the pre-monsoon season in Bangladesh. The squall lines/Nor'westers is simulated by considering six different microphysics (MP) schemes in combination with Kain-Fritsch (KF) and Betts-Millar-Janjic (BMJ) cumulus parameterization (CP) schemes. The different meteorological parameters in this study are wind speed at 10m level, temperature at 2m level, relative humidity at 2m level and sea level pressure. The different energies and instability indices are maximum Convective Available Potential Energy (MCAPE), maximum Convective Inhibition (MCIN), Level of Free convection (LFC), Lifted Condensation Level (LCL), Latent Heat Flux (LHF), Cross Total Index (CT), Vertical Total Index (VT), Total Totals Index (TT) and K-Index

(KI). These parameters have been calculated in the stations where squall/nor'westers occurred. Maximum vertical velocity has also been calculated from the model output, which indicates the maximum convection. Hydrometeors, relative humidity and vorticity have also been analyzed along the line of maximum vertical velocity.

Chapter 2

Review of Literatures

Bangladesh experiences a high frequency of severe thunderstorms during the pre-monsoon periods, which have great destructive potential and are characterized by tornadic violence, often accompanied by high magnitude squalls, torrential rains, and hail. Pre-monsoon season over Bangladesh extending from March to May is characterized by very good convective activity all over the country. Convective activity progressively increases from March onwards as the season advances. The thunderstorms form from a cumulonimbus cloud, which incur substantial vertical development where the tops usually reach well into the upper levels of the troposphere. However, most cumulonimbus cloud tops are restricted in height by the tropopause, the boundary between the troposphere and stratosphere (Krishnamurti, 2003). Though the thunderstorm activity may continue over the country even during the southwest monsoon season, the severity of thunderstorms is marked only in the pre-monsoon season, when they, on a number of occasions, are accompanied by squalls and hails (Srinivasan, *et al.*, 1973).

A stability index is a measure of the potential instability of the atmosphere over a specified region. Since such an indicator can be calculated hours prior to the actual development of any convective activity, it acts as timely identifier of areas within an air mass, which are capable of supporting convective activity. From mid-March to April the temperature in Bangladesh rises sharply compared to the preceding months (i.e. winter months). In the middle of April, the whole country, especially the northwestern part, records a sharp rise in day temperature. Presence of warm and moist air in the lower layer of the atmosphere is an essential precondition for the development of a nor'wester. Unstable atmosphere and intense convective activity are other important factors for their origin and growth. Nor'wester may be called air mass thunderstorms or convective thunderstorms, since they frequently occur in warm air masses and in the summer. Thunderstorms occur most frequently in the humid continental regions of the tropics. Bangladesh falls in the humid region of the tropics. As a result, the country faces severe thunderstorms especially during the pre-monsoon season. These thunderstorms are known as nor'westers in Bangladesh.

The main reason behind the nor'wester is the warm and moist air coming from the

south/southeast which rises up to 2 km or more, mixes with the relatively cold and dry air coming from the northwesterly and westerly directions. The mixing of these two dissimilar air masses causes storms. The warm and moist air rises due to the Chotanagpur Plateau, Himalayan ranges, and Assam Plateau. The life cycle of a nor'wester is associated with (i) cumulus; (ii) mature; and (iii) dissipating stages, which are determined by the magnitude and direction of the ascending or descending air currents. After 30 to 45 minutes the mature nor'wester begins to decrease in intensity and enters the dissipating stage. Because of very steep temperature lapse rate, high water content of clouds and the cumulous updrafts, hail is common to a nor'wester. The size of a hail is determined by the rate of uplift within a cloud and its high water content. Thunder and lightning are common with a nor'wester. Nor'wester is more frequent in the late afternoon because of the influence of surface heating in producing convection currents in the atmosphere. In the western region of Bangladesh, nor'wester come in the late afternoon and before evening but in the eastern side it comes generally after evening, moving from a northwesterly to a easterly and southeasterly direction. In this season, the morning remains calm. Temperature begins to rise from noon creating a convective current and the storm is formed. The average wind speed of a nor'wester is 40-60 km per hour. But in exceptional circumstances the wind speed may exceed 100 km. The duration of the storm is generally less than an hour but sometimes it may exceed an hour.

2.1 Pre-monsoon Rainfall

The pre-monsoon is normally occurring from March, although their arrival is often difficult to predict. Their intensity can range from light showers to heavy and persistent thunderstorms. The maximum amount of rainfall has been recorded in the northern part of Sylhet district and in the southeastern part of Cox's Bazar and Bandarban districts. The additional uplifting by the Meghalaya Plateau of the moist air causes higher amount of rainfall in the northeast. As the winter season progresses into the pre-monsoon hot season, rainfall increases due to intense surface heat and the influx of moisture from the Bay of Bengal. Rainfall during this season accounts for 10%-25% of the total annual rainfall which is caused by the thunderstorms or nor'wester [Kalbaishakhi].

2.2 Pre-monsoon Temperature

As the winter season progresses into the pre-monsoon hot season, temperature rises, reaching the maximum in April, which is the middle of the pre-monsoon hot season. Average

temperatures in April vary from about 27°C in the northeast to 30°C in the extreme west-central part of the country. In some places in Rajshahi and Kushtia districts, the maximum temperature in summer season rises up to 40°C or more. Widespread cloud covers causes dampening of temperature during the later part of the pre-monsoon season. Average temperatures in July vary from about 27°C in the southeast to 29°C in the northwestern part of the country.

2.3 Convective Inhibition (CIN)

Convective inhibition is a numerical measure in meteorology that indicates the amount of energy that will prevent an air parcel from rising from the surface to the level of free convection. CIN is the amount of energy required to overcome the negatively buoyant energy the environment exerts on an air parcel. In most cases, when CIN exists, it covers a layer from the ground to the level of free convection (LFC). The negatively buoyant energy exerted on an air parcel is a result of the air parcel being cooler (denser) than the air which surrounds it, which causes the air parcel to accelerate downward. The layer of air dominated by CIN is warmer and more stable than the layers above or below it. The situation in which convective inhibition is measured is when layers of warmer air are above a particular region of air. The effect of having warm air above a cooler air parcel is to prevent the cooler air parcel from rising into the atmosphere. This creates a stable region of air. Convective inhibition indicates the amount of energy that will be required to force the cooler packet of air to rise. This energy comes from fronts, heating, moistening, or mesoscale convergence boundaries such as outflow and sea breeze boundaries or Orographic lift (Colby, 1984).

2.4 Level of Free Convection (LFC)

The level of free convection is the altitude in the atmosphere where the temperature of the environment decreases faster than the moist adiabatic lapse rate of a saturated air parcel at the same level. The usual way of finding the LFC is to lift a parcel from a lower level along the dry adiabatic lapse rate until it crosses the mixing ratio line of the parcel: this is the lifted condensation level (LCL). From there on, follow the moist adiabatic lapse rate until the temperature of the parcel reaches the air mass temperature at the equilibrium level (EL). If the temperature of the parcel along the moist adiabat is warmer than the environment on further lift, one has found the LFC. Since the volume of the parcel is larger than the surrounding air after LFC by the ideal gas law ($PV = nRT$), it is less dense and becomes

buoyant rising until its temperature equals the surrounding air mass. If the air mass has one or many LFC, it is potentially unstable and may lead to convective clouds like cumulus and thunderstorms (<https://en.wikipedia.org/wiki/>).

2.5 Lifted Condensation Level (LCL)

The lifted condensation level is defined as the height at which the relative humidity (RH) of an air parcel will reach 100% when it is cooled by dry adiabatic lifting. The RH of air increases when it is cooled, since the amount of water vapor in the air (i.e., its specific humidity) remains constant, while the saturation vapor pressure decreases almost exponentially with decreasing temperature. If the air parcel is lifting further beyond the LCL, water vapor in the air parcel will begin condensing, forming cloud droplets. In the real atmosphere, it is usually necessary for air to be slightly supersaturated, normally by around 0.5%, before condensation occurs; this translates into about 10 meters or so of additional lifting above the LCL. The LCL is a good approximation of the height of the cloud base which will be observed on days when air is lifted mechanically from the surface to the cloud base (Lawrence, 2005).

2.6 Latent Heat (LH) Flux

Latent heat flux is the flux of heat from the Earth's surface to the atmosphere that is associated with evaporation of water at the surface and subsequent condensation of water vapor in the troposphere. It is an important component of Earth's surface energy budget. Latent heat flux is commonly measured with the Bowen ratio technique, or by eddy covariance (http://disc.gsfc.nasa.gov/hydrology/data-holdings/parameters/latent_heat_flux.shtml).

The atmosphere is a dynamic heat system designed to transfer heat from one place to another. Latent heat involved in the phase change of water plays essential roles in the transfer of heat. Just as much latent heat is released in the atmosphere through a phase change as the latent heat is absorbed at the Earth's surface. The latent heat fluxes and the transfer of sensible heat between the equator and the poles are major components of the energy balance of the Earth. The latent heat flux in the atmosphere is huge. Latent heat flux involved in the phase change of water drives the atmospheric circulation and plays essential roles in global climate.

Latent heat is also an important factor to better comprehend weather systems, because it is a primary source of energy that develops, promotes, and sustains severe weather systems, such as thunderstorms and tropical cyclones. Latent heat supplies weather energy. As water condenses, latent heat from the water molecule is released into the air, heats the air, makes it lighter, and makes it rise fast. As the air rises, more air flows in and promotes storms. In this process, some latent heat is changed into the kinetic energy that accelerates the speed of water molecules and powers up severe weather systems. Recent global warming increases the ability to evaporate and hold moisture in the atmosphere. As a greater amount of water vapor exists in the hot air, more latent energy is available to be released into severe storms. Another critical aspect of global warming is that it will increase variability of extreme weather, although the overall average of the atmospheric condition changes little. Thus rare, but extreme weather, often much beyond what we experience today, will be more common.

2.7 Classification of local severe storms

The thunderstorms are the local severe storms, which have been classified as follows.

Local severe storms		Maximum gusty wind (km/hr)
i.	Thunderstorms with gusty winds	: 31-40
ii.	Thunderstorms with squally winds/light nor'westers	: 41-60
iii.	Moderate nor'westers	: 61-90
iv.	Severe nor'westers	: 91-120
v.	Very severe nor'westers	: 121-150
vi.	Tornado	: >151

2.8 Nor'westers

Nor'westers/thunderstorms generally blows over Bangladesh usually in April-May from a northwesterly direction locally known as Kal-baishakhi. Nor'wester/thunderstorm coincides with the setting of the summer season. It occurs when the atmosphere becomes sufficiently unstable because of localized surface heating or other causes. Air that becomes buoyant rises and is cooled by adiabatic expansion until it eventually reaches saturation point and causes a cumulus cloud. If the atmosphere is unstable further, the cumulus cloud grows vertically to form cumulonimbus cloud and subsequently a thunderstorm, popularly known as nor'wester. The difference between an ordinary shower and this type of storm is that it is always associated with thunder and lightning. It is like a thermodynamic machine in which the latent

heat of condensation is rapidly converted into the kinetic energy of ascending air currents. Various aspects of these phenomena have been studied by different authors like Chowdhury and Karmakar (1986), Das *et al.* (1994), Karmakar and Alam (2007, 2006, 2005). In all of these studies, a number of important results have been obtained as regards formation, structure, timing and devastation of nor'westers, etc. There has been, of course, some difference of opinions among the authors as well.

2.9 Thunderstorm

Thunderstorm is defined as one or more sudden electrical discharges, manifested by a flash of light (lightning) and a sharp or rumbling sound (thunder). A typical thunderstorm is made up of a single cumulonimbus cloud. Thunderstorms are associated with strong winds, which are created by the downdraft, this downdraft in turn is created by cold air rushing out of the thunderstorm as precipitation inside of it evaporates and cools the air. If the environment outside the thunderstorm is particularly dry, evaporation will be enhanced, and so will the threat for severe winds. A downburst is defined as an area of strong winds produced by a downdraft. Once it comes in contact with the earth, it spreads out laterally and causes damage at ground level. There are two types of downbursts, a macro burst and a microburst. The macro burst covers an area larger than 4 km in diameter, and the microburst is smaller than 4 km in diameter, as defined by Fujita (1985). Both are a serious threat to structures on the ground and to planes in the air. Damage caused by downbursts is frequently mistaken for tornado damage. People who have experienced this phenomenon describe it as a loud (sometimes dark) cloud rushing toward them and when it reaches them, the wind becomes very violent. There are four types of thunderstorms. These are the single cell (ordinary), multi cell (squall line), multi cell cluster and super cell.

2.9.1 Single-cell Thunderstorm

The ordinary or single cell thunderstorm is nothing more than ephemeral bursts of convection. Each burst creates a towering cumulus or "cell" of convection. Once the cell gets large and tall enough, it is classified as a cumulonimbus, or thunderstorm (<https://upload.wikimedia.org/wikipedia/commons>).

The updraft and of this small cloud interfere with each other, resulting in a fairly short-lived cell, but the downdraft from one single cell may give rise to a new cell nearby. This “parent-daughter” effect allows an ordinary thunderstorm to pulse with convection for up to one hour.



Fig. 1.1: Single cell thunderstorm

2.9.2 Multi-cell clusters

The multi-cell cluster is the most common type of thunderstorm. The name multi-cell simply means that there are many cells that grow to form a group of cells that move together as one unit. A multi-cell cluster thunderstorm results from a vigorous parent-daughter effect (<https://en.wikipedia.org/wiki/Thunderstorm>). In this case, an ordinary thunderstorm creates neighboring storms via the downdraft and a gust front.

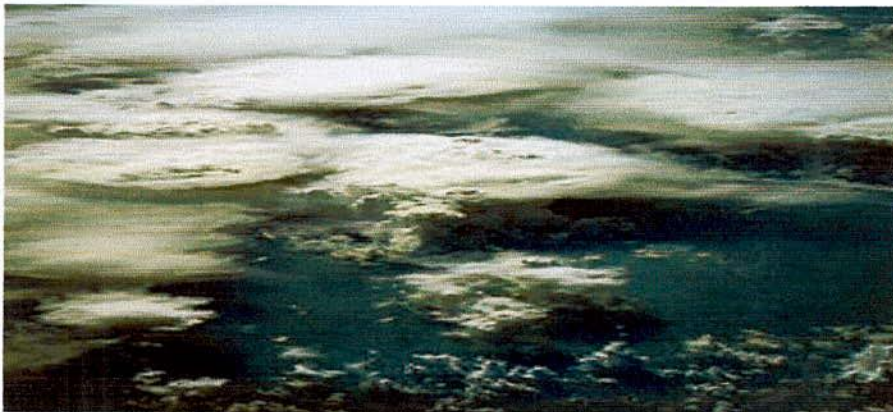


Fig. 1.2: Multi-cell thunderstorm

If the surrounding atmosphere is unstable and moist enough, new cells will be created around the old one, giving birth to cluster of active thunderstorms. Each cell will be in a different

phase of the life cycle. Each individual cell will have its turn to be the dominant one. New cells tend to form on the western or southwestern edge of the cluster, while the more mature cells are usually found in the centre. The dissipating cells are often found on the eastern or northeastern edge of the cluster. The multi-cell cluster storms last a bit longer than ordinary or single cell storms and cover a larger area. Each cell in a multi-cell cluster storm usually lasts about 20 minutes, but the cluster of storms itself can persist for several hours.

2.9.3 Squall line thunderstorms

The multi-cell line or squall line thunderstorms form in long lines with a well-developed gust front at the leading edge of the line. Squall lines are prolific downburst producers. Occasionally an extreme strong downburst will accelerate a portion of the line forward causing it to form what is called *bow*. On the leading edge of this bow formation is where the most damaging winds are found. Tornadoes will sometimes form just to the north of this bow, or on the line's southernmost cell, which is called the *anchor cell*. Cells that form on the southern ends of squall lines tend to inherit super-cell characteristics since there is nothing to the south of them to disrupt air flow being entrained into them (<http://spotterguides.us/advanced/advanced05.htm>).

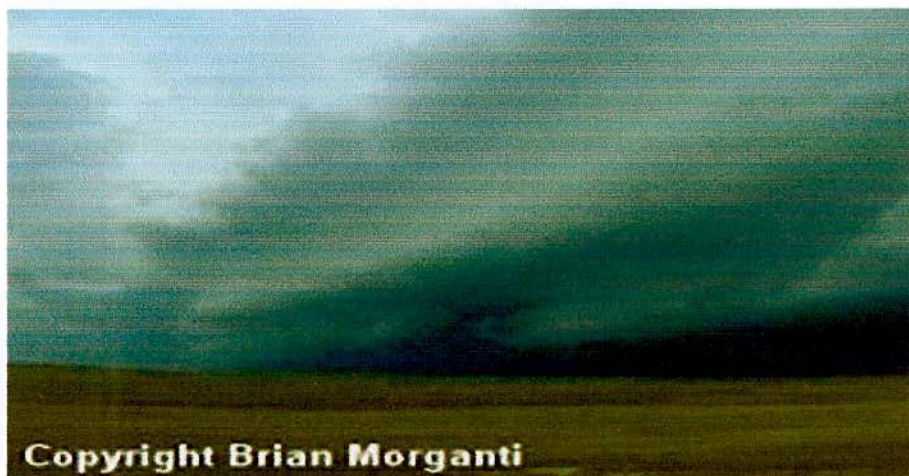


Fig. 1.3: Squall line thunderstorm

2.9.4 Super cell thunderstorm

The super cell thunderstorm is the classic cumulonimbus tower with the anvil top and on occasion the overshooting updraft tower. These storms are notorious for producing damaging straight-line winds, frequent lightning, flash floods, large hail, and violent tornadoes. The

base of the storm may be only 20-50 km across, but the anvil aloft can stretch for many hundreds of kilometers. The super cell is unique because the updraft actually rotates; this rotating updraft is called a mesocyclone. Organization within the storm is incredible. The updraft and downdraft regions do not interfere each other like the ordinary thunderstorm; instead, they collaborate to prolong the life of the storm (<https://en.wikipedia.org/wiki/Thunderstorm>).



Fig. 1.4: Super cell thunderstorm

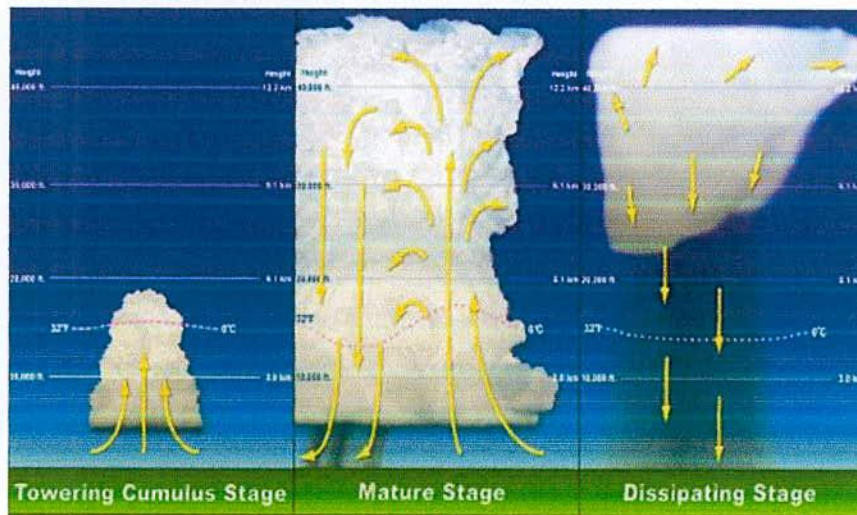


Fig. 1.5: Life cycle of a thunderstorm

The inflow, outflow, updrafts, and downdrafts all work together like a living, breathing creature. A super cell can exist in a quasi-steady state for hours, advecting along the ground with the ambient wind. In order to form a super cell, three ingredients are necessary: (i) high

thermal instability, (ii) strong winds in the middle and upper troposphere, and (iii) veering of the wind with height in the lowest kilometer. As the precipitation is produced in the updraft, the strong upper-level winds blow the precipitation away from the updraft, allowing little or none of it fall back down through the updraft core. Keeping the precipitation away from the updraft is what allows the supercell to thrive for many hours, capable of producing violent weather throughout its lifetime. Light rain will begin as the super cell approaches. As the updraft area comes closer, the areas to the north and east will see an increase in rain and hail, and then near the updraft itself is where most severe weather (tornadoes) will occur. The life cycle of a thunderstorm has three stages: (a) Cumulus stage, (b) Mature stage and (c) Dissipating stage (<https://en.wikipedia.org/wiki/Thunderstorm>). The three stages are shown in Fig. 1.5.

2.10 Tornado

A tornado is a violently rotating column of air that is in contact with both the surface of the earth and a cumulonimbus cloud or, in rare cases, the base of a cumulus cloud. They are often referred to as twisters or cyclones, although the word cyclone is used in meteorology, in a wider sense, to name any closed low pressure circulation is seen as a funnel-shaped cloud pendant from a cloud base (Fig. 1.5). The funnel does not always extend to the ground, and may be obscured by dust (Ghose, 1986). The tornadoes move in a zigzag path.

2.10.1 Life Cycle of Tornado

The tornado life cycle may broadly be divided into the following five stages (Davies Jones, 1982)

- (i) The dust whirl stage – when the first signs of circulation are visible as dust swirling upwards from the surface.
- (ii) The organizing stage – characterized by overall downward descent of the funnel.
- (iii) The mature stage – when the funnel reaches its greatest width and is almost vertical and when damage is most intense.
- (iv) The shrinking stage – marked by decreasing funnel width, increasing funnel tilt and a narrow damage sweep.
- (v) The decay stage – when the vortex is stretched into a rope shape.

2.10.2 Damage by a Tornado

A tornado inflicts damage in various ways as in the following (Holford, 1977):

- a) By the direct impact of wind, whose force is proportional to the square of wind speed.
- b) By twist due to unequal wind speeds within the very narrow band of the circulation. Winds are often so much greater on one side of a tree than on the other that they screw off the tops of trees.
- c) By explosion when a tornado passes directly over a building which contains air at normal atmospheric pressure. Extremely high pressure gradients exist across the narrow circulation, which would result in a momentary inequality of pressure between the outside and inside of a building. Roofs are sucked off and walls explode outwards. The advice given in tornado safety rules in the USA is to open doors and windows on the opposite side of the building from that of the approaching tornado, so as to facilitate the equalization of atmospheric pressure.
- d) By lift and drop in the vertical currents within the tornado. Sheds, cattle and human beings are carried high into the air (Nandi and Mukherjee, 1966). Even vehicles such as buses with several persons inside are reported to have been lifted a few meters above the ground (Mukherjee and Bhattacharya, 1972; Gupta and Ghosh, 1980).

2.10.3 Favorable conditions for tornado genesis

The following conditions favorable for formation of tornadoes:

- (a) Abundant moisture in the surface layer to a depth of at least 1 km. The presence of a dry air mass at intermediate level (1 to 2.5 km), providing the potential for strong downdrafts through evaporative cooling, is also favorable.
- (b) Deep conditional and convective instability i.e., large lapse rate of temperature and moisture through a great depth.
- (c) The presence of a stable layer or inversion. This acts to prevent deep convection from occurring until the potential for explosive overturning is established.
- (d) A mechanism to remove the stable layer. The most common mechanism is dynamic lifting with surface heating and warm air advection below the inversion. Other possible mechanism includes lifting by terrain and by gravity waves. Dynamic lifting is strongest

near thin zones of low-level convergence such as fronts or dry lines (dew-point fronts) and beneath regions of pronounced upper level divergence. Typically, these features occur in combinations to provide sustained lifting through deep layers.

- (e) Moderate to strong winds that veer with height, with large values in a narrow horizontal band at altitudes above 6 km.

2.11 Climatological aspects of nor'westers

Nor'wester activities in these parts of the region are directly linked up with the apparent movement of the sun towards north causing steady rise in temperature over Southern India and gradually extending to the north. Such a situation becomes increasingly prominent from March and prolongs up to the end of May. Frequency of nor'westers in Bangladesh usually reaches its maximum in May, having maximum value over the Sylhet-Mymensingh-Dhaka region (Chowdhury and Karmakar, 1986) and has comparatively minimum over the northwestern and southwestern parts of Bangladesh. There are occasions when nor'westers has been observed to occur in late February and early June. The occurrences of nor'westers in late February can be attributed to the early withdrawal of winter from Bangladesh, Assam, Bihar, West Bengal and adjoining area as well as due to the penetration of the easterly lows through the southern tip of India and their subsequent movement towards north-east (Das *et al.*, 1994), while those in early June are due to delay in the onset of south-west monsoon over this region. The delay in the occurrence of nor'wester over Bangladesh is due to presence of intense subtropical high over the Bay of Bengal.

2.12 Weather Research & Forecasting (WRF) Model

The Weather Research and Forecasting (WRF) Model is a next-generation mesoscale numerical weather prediction (NWP) system designed to serve both atmospheric research and operational forecasting needs. It features two dynamical cores, a data assimilation system, and a software architecture facilitating parallel computation and system extensibility. The model serves a wide range of meteorological applications across scales from tens of meters to thousands of kilometers. The effort to develop WRF began in the latter part of the 1990's and was a collaborative partnership principally among the National Center for Atmospheric Research (NCAR), the National Oceanic and Atmospheric Administration (NOAA) represented by the National Centers for Environmental Prediction (NCEP) and the Forecast Systems Laboratory (FSL) the Air Force Weather Agency (AFWA), the Naval Research

Laboratory, the University of Oklahoma, and the Federal Aviation Administration (FAA).

The WRF model is an atmospheric simulation system which is designed for both operational and research use. WRF is currently in operational use at the NOAA national weather service as well as at the air force weather agency and meteorological services worldwide. Getting weather predictions in time using latest advances in atmospheric sciences is a challenge even on the fastest super computers. Timely weather predictions are particularly useful for severe weather events when lives and property are at risk. Microphysics is a crucial but computationally intensive part of WRF. WRF offers two dynamical solvers for its computation of the atmospheric governing equations, and the variants of the model are known as WRF-ARW and WRF-NMM. The Advanced Research WRF (ARW) is supported to the community by the NCAR Mesoscale and Microscale Meteorology Division. The WRF-NMM solver variant was based on the Eta Model, and later Non hydrostatic Mesoscale Model, developed at NCEP. The WRF-NMM is supported to the community by the Developmental Test bed Center.

2.12.1 Microphysics schemes in WRF-ARW Model

Microphysics includes explicitly resolved water vapor, cloud and precipitation processes. The model is general enough to accommodate any number of mass mixing-ratio variables, and other quantities such as number concentrations. Four-dimensional arrays with three spatial indices and one species index are used to carry such scalars. Memory, i.e., the size of the fourth dimension in these arrays, is allocated depending on the needs of the scheme chosen, and advection of the species also applies to all those required by the microphysics option. In the current version of the ARW, microphysics is carried out at the end of the time-step as an adjustment process, and so does not provide tendencies. The rationale for this is that condensation should be at the end of the time-step to guarantee that the final saturation balance is accurate for the updated temperature and moisture. However, it is also important to have the latent heating forcing for potential temperature during the dynamical sub-steps and this is done by saving the microphysical heating as an approximation for the next time-step as described.

2.12.1.1 Kessler Scheme

The Kessler scheme is a simple warm cloud scheme that includes water vapor, cloud water and rain. The microphysical process consists of the production, fall and evaporation of rain,

the accumulation and auto conversion of cloud water and the production of cloud water from condensation. A warm-rain scheme has been used commonly in idealized cloud modeling studies. Kessler scheme is one moment scheme. The purpose of the scheme is to increase understanding of the roles of cloud conversion, accretion, evaporation, and entrainment processes in shaping the distributions of water vapor, cloud, and precipitation associated with tropical circulations. This scheme is idealized microphysics process without the consideration of ice phase and melting zone. Kessler scheme has been used widely in cloud modeling studies due to its simplicity. The equation represented the processes between cloud, vapor and rain are also much simplified compared with other scheme. Kessler scheme produced much heavier precipitation and can show unrealistic precipitation profiles in some studies (Kessler, 1969).

2.12.1.2 Lin *et al.* Scheme

A sophisticated scheme that has ice, snow and graupel processes, suitable for real-data high-resolution simulations. Lin *et al.* (1983) scheme includes six classes of hydrometeors are included: water vapor, cloud water, rain water, cloud ice, snow, and graupel. All parameterization production terms are based on Lin *et al.* (1983). This is a relatively sophisticated microphysics scheme in WRF, and it is more suitable for use in research studies. The scheme is taken from Purdue cloud model and the details can be found in Chen and Sun *et al.* (2002) 2-D microphysics scheme. This is one of the first schemes to parameterize snow, graupel, and mixed-phase processes. It has been used extensively in research studies and in mesoscale NWP Model. The scheme includes ice sedimentation and time-split fall terms.

2.12.1.3 WRF Single-Moment 6-class Microphysics Scheme (WSM6)

The WRF-single-moment-6-class (WSM6) microphysics scheme has been one of the options of microphysical process in the WRF model. This scheme predicts the mixing ratios for water vapor, cloud water, cloud ice, snow, rain, and graupel. We attempt to improve such existing deficiencies in the WSM6 scheme by incorporating the prediction of number concentrations for warm rain species. A new method for representing mixed-phase particle fall speeds for the snow and graupel by assigning a single fall speed to both that is weighted by the mixing ratios, and applying that fall speed to both sedimentation and accumulation processes is introduced of the three WSM schemes, the WSM6 scheme is the most suitable for cloud-

resolving grids, considering the efficiency and theoretical backgrounds (Hong *et al.*, 2006). The WSM6 scheme has been developed by adding additional process related to graupel to the WSM5 scheme (Hong and Lim, 2006).

2.12.1.4 Thompson Scheme

A bulk microphysical parameterization (BMP) developed for use with WRF or other mesoscale models. The snow size distribution depends on both ice water content and temperature and is represented as a sum of exponential and gamma distributions. Furthermore, snow assumes a non-spherical shape with a bulk density that varies inversely with diameter as found in observations. A new scheme with ice, snow and graupel processes suitable for high-resolution simulations. This adds rain number concentration and updates the scheme from the one in Version 3.0 New Thompson *et al.* scheme in V3.1. Replacement of Thompson *et al.*, (2007) scheme that was option 8 in V3.0 6-class microphysics with graupel, ice and rain number concentrations also predicted.

2.12.1.5 Stony Brook University (SBU) Microphysics

Stony Brook University scheme is a 5-class scheme with riming intensity predicted to account for the mixed-phase processes. A new approach for representing the ice microphysics is presented, which considers both temperature and riming effects on ice properties. The SBU-YLIN scheme includes five prognostic mixing ratios: water vapor, cloud ice, precipitating ice (PI), cloud liquid water, and rain. Dry snow, rimed snow, and graupel are included in the PI category through the introduction of a varying riming intensity parameter. The new scheme (SBU-YLIN) allows for physically based representation of the ice particles with temperature- and riming intensity-dependent properties, such as the mass, cross-sectional area, and fall velocity relationships. Riming intensity is diagnosed from LWC, PI mass, and temperature. One advantage of the new approach is the simplification of the scheme and the reduction of the computation time. Also, it is more physically based than many existing schemes, since it considers partially rimed particles (Lin and Colle, 2011).

2.12.1.6 WRF Double-Moment 6-class Microphysics Scheme (WDM6)

The WRF double-moment 6-class microphysics scheme (WDM6) implements a double-moment bulk micro physical parameterization of clouds and precipitation and is applicable in mesoscale and general circulation models. The WDM6 scheme enables the investigation of the aerosol effects on cloud properties and precipitation processes with the prognostic

variables of cloud condensation nuclei (CCN), cloud water and rain number concentrations. WDM6 extends the WRF single-moment 6-class microphysics scheme (WSM6) by incorporating the number concentrations for cloud and rainwater along with a prognostic variable of CCN number concentration. Moreover, it predicts the mixing ratios of six water species (water vapor, cloud droplets, cloud ice, snow, rain, and graupel), similar to WSM6. Prognostic water substance variables include water vapor, clouds, rain, ice, snow, and graupel for both the WDM6 and WSM6 schemes. Additionally, the prognostic number concentrations of cloud and rain waters, together with the CCN, are considered in the WDM6 scheme. The number concentrations of ice species such as graupel, snow, and ice are diagnosed following the ice-phase microphysics of Hong *et al.* (2004).

2.12.2 Cumulus Parameterization

These schemes are responsible for the sub-grid-scale effects of convective and/or shallow clouds. The schemes are intended to represent vertical fluxes due to unresolved updrafts and downdrafts and compensating motion outside the clouds. They operate only on individual columns where the scheme is triggered and provide vertical heating and moistening profiles. Some schemes provide cloud and precipitation field tendencies in the column, and future schemes may provide momentum tendencies due to convective transport of momentum. The schemes all provide the convective component of surface rainfall. Cumulus parameterizations are theoretically only valid for coarser grid sizes, (e.g., greater than 10 km), where they necessary to properly release latent heat on a realistic time scale in the convective columns. Where the assumptions about the convective eddies being entirely sub-grid-scale break down for finer grid sizes, sometimes these schemes have been found to be helpful in triggering convection in 5-10 km grid applications. Generally they should not be used when the model can resolve the convective eddies itself. These schemes are responsible for the sub-grid-scale effects of convective and shallow clouds. The schemes are intended to represent vertical fluxes due to unresolved updrafts and downdrafts and compensating motion outside the clouds.

2.12.2.1 Kain-Fritsch (KF) Scheme

In the KF scheme the condensates in the updraft are converted into precipitation when their amount exceeds threshold value. In this scheme the convection consumes the convective available potential energy in a certain time scale. The KF scheme also includes the shallow

convection other than deep convection. The shallow convection creates non-perceptible condensates and the shallowness of the convection is determined by a vertical extent of the cloud layer that is known by a function of temperature at LCL of rising air parcel. The KF scheme was derived from the Fritsch–Chappell, and its fundamental framework and closure assumptions are described by Fritsch and Chappell (1980). KF (1990) modified the updraft model in the scheme and later introduced numerous other changes, so that it eventually became distinctly different from the Fritsch–Chappell scheme. It was distinguished from its parent algorithm by referring to the more elaborate code as the KF scheme, beginning in the early 1990s. This is also deep and shallow convection sub-grid scheme using a mass flux approach with downdrafts and CAPE removal time scale. Updraft generates condensate and dump condensate into environment downdraft evaporates condensate at a rate that depends on RH and depth of downdraft leftover condensate accumulates at surface as precipitation.

2.12.2.2 Betts-Miller-Janjic (BMJ) Scheme

The BMJ cumulus parameterization scheme is a nudging type adjustment of temperature and humidity in grid scale. The scheme adjusts the sounding towards a pre-determined, post convective profile derived from climatology. This post convective profile has been defined by points at the cloud base, cloud top and freezing level. In this scheme there is no explicit updraft or downdraft and no cloud detrainment occur. Convection is initiated when soundings are moist through a deep layer and when CAPE and convective cloud depth thresholds are exceeded. Betts and Miller proposed a convective adjustment scheme that includes both deep and shallow convection. The deep convection in the Betts–Miller scheme is similar to the other adjustment schemes except that it uses empirically based quasi-equilibrium thermodynamic profiles as a reference state rather than a moist adiabatic. The basic shape of these quasi-equilibrium reference profiles is based on the numerous observations. The construction of the reference profiles and the specification of the relaxation timescale are two major components of the Betts–Miller scheme (Janjic, 1994).

These points and thresholds can vary by season and between the tropics and extra tropics. Compared with the original sounding, the sounding modified to the post convective profile will note a net change in perceptible water as well as changes in net heating and cooling. Convection is initiated when soundings are moist through a deep layer and when CAPE and convective cloud depth thresholds are exceeded. Important vertical structures may be

eliminated since the reference profiles are based on climatology. Convection only initiated for soundings with deep moisture profile. When convection is initiated the scheme often rains out too much water. This is because the reference profile is too dry for the forecast scenario or the transition to the reference profile was too rapid. Scheme does not account for the strength of CAPE inhibiting convective development. Scheme does not account for any changes below the cloud base.

2.12.3 Planetary Boundary Layer (PBL)

The PBL is the layer in the lower part of the troposphere with thickness ranging from a few hundred meters to a few kilometers within which the effects of the Earth's surface are felt by the atmosphere. The PBL processes represent a consequence of interaction between the lowest layer of air and the underlying surface. The interactions can significant impact on the dynamics of the upper air flows. The influences of the small-scale eddy on large scale atmospheric circulations may be included in the model equations. Accurate depiction of meteorological conditions, especially within the PBL, is important for air pollution modeling, and PBL parameterization schemes play a critical role in simulating the boundary layer. It is a very important portion of the atmosphere to correctly model to provide accurate forecasts, e.g., air pollution forecasts (Deardorff 1972; Pleim 2007). As important as the PBL is, it has one basic property whose accurate and realistic prediction is paramount to its correct modeling: its height. After all, the height of the top of the PBL defines its upper boundary. This is critical since PBL parameterizations schemes in WRF-ARW models need to know the extent through which to mix properties such as heavy rainfall, relative humidity, outgoing long wave flux, downward long wave flux.

PBL schemes were developed to help resolve the turbulent fluxes of heat, moisture, and momentum in the boundary layer. Another important issue is the interaction between the atmosphere and the surface. The PBL schemes handle the latent and sensible heat fluxes into the atmosphere, the frictional effects with the surface and the strong sub-grid-scale mixing which takes place in the lower levels due to these processes.

2.12.3.1 Yonsei University (YSU) scheme

The Yonsei University (YSU) PBL is the next generation of the Medium Range Forecast (MRF), Non local-K scheme with explicit entrainment layer and parabolic K profile in unstable mixed layer. The YSU scheme is a bulk scheme that expresses non-local mixing by

convective large eddies. Non-local mixing is achieved by adding a non-local gradient adjustment term to the local gradient. At the top of the PBL, the YSU scheme uses explicit treatment of the entrainment layer, which is proportional to the surface layer flux (Shin and Hong 2011; Hong *et al.* 2006).

2.12.4 Map Projection

Commonly, a map projection is a systematic transformation of the latitudes and longitudes of locations on the surface of a sphere or an ellipsoid into locations on a plane. Map projections are necessary for creating maps. All map projections distort the surface in some fashion. Depending on the purpose of the map, some distortions are acceptable and others are not; therefore, different map projections exist in order to preserve some properties of the sphere-like body at the expense of other properties. There is no limit to the number of possible map projections. More generally, the surfaces of planetary bodies can be mapped even if they are too irregular to be modeled well with a sphere or ellipsoid. Even more generally, projections are the subject of several pure mathematical fields, including differential geometry and projective geometry. However, map projection refers specifically to a cartographic projection (Snyder, 1989).

2.12.4.1 Mercator projection

The Mercator projection is a cylindrical map projection presented by the Flemish geographer and cartographer Gerardus Mercator in 1569. It became the standard map projection for nautical purposes because of its ability to represent lines of constant course, known as rhumb lines loxodromes, as straight segments which conserve the angles with the meridians. While the linear scale is equal in all directions around any point, thus preserving the angles and the shapes of small objects, the Mercator projection distorts the size and shape of large objects, as the scale increases from the Equator to the poles, where it becomes infinite. Although the Mercator projection is still used commonly for navigation, due to its unique properties, cartographers agree that it is not suited to general reference world maps due to its distortion of land area. Mercator himself used the equal-area sinusoidal projection to show relative areas. As a result of these criticisms, modern atlases no longer use the Mercator projection for world maps or for areas distant from the equator, preferring other cylindrical projection or forms of equal-area projection. The Mercator projection is still commonly used for areas near the equator, however, where distortion is minimal.

2.12.5 Arakawa Staggered C-grids

The Arakawa grid system depicts different ways to represent and compute orthogonal physical quantities on rectangular grids used for Earth system models for meteorology and oceanography. For example, the Weather Research and Forecasting Model use the Arakawa Staggered C-Grid in its atmospheric calculations when using the ARW core. The staggered Arakawa C-grid further separates evaluation of vector quantities compared to the Arakawa B-grid e.g., instead of evaluating both east-west (u) and north-south (v) velocity components at the grid center, one might evaluate the u components at the centers of the left and right grid faces, and the v components at the centers of the upper and lower grid faces (Arakawa and Lamb, 1977).

Chapter III

Methodology

3.1 Methodology of Stability Index

3.1.1 Cross Total Index (CT)

This is the 500-hPa Dry-bulb temperature subtracted from the 850-hPa dew point (T_d) temperature (<http://www.skystef.be/>).

CT	< 18	Weak potential for thunderstorms.
CT	18 to 19	Moderate potential for thunderstorms.
CT	20 to 21	Strong potential for thunderstorms.
CT	22 to 23	Weak potential for severe thunderstorms.
CT	24 to 25	Moderate potential for severe thunderstorms.
CT	> 25	Strong potential for severe thunderstorms.

The Mathematical expression: $CT = T_{d850} - T_{500}$

3.1.2 Vertical total Index (VT)

The VT represents static stability or the lapse rate between 850 and 500 hPa. This is defined as the 500-hPa dry-bulb temperature subtracted from the 850-hPa dry-bulb temperature (<http://www.skystef.be/>). That is

$$VT = T_{850} - T_{500}$$

VT \Rightarrow 26 Favorable for the occurrence of a thunderstorm.

VT > 28 Strong potential for thunderstorms.

3.1.3 Total Totals Index (TT)

Total Totals Index is a measure of thunderstorm potential. If low-level moisture extends through the 850 hPa level generally its value is higher. The TT is a combination of the Vertical Totals (VT) and Cross Totals (CT). The VT is the temperature difference between 850 and 500 hPa while the CT is 850 hPa dew point temperatures minus the 500 hPa temperatures (<http://www.theweatherprediction.com/habyhints/302>).

$$\begin{aligned} TT &= CT + VT \\ &= T_{d850} - T_{500} + T_{850} - T_{500} \\ &= (T_{850} + T_{d850}) - 2T_{500} \end{aligned}$$

TT	<44	Convection not likely.
TT	44 to 50	Likely thunderstorms.
TT	51 to 52	Isolated severe storms.
TT	53 to 56	Widely scattered severe.
TT	>56	Scattered severe storms.

3.1.4 K-Index (KI)

K-Index is a measure of thunderstorm potential based on the vertical temperature lapse rate, and the amount and vertical extent of low-level moisture in the atmosphere (<http://www.skystef.be/calculator-k-index.htm>).

The K-Index can be computed by

$$\text{K-Index} = (T_{850} - T_{d850}) - (T_{d700} + T_{500})$$

Where T_{850} = Temperature at 850 hPa in °C

T_{d850} = Dew-point temperature at 850 hPa in °C

T_{d700} = Dew-point temperature at 700 hPa in °C

T_{500} = Temperature at 500 hPa in °C

KI	0 to 18	Stable. No Thunderstorms
KI	19 to 20	Marginally unstable. Thunderstorms Unlikely.
KI	21 to 25	Moderately unstable. Isolated Thunderstorms.
KI	26 to 30	Widely Scattered Thunderstorms
KI	31 to 35	Numerous Thunderstorms
KI	36 to 40	Very Unstable. Thunderstorms Very Likely
KI	>40	Extremely Unstable. 100% Chance of Thunderstorms

3.1.5 Convective Available Potential Energy (CAPE)

Convective Available Potential Energy (CAPE) is a measure of the instability of the atmosphere and defines the vertically integrated positive buoyancy of a rising parcel. It is the amount of energy a parcel of air would have if lifted a certain distance vertically through the atmosphere. In the real world, CAPE is usually an overestimate of updraft strength due to water loading and entrainment of unsaturated environmental air. It is an indicator of atmospheric instability and is related to updraft strength in thunderstorms.

CAPE for different stability regimes are given as follows (<http://wind.mit.edu/~btangy/Home/convection.htm>):

CAPE < 1000 J/Kg	:	Instability is weak
CAPE > 1000 < 2500 J/Kg	:	Moderately unstable
CAPE > 2500 J/Kg	:	Extremely unstable

3.1.6 Convective Inhibition (CIN)

Convective Inhibition (CIN) is a measure of the stability of the atmosphere and defines the vertically integrated negative buoyancy of a rising parcel. It is a good indicator of general stability, and convection tends to be less vigorous with higher values. (<http://wind.mit.edu/~btangy/Home/convection.htm>)

CIN	< 100	Potential Instability.
CIN	100 to 200	Marginally stable.
CIN	200 to 300	Moderately stable.
CIN	>400	Very stable.

3.2 Model Setup

In the present study the Weather Research and Forecast (WRF-ARW Version 3.5.1) model have been used to simulate Nor'wester/Tornado over Bangladesh. Advance Research WRF (ARW) is a dynamic solver which is compatible with WRF system to simulate broad spectrum of meteorological phenomena. Weather Research and Forecast model consists of fully compressible non-hydrostatic equations and different prognostic variables. The model vertical coordinate is terrain following hydrostatic pressure and the horizontal grid is Arakawa C-grid staggering. The model has different microphysics options. In this research six microphysics e. g. Kessler, Lin, WSM6, Thompson, Stony Brook University (SBU) and WDM6 have been used. The model has integrated by using initial and lateral boundary conditions (LBCs) from NCEP-FNL analysis at six hourly intervals. Surface layer is using Monin-Obukhov and planetary boundary layer (PBL) is treated with Yonsei University scheme. Dudhia (1989) scheme has been used for short wave radiation and Rapid Radiative Transfer Model (RRTM) for long wave (Mlawer *et al.* 1997). Kain-Fritsch (KF) (1993) and Bets-Millar-Janjic (BMJ) cumulus parameterization (CP) schemes have been used for simulating Nor'wester/Tornado.

3.3 Model Domain and Configuration

The model has been configured in single domain, 3 km horizontal grid spacing with 173×225 grids in the east-west and north-south directions and 28 vertical levels. Time step of integration is set to 15 seconds for maintaining computational stability as the model uses third-order Runge-Kutta time integration scheme. The model has been run for 24 hours from 0000 UTC of 27 April to 0000 UTC 28 April 2014, 0000 UTC of 15 May to 0000 UTC 16 May 2014, 0000 UTC 07 April to 0000 UTC of 08 April 2012 and 0000 UTC of 28 April to 0000 UTC of 29 April 2012. The detail of the model and domain configuration is given in Table I and the model domain is given in Fig. 3.1.



Fig. 3.1: WRF Model Domain for simulating Nor'wester/Tornado in Bangladesh

Table 1: Observed and studied Squall line/Nor'wester in Bangladesh

Date	Station	Time (UTC)	Speed km/h	Status
07-04-2012	Dhaka (Gusty Wind)	0400	41	light nor'westers
	Chittagong (Squall)	0740	102	Severe nor'westers
28-04-2012	Khulna (Squall)	0325	65	Moderate nor'westers
	Chittagong (Gusty Wind)	0640	72	Moderate nor'westers
	Chittagong (Gusty Wind)	0647	78	Moderate nor'westers
	Chittagong (Gusty Wind)	0702	69	Moderate nor'westers
27-04-2014	Sylhet (Squall)	1848-1851	83	Moderate nor'westers
	Srimangal (Squall)	1803-1825	83	Moderate nor'westers
15-05-2014	Barisal (Squall)	0935	120	Severe nor'westers
	Chittagong (Squall)	1203	42	light nor'westers

Table 2: WRF Model and Domain Configurations

Dynamics	Non-hydrostatic
Number of domain	1
Central points of the domain	Central Lat.: 23.7°N, Central Lon.: 90.55°E
Horizontal grid distance	3 km
Integration time step	15 s
Number of grid points	X-direction 173 points, Y-direction 225 points
Map projection	Mercator
Horizontal grid distribution	Arakawa C-grid
Nesting	One way
Vertical co-ordinate	Terrain-following hydrostatic-pressure co-ordinate (30 sigma levels up to 100 hPa)
Time integration	3 rd order Runge-Kutta
Spatial differencing scheme	6 th order centered differencing
Initial conditions	Three-dimensional real-data (FNL: 1° × 1°)
Lateral boundary condition	Specified options for real-data
Top boundary condition	Gravity wave absorbing (diffusion or Rayleigh damping)
Bottom boundary condition	Physical or free-slip
Diffusion and Damping	Simple Diffusion
Microphysics	i. Kessler ii. Lin <i>et al.</i> iii. WSM 6-class graupel iv. Thompson v. Stony Brook University (SBU) vi. WDM6
Radiation scheme	Dudhia (1989) for short wave radiation/ RRTM long wave Mlawer <i>et al.</i> (1997)
Surface layer	Monin-Obukhov similarity theory Scheme (Hong and Pan, 1996)
Land surface parameterization	5 Layer Thermal diffusion Scheme (Ek <i>et al.</i> , 2003)
Cumulus parameterization schemes	i. Kain-Fritsch (KF) scheme (Kain and Fritsch, 1990, 1993; Kain, 2004) ii. Betts-Millar-Janjic (BMJ) scheme
PBL parameterization	Yonsei University Scheme (YSU) (Hong <i>et al.</i> , 2006)

3.4 Data and Methodology

Final Reanalysis (FNL) data (1° x1°) from National Centre for Environment Prediction (NCEP), USA will be used as initial and lateral boundary conditions (LBCs) which is updated at six hourly interval i.e. the model will be initialized with 0000, 0600, 1200 and

1800 UTC initial field of corresponding date. The NCEP FNL data will be interpolated to the model horizontal and vertical grids. There are many MP and CP schemes in WRF-ARW Model.

In this research we have used six different MP (e.g. Kessler, Lin *et al.*, WSM6-class graupel scheme, Thompson graupel, SBU and WDM6,) schemes in combination with two different CP (Kain-Fritsch and Betts-Miller-Janjic) schemes. The Tornado/Nor'wester occurred within short period of time. The time span has not more than one hour for the formation to dissipation of the system. For the study of these short period events it has to simulate/analyze data within the occurring time of the events. To study the short period events WRF outputs have to generate every 5 minutes. WRF output file will be converted to data file using ARW post software. By using Grads software the different meteorological parameters, stability indices and energies have to produce, which are related to Tornado/Nor'wester. The study of different meteorological parameters of this research is wind speed at 10m levels, temperature at 2m levels, relative humidity at 2m levels and sea level pressure. The different energies and instability indices are maximum Convective Available Potential Energy (MCAPE), maximum Convective Inhibition (MCIN), Level of Free convection (LFC), Lifted Condensation Level (LCL), Latent Heat (LH) flux, Cross Total Index (CT), Vertical Total Index (VT), Total Totals Index (TT) and K-Index (KI) have been calculated at the stations where squall/nor'wester/Tornado occurs. We have also calculated maximum vertical velocity from the model output, which indicates the maximum convection. Along the line of maximum vertical velocity hydrometeors, relative humidity and vorticity have also been calculated.

Txt format data from control (ctl) file of WRF model output has been found using Grid Analysis and Display System (GrADS). These txt data have been converted into Microsoft Excel format and then plotted.

CHAPTER IV

RESULTS AND DISCUSSION

In this research we have been studied four nor'westers/squall line those formed in the different regions of Bangladesh. The studied nor'wester/squall lines are 7 April 2012, 28 April 2012, 27 April 2014 and 15 May 2014. The different meteorological parameters, energies and instability indices of the above mentioned events have been analysed and presented in the following section. The parameters are wind speed at 10m level, temperature at 2m level, relative humidity at 2m level and sea level pressure (SLP), maximum Convective Available Potential Energy (CAPE), maximum Convective Inhibition (CIN), Level of Free convection (LFC), Lifted Condensation Level (LCL), Latent Heat (LH) flux, Cross Total Index (CT), Vertical Total Index (VT), Total Totals Index (TT) and K-Index (KI) have been calculated at the stations where squall/nor'wester occurs. We have also analysed and presented the maximum vertical velocity and cloud water mixing ratio, rain water mixing ratio, relative humidity and vorticity along the line of maximum vertical velocity in the following section.

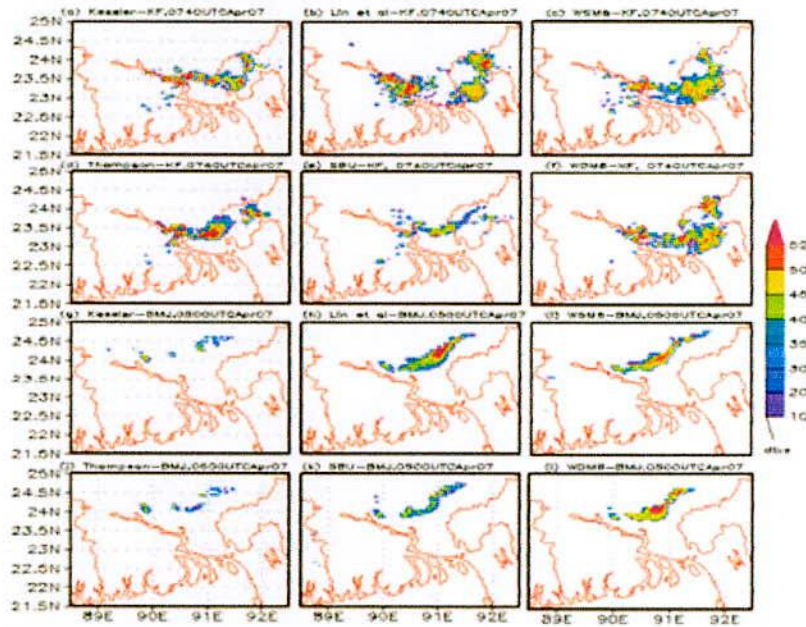
4.1 Nor'wester of 07 April 2012

The squall line/gusty wind are observed at Dhaka (23.76N and 90.38E) and Chittagong (22.26 N and 91.81 E) on 07 April 2012. The observed time of gusty wind at Dhaka was 0400 UTC and the nor'wester moved from the westerly direction with the maximum sustained wind speed 11.4 m/s. On that day, the squall was also observed at Chittagong at 0740 UTC and was found to moved from the northwesterly direction with the maximum sustained wind speed 28.3 m/s. Six different microphysics schemes are considered e.g. Kessler, Lin *et al.*, WSM6, Thomson, SBU and WDM6 and KF and BMJ cumulus parameterization schemes for the simulation of squall/nor'wester over Dhaka and Chittagong on 07 April 2012. All six different MPs in combination with KF scheme has simulated squall at 0740 UTC and BMJ scheme at 0500 UTC over Bangladesh as shown in Figs. 4.1.1(a-l). The model simulated time and position of the squall is different than observed.

4.1.1 Sea Level Pressure (SLP)

Model simulated time variations of SLP for six different microphysics (MP) e.g. Kessler, Lin, WSM6, Thomson, SBU, WDM6 coupling with KF and BMJ schemes at Chittagong are

presented in Figs. 4.1.2(a-b). Starting from 0600 UTC, the SLP has sharply decreased (Fig. 4.1.2a) for all MPs coupling with KF scheme up to around 0900 UTC.



Figs. 4.1.1: Model simulated squall line for different MP schemes coupling with (a-f) KF and (g-l) BMJ schemes on 7 April 2012.

The minimum values of SLP are 1008.89, 1009.31, 1009.74, 1008.53 and 1008.31 hPa found at 0920, 0840, 0830, 0910 and 0940 UTC for Kessler, Lin *et al.*, WSM6, Thompson and SBU in combination with KF schemes. After that the SLP fluctuates continuously before 1900 UTC and then again decreased for all MPs. From Fig. 4.1.2b, it is found that the SLP is decreased continuously from 0200 UTC to 1300 UTC and after that it has increased for all MPs in combination with BMJ cumulus parameterization. The decreasing tendency for all MPs in combination with BMJ is similar in nature up to the simulation time. The time of occurrence of squall at Chittagong was 0740 UTC, and WSM6-KF and Lin-KF combination have simulated minimum SLP at 0830 and 0840 UTC, which are close to the observed times. The minimum SLP simulated for other combinations are much more delayed than that of observed.

Figs. 4.1.2(c-d) depict model simulated SLP at Dhaka. From Fig. 4.1.2c, it is found that SLP continuously fluctuates for all MPs and first minimum 1009.98 hPa is found at 0440 UTC and 2nd minimum SLP of 1008.5 hPa at 0910 UTC by Lin *et al.* in combination with KF. The

minimum SLP values of 1006.9, 1007.4, 1007.6 and 1008.4 hPa are found for SBU-KF, TH-KF, WSM6-KF and WDM6-KF combination at 0930, 1010, 1000 and 0950 UTC respectively. After that SLP is found oscillatory and increased sharply for Kessler, Lin et al. WSM6, WDM6 coupling with KF scheme. From Fig. 4.1.2d, the minimum SLP of 1009.63 and 1009.37 hPa are simulated for Lin *et al.* and WDM6 coupling with BMJ scheme at 0420 UTC, which are close to the observed time (0400 UTC) of occurrence of gusty wind at Dhaka.

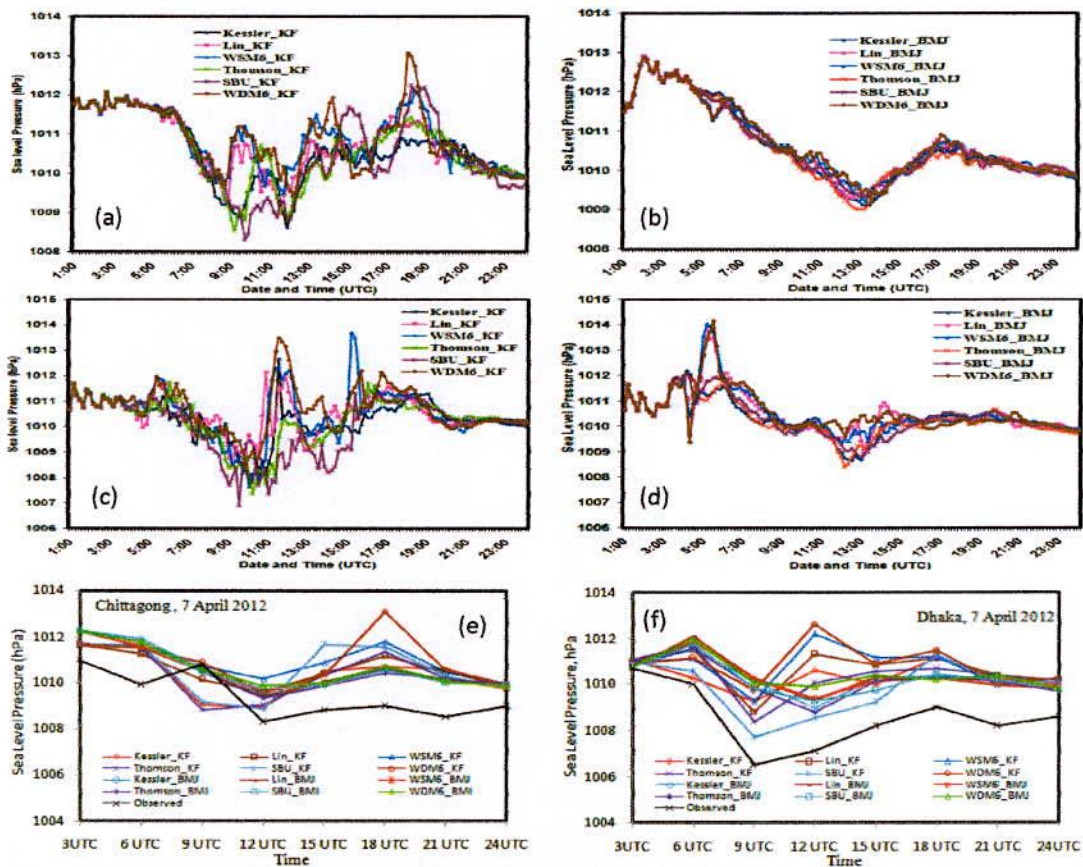


Fig. 4.1.2: Time variation (5 minute interval) of SLP at (a-b) Chittagong and (c-d) Dhaka and comparison of observed and model simulated 3-hourly SLP at (e-f) Chittagong and Dhaka using six different MP schemes coupling with KF and BMJ schemes respectively on 7 April 2012.

Comparison of observed and model simulated 3-hourly SLP at Chittagong and Dhaka using six different MP schemes coupling with KF and BMJ schemes are presented in Figs. 4.1.2(e-f) respectively. From Fig. 4.1.2e, it is found from the observation that the SLP increased from 0600 to 0900 UTC and after that it has decreased at 1200 UTC but KS-KF, TH-KF and SBU-

KF has simulated minimum at 0900 UTC and all other combinations have simulated minimum at 1200 UTC. The minimum SLP is found at 0900 UTC from observation and all combination of MPs and CPs at Dhaka.

4.1.2 Maximum Wind Speed (MWS) at 10 m Level

Time variations of maximum wind speed (m/s) at 10m level simulated by six different MP schemes coupling with KF and BMJ schemes at Chittagong are presented in Figs. 4.1.3(a-b). The model simulated MWS at 10m level by all MPs coupling with KF scheme after 0900 UTC (Fig. 4.1.3a) at Chittagong.

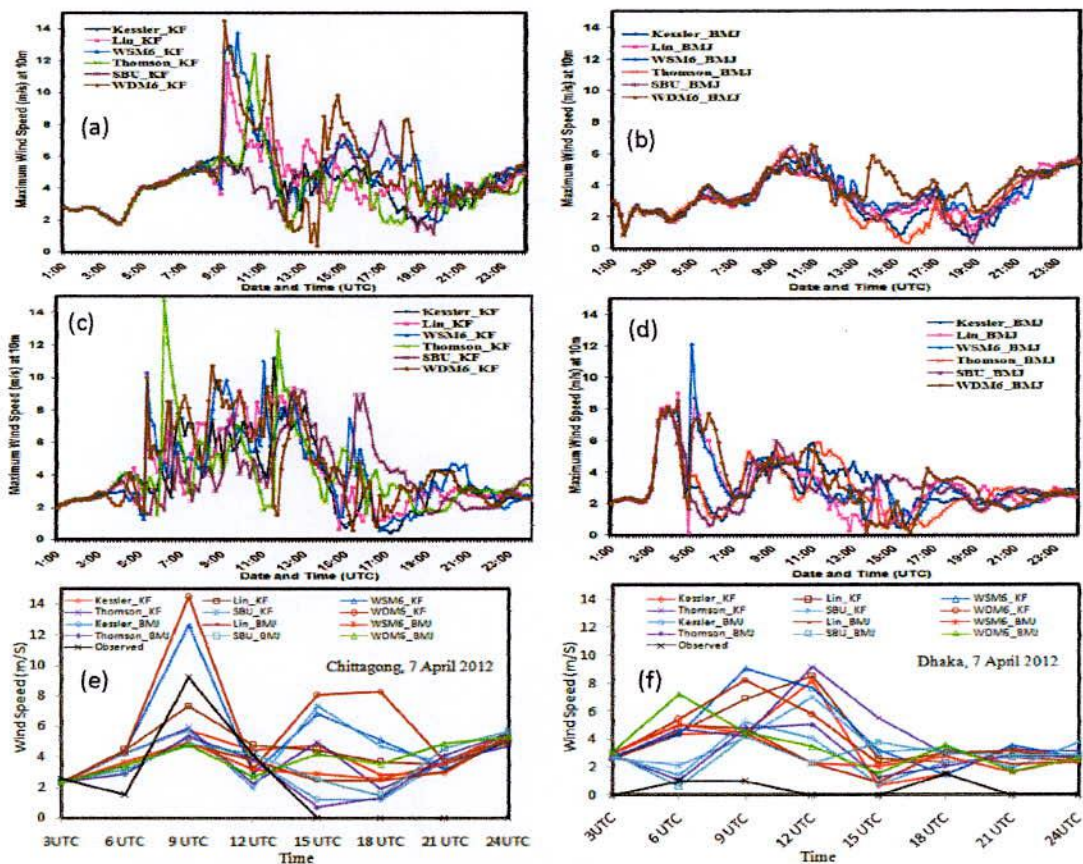


Fig. 4.1.3: Time variation (5 minute interval) of MWS at 10m level at (a-b) Chittagong and (c-d) Dhaka and comparison of observed and model simulated 3-hourly MWS at (e-f) Chittagong and Dhaka using six different MP schemes coupling with KF and BMJ schemes respectively on 7 April 2012.

The simulated first maxima of MWS of 14.5, 12.6, 12.4 and 11.8 m/s are found at 0900, 0900, 1030 and 0910 UTC for WDM6, WSM6, Thompson and Lin *et al.* schemes coupling

with KF scheme. Different MPs schemes coupling with BMJ scheme (Fig. 4.1.3b) have simulated very little wind speed at Chittagong on that day. The observed wind found at Chittagong was 28.3 m/s.

Figs. 4.1.3(c-d) depict model simulated maximum wind speed (m/s) at 10m level at Dhaka. From Fig. 4.1.3c, the maximum wind speeds of 10, 10.3 and 10.3 m/s are found for WDM6, Lin *et al.* and WSM6 coupling with KF scheme at 0520 UTC. The maximum wind speed of 14.8 m/s is also found at 0610 UTC for Thompson-KF combination. From Fig. 4.1.3d, the first maxima of wind speeds at 10m level are found to be 9.00 and 8.5 m/s for Lin *et al.* and WDM6 coupling with BMJ scheme at 0420 UTC, which is close to the observed time at Dhaka. The MWS equal to 12.1 m/s is also found at 0500 UTC for WSM6-BMJ combination. The maximum observed wind speed at Dhaka was 11.4 m/s at 0400 UTC. The MWS almost close to the observed wind speed for WDM6-KF, Lin-KF, WSM6-KF and WDM6-BMJ but the simulated time is ahead almost by 1 hour.

Comparison of observed and model simulated 3-hourly MWS at 10m level at Chittagong and Dhaka using six different MP schemes coupling with KF and BMJ schemes are presented in Figs. 4.1.3(e-f) respectively. The simulated 3-hourly MWS 12.6 and 14.5 m/s at 0900 UTC for WSM6-KF and WDM6-KF combinations at Chittagong (Fig. 4.1.3e) matched with the observed maximum winds 9.2 m/s at 0900 UTC. The Observed wind is very low at Dhaka (Fig. 4.1.3f) but model simulated wind is high for WDM6-BMJ at 0600 UTC, WSM6-KF & WDM6-KF at 0900 UTC and TH-KF & Lin-KF at 1200 UTC.

The model simulated maximum wind speeds at 10m level are 28.8, 30.7, 29.5, 31.6, 24.8 and 31.9 m/s at 0610, 0630, 0750, 0630, 1030 and 0550 UTC at (24.11°N & 90.83°E), (23.98°N & 90.71°E), (23.2°N & 90.57°E), (23.66°N & 90.66°E), (22.68°N & 90.33°E) and (23.96°N & 90.95°E) respectively using Kessler, Lin, WSM6, Thompson, SBU and WDM6 coupling with KF scheme and 24.6, 24.5, 17.9, 26.7, 12.7 and 29.6 m/s at 1250, 0500, 0920, 1230, 0510 and 0450 UTC (23.35°N & 89.83°E), (24.14°N & 90.97°E), (22.50°N & 89.8°E), (23.3°N & 89.91°E), (24.2°N & 89.8°E) and (24.04°N & 90.74°E) respectively using Kessler, Lin, WSM6, Thompson, SBU, WDM6 coupling with BMJ scheme. The simulated wind speeds for different MP schemes in combination with KF scheme are almost similar to that of observed wind speed at Chittagong but time and location is different.

4.1.3 Temperature at 2m Level

Figs. 4.1.4 (a-b) represent the time variation of temperature ($^{\circ}\text{C}$) at 2m Level at Chittagong simulated by six different MPs in combination with KF and BMJ schemes. The temperature has increased sharply (Fig. 4.1.4a) for all MPs up to 0900 UTC and after that it has decreased significantly at 0910 UTC for Lin-KF, at 0910 UTC for WSM6-KF and at 0950 UTC for WDM6-KF. After that the temperature is fluctuating continuously for all MPs coupling with KF scheme. The temperature at 2m level has increased continuously up to 1230 UTC and after that it has decreased linearly for all MPs in combination with BMJ scheme (Fig. 4.1.4b).

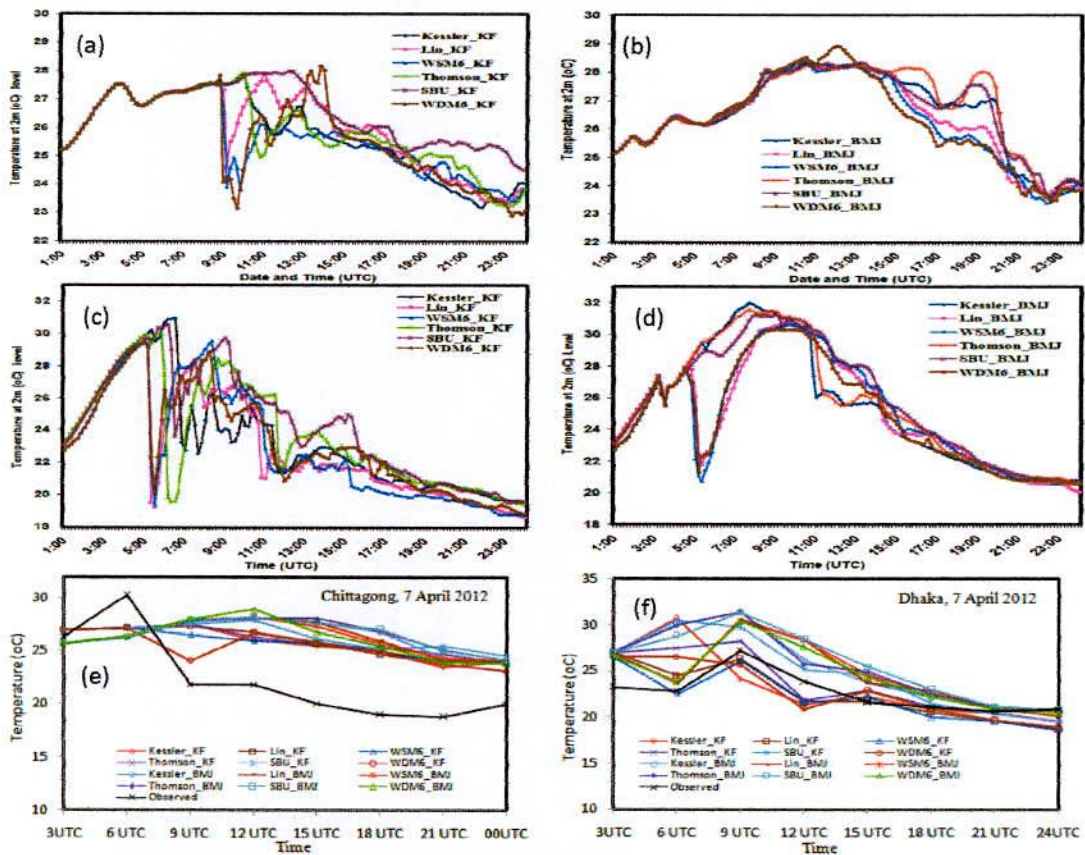


Fig. 4.1.4: Time variation (5 minute interval) of temperature at 2m level at (a-b) Chittagong and (c-d) Dhaka and comparison of observed and model simulated 3-hourly temperature at (e-f) Chittagong and Dhaka using six different MP schemes coupling with KF and BMJ schemes respectively on 7 April 2012.

No significant change is observed for BMJ combination all through the day. But significant changes have found for Lin-KF, WSM6-KF and WDM6-KF after 0900 UTC. Due to this sharp decrease of temperature after 0900 UTC, it can be said that there is something occurring at Chittagong at that time.

WRF model simulated 2m level temperature ($^{\circ}\text{C}$) at Dhaka has been described in Figs. 4.1.4(c-d). From Fig. 4.1.4c, the maximum temperatures simulated are 29.2, 29.3 and 29.1 $^{\circ}\text{C}$ by Lin-KF, WSM6-KF and WDM6-KF combination at 0510 UTC. After that the temperatures have sharply decreased to 19.2, 19.4 and 20.1 $^{\circ}\text{C}$ for these combinations at 0530 UTC. Almost 10 $^{\circ}\text{C}$ has fallen within short period (20 minutes) of time. The gusty wind is observed over Dhaka during the rapid change of temperature within short period of time by different combination of MPs. This may be due to the strong downdraft of cold air with hails from the upper air during the storm. From Fig. 4.1.4d, it is found that the temperature has decreased significantly after 0440 UTC from 27.87 to 21.3 $^{\circ}\text{C}$ for WDM6-BMJ, from 28.25 to 21.8 $^{\circ}\text{C}$ for Lin-BMJ and from 27.24 to 20.7 $^{\circ}\text{C}$ for WSM6-BMJ combinations. The rapid change of temperature is also observed for Lin, WSM6 and WDM6 in combination with KF and BMJ schemes.

Comparison of observed and model simulated 3-hourly temperature at 2m level at Chittagong and Dhaka using six different MP schemes coupling with KF and BMJ schemes are presented in Figs. 4.1.4(e-f). The 3-hourly observed maximum temperature is found 28.92 $^{\circ}\text{C}$ (Fig. 4.1.4e) at 0600 UTC but model simulated maximum temperature has found at 1200 UTC for WDM6-BMJ at Chittagong. The 3-hourly observed maximum temperature is 27.2 $^{\circ}\text{C}$ at 0900 UTC (Fig. 4.1.4f) but KS-KF and SBU-KF has simulated maximum temperature at 0600 UTC and all other combinations have simulated at 0900 UTC.

4.1.4 Vertical Velocity

The maximum updrafts for the heavy rainfall event on 7 April 2012 using different MPs coupling with KF and BMJ schemes is simulated and are presented in Figs. 4.1.5(a-l). The times and positions of maximum updrafts simulated are different in different combination of MPs and CP schemes (Figs. 4.1.5). The maximum updrafts are 37, 53, 48, 42, 50 and 46 m s^{-1} as simulated by Kessler, Lin *et al.*, WSM6, Thomson, SBU and WDM6 schemes coupling with KF scheme at the times of 0820, 0830, 0920, 0830, 0930 and 0920 UTC (Fig. 4.1.5) on 7 April respectively. The maximum updrafts of 32, 36, 29, 34, 34 and 29 m s^{-1} are simulated by Kessler, Lin *et al.*, WSM6, Thomson, SBU and WDM6 schemes coupling with BMJ scheme at the times of 1340, 1200, 0840, 1240, 0810 and 0420 UTC respectively.

The maximum updraft is simulated at around 500–200 hPa by KS-KF, Lin-KF, WSM6-KF, Thompson-KF, SBU-KF and WDM6-KF combinations on 7 April 2012. The maximum

updraft is also simulated by KS-BMJ, Lin-BMJ, TH-BMJ and SBU-BMJ combination at around 500-300 hPa on 7 April 2012. The updraft is simulated much less by WSM6-BMJ and WDM6-BMJ combinations. The downdraft is generally weaker but has been seen throughout the depth of the troposphere and updraft in the middle and upper troposphere. The low-level descent and high-level ascent is expected from a mature convective system and is consistent with earlier studies. The descent in the lower troposphere could be due to evaporation and precipitation loading (Srivastava, 1985). The updraft in the upper troposphere could be due to the latent heat release during glaciations and vapor deposition.

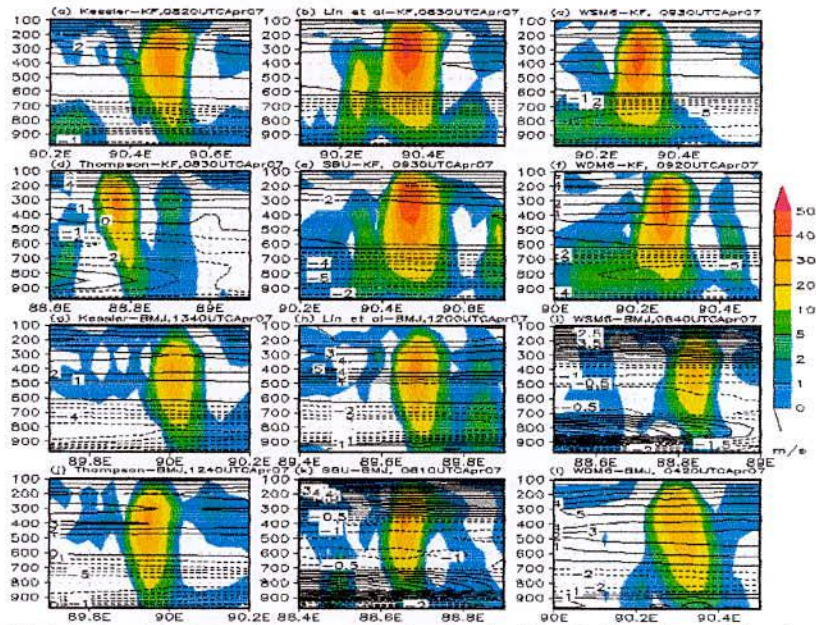


Fig. 4.1.5: Model simulated maximum vertical velocity (shaded) and vorticity (contour, $\times 10^{-5}$ /s) using Kessler, Lin *et al.*, WSM6, Thomson, SBU and WDM6 schemes coupling with (a-f) KF and (g-l) BMJ schemes on 7 April 2012.

4.1.5 Vorticity

Along the lines of maximum updraft, vorticity (contour, $\times 10^{-5}$ /s) have been simulated by different MP schemes coupling with KF and BMJ schemes on 07 April 2012 and are presented as in Figs. 4.1.5(a-l). All MPs in combination with KF and BMJ schemes are found to simulate positive vorticity from 500-100 hPa except WSM6-BMJ and SBU-BMJ combinations along the line of maximum vertical velocity. Below these levels all combinations have simulated negative vorticity, which indicates that the lower level has anticyclonic circulation and upper atmosphere has cyclonic circulation.

4.1.6 Relative Humidity (RH)

The model simulated time variation of RH at 2m level for six different MPs in combination with KF and BMJ schemes at Chittagong and are shown in Figs. 4.1.6(a-b). The RH is found maximum in the morning and first minimum is simulated at 0350 UTC for all MPs coupling with KF and BMJ schemes. After that it has increased again up to 0450 UTC and then decreased. The irregularity of RH has simulated after 0840 UTC for different MPs coupling with KF and BMJ schemes. The RH is higher for Kessler-KF, Thompson-KF and SBU-KF combination (Fig. 4.1.6a) after 0840 UTC, WDM6-KF at 0930, WSM6-KF at 0940 and Lin-KF at 1110 UTC respectively. Again, the model has simulated irregular pattern of RH for all MPs in combination with KF scheme. The RH has increased for Kessler-BMJ, Thompson-BMJ and SBU-BMJ at 0820, 0810 and 0810 UTC respectively and after that it has shown irregular patterns (Fig. 4.1.6b) for all MPs coupling with BMJ scheme at Chittagong station.

Figs. 4.1.6(c-d) depict model simulated RH at 2m level at Dhaka. The RH has decreased sharply up to 0510 UTC (Fig. 4.1.6c) for all MPs coupling with KF scheme. Then it has increased sharply for Lin-KF, WSM6-KF and WDM6-KF combination at 0520 UTC and it continues up to 0540 UTC. It has decreased further significantly and minimum RH has sustained up to 1000 UTC and then found to increase in an oscillatory nature. After decreasing continuously the RH has increased significantly for TH-KF and KS-KF combinations at 0610 and 0650 UTC respectively. The RH has decreased sharply (Fig. 4.1.6d) up to 0450 UTC for all MPs coupling with KF scheme, after that it has increased significantly for Lin-BMJ, WSM6-BMJ and WDM6-BMJ at 0510, 0500 and 0510 UTC respectively. Due to this sharp increase of RH after 0500 UTC was favorable for the formation of nor'wester. The RH has increased at 0820, 0810 and 0810 UTC for Kessler-BMJ, Thompson-BMJ and SBU-BMJ combinations respectively, which is closer to the observed time of squall at Chittagong. The simulated RH is maximum at 0520 UTC for Lin-KF, WSM6-KF and WDM6-KF combinations and at 0510, 0500 and 0510 UTC for Lin-BMJ, WSM6-BMJ and WDM6-BMJ respectively, which is closer to the observed time of gusty wind at Dhaka.

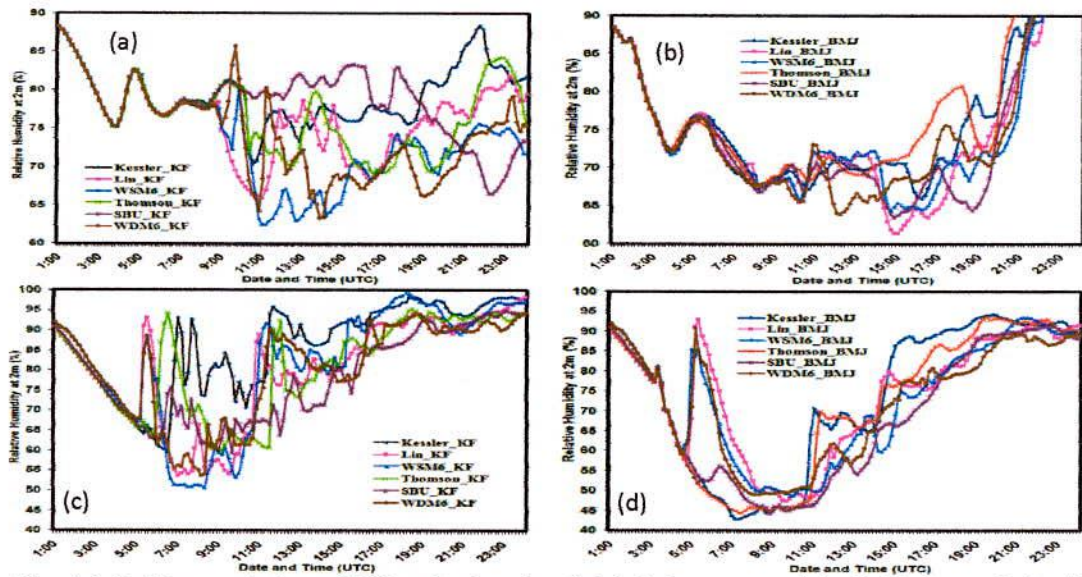


Fig. 4.1.6: Time variation of RH at 2m level at (a-b) Chittagong and (c-d) Dhaka on 7 April 2012 using six different MP schemes coupling with KF and BMJ schemes.

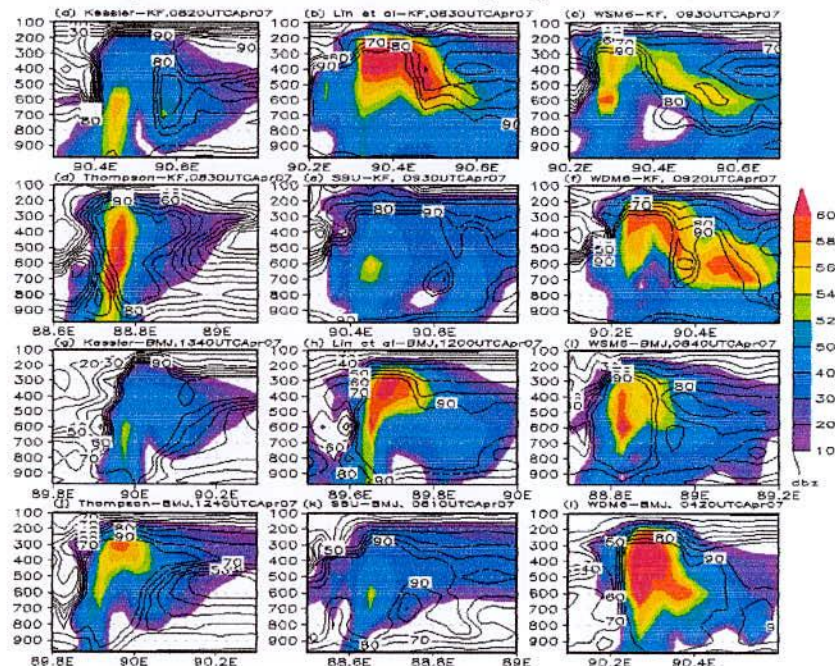


Fig. 4.1.7: WRF Model simulated reflectivity (shaded) and relative humidity (contour) along the line of maximum vertical velocity using Kessler, Lin *et al.*, WSM6, Thomson, SBU and WDM6 schemes coupling with (a-f) KF and (g-l) BMJ schemes on 7 April 2012.

The RH (contour) is simulated along the line of maximum vertical velocity using different MPs coupling with KF and BMJ schemes and is presented in Figs. 4.1.7(a-l). Kessler scheme

coupling with KF and BMJ schemes has simulated RH up to 100 hPa. All other MPs coupling with KF and BMJ schemes have simulated RH up to 200 hPa. The maximum RH > 90% is simulated for all MPs in combination with CPs up to 200 hPa level where the vertical velocity is found maximum.

4.1.7 Maximum Reflectivity (MR)

The model simulated time variation of MR (dBZ) for six different MPs coupling with KF and BMJ schemes at Chittagong is presented in Figs. 4.1.8(a-b). Starting from 0920 to 2100 UTC reflectivity has been found for all MPs coupling with KF schemes (Fig. 4.1.8a). The reflectivity is maximum and 44.32dBZ for SBU-KF at 1300 UTC, 36.41dBZ for WDM6-KF at 1400 UTC and 30.61dBZ for WSM6-KF at 1150 UTC. From Fig. 4.1.8b, reflectivity is found during 0130-0200, 0940-1230, 1440-1740 UTC, where reflectivity 14.16, 22.90 and 22.93dBZ are maximum for Lin *et al*, SBU and WDM6 schemes coupling with BMJ scheme at 0140, 1730 and 1130 UTC respectively. The reflectivity is not found significant for any combination of MP and CP schemes.

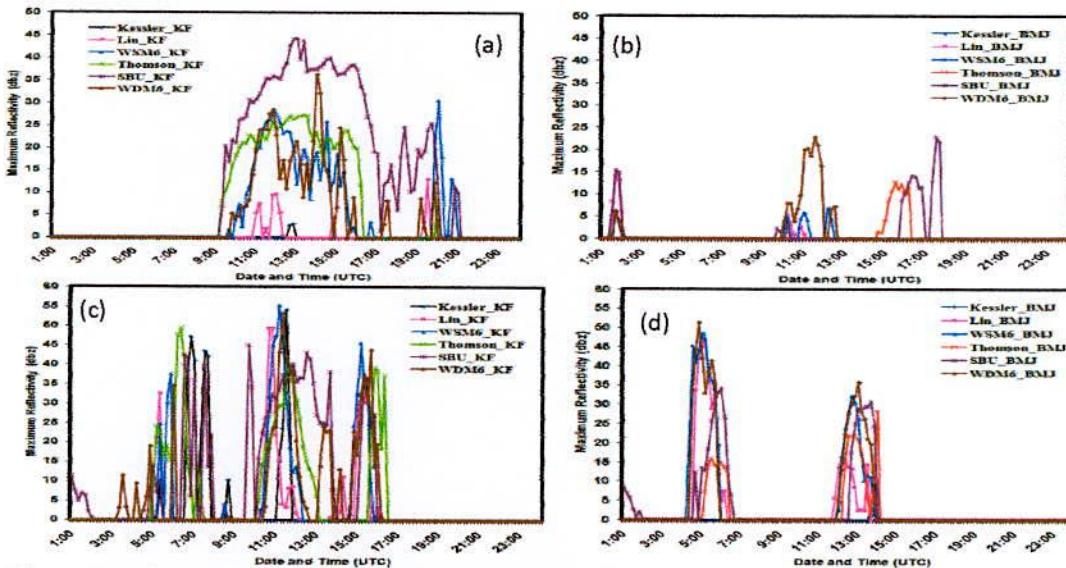


Fig. 4.1.8: Time variation of reflectivity at (a-b) Chittagong and (c-d) Dhaka on 7 April 2012 using six different MP schemes coupling with KF and BMJ schemes.

Figs. 4.1.8(c-d) depict model simulated MR at Dhaka. The significant reflectivity has been found (Fig. 4.1.8c) for all MPs coupling with KF scheme from 0500 to 1620 UTC. The maximum reflectivity of 49.4, 47.1, 42.5, 37.5, 34.6 and 32.6 dBZ are simulated before noon for TH, KS, SBU, WSM6, WDM6 and Lin schemes in combination with KF scheme at 0620,

0650, 0630, 0550, 0600 and 0520 UTC respectively. On that day the MR are also simulated to be 54.2, 49.5, 55.3, 49.4, 45 and 53.3 dBZ by KS, Lin, WSM6, TH, SBU and WDM6 schemes coupling with KF scheme at 1130, 1040, 1110, 0620 0940 and 1120 UTC respectively. Different MPs in combination with BMJ scheme are simulated reflectivity during 0420-0620 and 1200-1350 UTC (Fig. 4.1.8d). The maximum reflectivity of 51.4, 48.6 and 46.5 dBZ are found for WDM6-BMJ, WSM6-BMJ and Lin-BMJ combinations at 0450, 0500 and 0500 UTC respectively, which is close to the observed time of squall at Dhaka.

The Reflectivity (shaded, dBZ) is simulated along the line of maximum vertical velocity using different MPs coupling with KF and BMJ schemes and are presented in Figs. 4.1.7(a-l). The maximum reflectivity > 60dBZ has simulated for Lin *et al.*, WSM6, Thompson and WDM6 schemes in combination with KF and BMJ schemes where the up draught has found maximum.

4.1.8 Cross Total Index (CT)

The model simulated time variation of CT at Chittagong for six different MPs coupling with KF and BMJ schemes have been presented in Figs. 4.1.9(a-b). Up to 0220 UTC (Fig. 4.1.9a) the CT is > 23°C for all MPs coupling with KF scheme and after that it decreased up to 0710 UTC by Lin-KF, WSM6-KF and WDM6-KF combinations. The CT is found to decrease for all other MPs up to 0800 UTC. In the morning the CT greater than 23°C indicates weak potential for severe thunderstorms. Then it has increased significantly for all MPs coupling with KF schemes and maximum CTs are found 27.48, 25.33, 25.26, 25.06, 25.01 and 24.47°C at 1130, 1000, 0900, 1000, 1030 1010 UTC for SBU, WDM6, Lin *et al.*, WSM6, TH and KS schemes respectively. All MPs have simulated CT greater than 25°C, indicates strong potential for severe thunderstorms. Out of all MPs, Lin-KF, WDM6-KF and WSM6-KF combinations have simulated much earlier than all other MPs. From Fig. 4.1.9b, the maximum value of CT is greater than 24°C for all MPs coupling with BMJ schemes at 0140 UTC which indicates CT is moderate potential for severe thunderstorms in the morning at Chittagong. After that, it has decreased significantly up to 0730 UTC, when CT is less than 18°C for all MPs coupling with BMJ scheme. After 0730 UTC again it has been increased and 2nd maxima (< 24°C) are simulated at 0930 UTC or later for all MPs coupling with BMJ scheme. But this maximum is weak potential for severe thunderstorms at Chittagong.

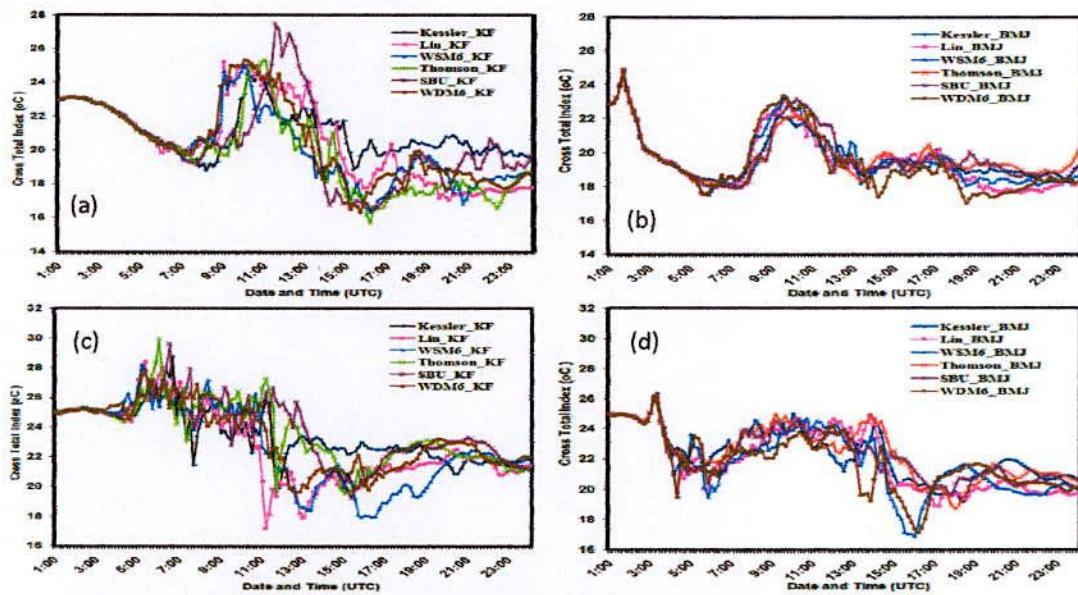


Fig. 4.1.9: Time variation of CT at (a-b) Chittagong and (c-d) Dhaka on 7 April 2012 using six different MP schemes coupling with KF and BMJ schemes.

Figs. 4.1.9(c-d) depict model simulated CT at Dhaka. The CT is found $>25^{\circ}\text{C}$ for all MPs coupling with KF schemes except SBU-KF combination from 0130 to 0310 UTC (Fig. 4.1.9c), which indicates strong potential for severe thunderstorms and then it has decreased ($<24^{\circ}\text{C}$) up to 0420 UTC by KS-KF, Lin-KF, TH-KF, and SBU-KF combinations, which indicates weak potential for severe thunderstorms. Then, up to 0700 UTC, it has increased ($>29^{\circ}\text{C}$) significantly for TH-KF and SBU-KF combinations and then fluctuates continuously for all MPs coupling with KF schemes. Up to 0250 UTC (Fig. 4.1.9d), the simulated CT is $>24^{\circ}\text{C}$ for all MPs coupling with BMJ scheme, which indicates moderate potential for the occurrence of severe thunderstorms in the morning at Dhaka. After that it has increased during short period for all MPs coupling with BMJ scheme and the maximum value of CT is $>26^{\circ}\text{C}$ for all MPs coupling with BMJ scheme at 0310 UTC, which indicates strong potential for the occurrence of severe thunderstorms. It has decreased to $22 - 23^{\circ}\text{C}$ up to 0400 UTC for all MPs coupling with BMJ scheme and then increased and fluctuates continuously for all MPs coupling with BMJ scheme.

4.1.9 Vertical Totals Index (VT)

The model simulated time variation of VT for six different MPs coupling with KF and BMJ schemes at Chittagong are presented in Figs. 4.1.10(a-b). The VT has increased continuously (Fig. 4.1.10a) and reached $> 30^{\circ}\text{C}$ at around 0850 UTC for all MPs coupling with KF

schemes and after that it has decreased sharply by Lin-KF, WSM6-KF and WDM6-KF combinations. The $VT > 28^{\circ}\text{C}$ indicates strong potential for the occurrence of severe thunderstorms. After that it has started to increase in an oscillatory nature.

In the morning, VT has decreased sharply and then increased from 0150 to 0700 UTC (Fig. 4.1.10b) for all MPs coupling with BMJ scheme. From 0240 to 0810 UTC the $VT > 28^{\circ}\text{C}$ indicates strong potential for the occurrence of severe thunderstorms. Figs. 4.1.10(c-d) depict the model simulated VT at Dhaka. Up to 0350 UTC (Fig. 4.1.10c), the VT is $> 31^{\circ}\text{C}$ for all MPs coupling with KF scheme and then it has decreased slowly and fluctuates for all MPs coupling with KF scheme at around 0630 UTC. From 0100 to 0500 UTC, VT is $> 28^{\circ}\text{C}$ for all MPs coupling with KF scheme indicates strong potential of VT for the occurrence of severe thunderstorms at Dhaka. Up to 0310 UTC (Fig. 4.1.10d) the $VT > 28^{\circ}\text{C}$ for all MPs coupling with BMJ scheme indicates strong potential for the occurrence of severe thunderstorms and then significantly decreased for all MPs coupling with BMJ scheme at 0320 UTC. After 0410 UTC it has again increased for all MPs coupling with BMJ scheme and the value is found $> 26^{\circ}\text{C}$, which is favorable for the occurrence of thunderstorm.

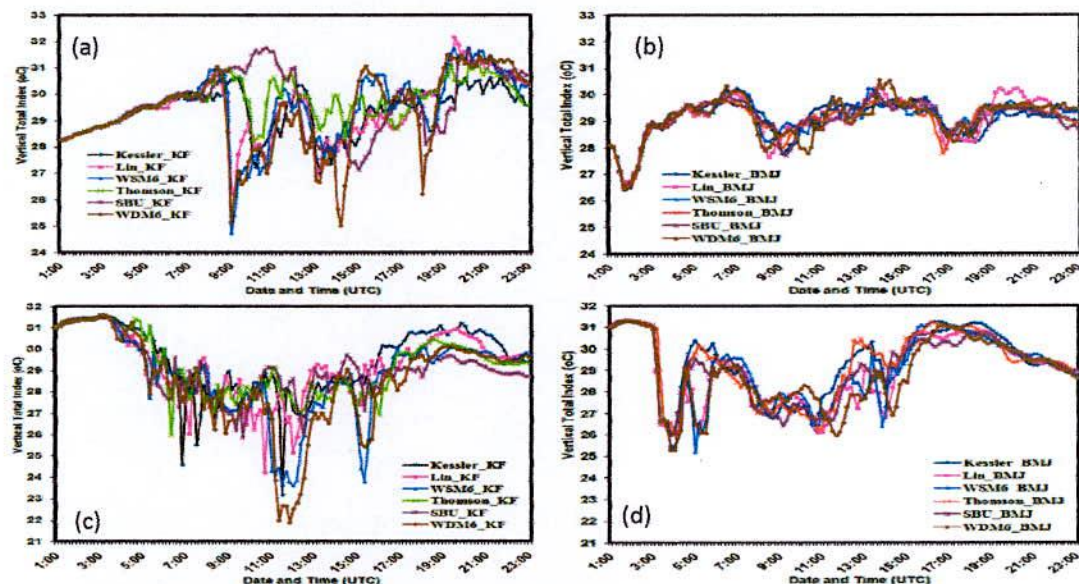


Fig. 4.1.10: Time variation of VT at (a-b) Chittagong and (c-d) Dhaka on 7 April 2012 using six different MP schemes coupling with KF and BMJ schemes.

4.1.10 Total Totals Index (TT)

The model simulated time variations of TT Index for six different MPs coupling with KF and BMJ schemes at Chittagong are shown in Figs. 4.1.11(a-b). Up to 0410 UTC (Fig. 4.1.11a), the $TT > 51^{\circ}\text{C}$ is found for all MPs coupling with KF schemes. In the morning, the TT simulated greater than 51°C indicates the occurrence of isolated severe storms. After that it has decreased for all MPs up to 0710 UTC and then increased in an oscillatory pattern. From 0430 to 0740 UTC, the $TT > 49^{\circ}\text{C}$ or equal for all MPs coupling with KF scheme indicates the occurrence of likely thunderstorms. The maximum TT is found to be 58.09°C at 1130 UTC for SBU-KF combination, which indicates the occurrence of scattered severe storms. In the morning, the maximum TT is found $> 51^{\circ}\text{C}$ (Fig. 4.1.11b) for all MPs coupling with BMJ schemes and is decreased up to 0630 UTC and then increased reaching maximum after 0900 UTC to 52°C . After that it shows oscillatory pattern for all MPs coupling with BMJ scheme.

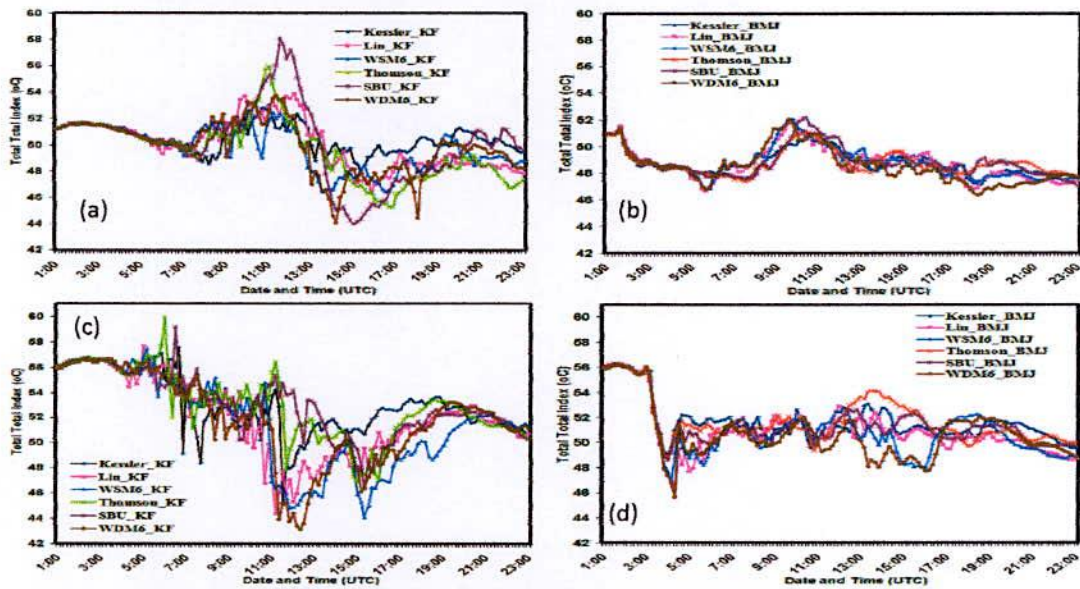


Fig. 4.1.11: Time variation of TT at (a-b) Chittagong and (c-d) Dhaka on 7 April 2012 using six different MP schemes coupling with KF and BMJ schemes.

Figs. 4.1.11(c-d) depict model simulated TT at Dhaka. The TT is found $> 56^{\circ}\text{C}$ for all MPs coupling with KF scheme from 0120 to 0340 UTC (Fig. 4.1.11c). In the morning, the $TT > 56^{\circ}\text{C}$ indicates the occurrence of scattered severe storms. After that it has decreased slowly and fluctuates continuously for all MPs coupling with KF scheme up to 1000 UTC. From 0400 to 0600 UTC, the value of TT lies between 53 to 56°C which indicates the occurrence of widely scattered severe storms. The maximum value of TT is 59.98 and 59.19°C has been

simulated by TH-KF and SBU-KF combinations at 0600 and 0630 UTC respectively. The TT simulated is $> 56^{\circ}\text{C}$ for all MPs coupling with BMJ scheme up to 0210 UTC (Fig. 4.1.11d), which indicates the occurrence of scattered severe storms. After that the TT is found $>55^{\circ}\text{C}$ for all MPs coupling with BMJ scheme up to 0310 UTC which is favorable for the occurrence of widely scattered severe storms. After 0310 UTC, the TT has decreased significantly and after 0410 UTC, the TT has increased again for all MPs coupling with BMJ scheme. From 0320 to 0420 UTC, the TT lies between 45 to 52°C for all MPs coupling with BMJ scheme and indicates the occurrence of likely thunderstorms and from 0430 to 0600 UTC, the TT $> 51^{\circ}\text{C}$ for KS-BMJ and TH-BMJ combinations, indicating the occurrence of isolated severe storms and then it has been changing in an oscillatory pattern for all MPs coupling with BMJ scheme.

4.1.11 K Index (KI)

The model simulated time variation of KI for six different MPs coupling with KF and BMJ schemes at Chittagong has been presented in Figs. 4.1.12(a-b). Up to 0420 UTC (Fig. 4.1.12a) the KI $> 41^{\circ}\text{C}$, which indicates extremely unstable atmosphere for all MPs coupling with KF schemes. In the morning, the KI greater than 40°C , indicates maximum possibility for the occurrence of thunderstorm. After that it has decreased gradually up to 0750 UTC and then again increased up to 1140 UTC for all MPs coupling with KF scheme.

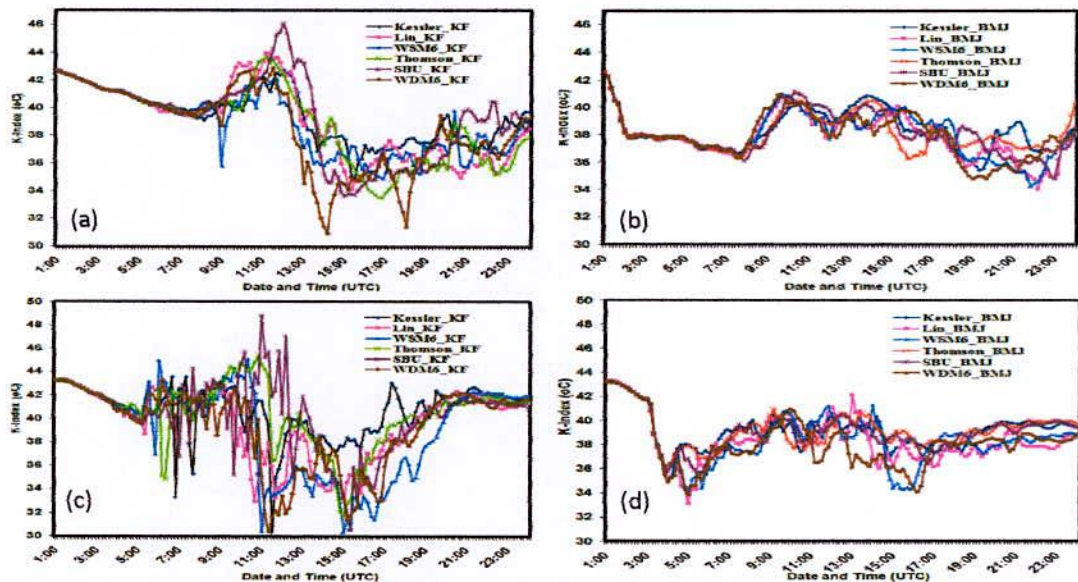


Fig. 4.1.12: Time variation of K Index at (a-b) Chittagong and (c-d) Dhaka on 7 April 2012 using six different MP schemes coupling with KF and BMJ schemes.

K index has decreased sharply to 35.83°C for WSM6-KF combination at 0900 UTC, which has the probability of numerous thunderstorms. From 0430 to 0910 UTC, the KI > 39°C or equal, which is very unstable case for all MPs coupling with KF scheme and indicates the occurrence of very likely thunderstorms. Up to 0140 UTC (Fig. 4.1.12b), the KI is > 40°C, which extremely unstable case for all MPs coupling with BMJ schemes. In the morning, the KI greater than 40°C, indicates maximum possibility for the occurrence of thunderstorm. After that it has decreased gradually up to 0740 UTC and then again increased up to 0940 UTC for all MPs coupling with BMJ scheme. From 0150 to 0940 UTC the KI is >39°C or equal, which is very unstable atmosphere, simulated for all MPs coupling with KF scheme, and indicates the occurrence of very likely thunderstorms.

Figs. 4.1.12(c-d) depict model simulated KI at Dhaka. The simulated KI is > 40°C up to 0420 UTC (Fig. 4.1.12c), which indicates extremely unstable atmosphere for all MPs coupling with KF scheme and the possibility of maximum for the occurrence of thunderstorm. Then it has decreased and subsequently fluctuates continuously for all MPs coupling with KF scheme. At 0640 UTC, the KI is > 40°C for KS-KF combination. The KI is > 40°C from starting up to 0310 UTC (Fig. 4.1.12d), indicates extremely unstable situation for all MPs coupling with BMJ scheme. In the morning, the KI greater than 40°C, indicates the maximum possibility of the occurrence of thunderstorm at Dhaka. After that it has significantly decreased and fluctuates continuously. The KI > 36°C during 0320 to 0340 UTC indicates very unstable atmosphere for the occurrence of very likely thunderstorms for all MPs coupling with BMJ scheme. The KI > 32°C during 0340 to 1500 UTC for all MPs coupling with BMJ scheme indicates for the occurrence of numerous thunderstorms.

4.1.12 Convective Available Potential Energy (CAPE)

Model simulated time variations of CAPE for six different MPs coupling with KF and BMJ schemes at Chittagong are presented in Figs. 4.1.13(a-b). Starting from 0420 UTC (Fig. 4.1.13a) the CAPE has decreased sharply up to 0610 UTC for all MPs coupling with KF scheme and then increased continuously for KS-KF, TH-KF and SBU-KF combinations. The CAPE > 2500 J/kg has been simulated by all MPs coupling with KF scheme for short period of time during 0420-0440 UTC, which is extremely unstable condition of atmosphere for the formation of nor'wester. The CAPE >1800 J/kg during 0440 to 0850 UTC is moderately unstable condition for all MPs coupling with KF scheme.

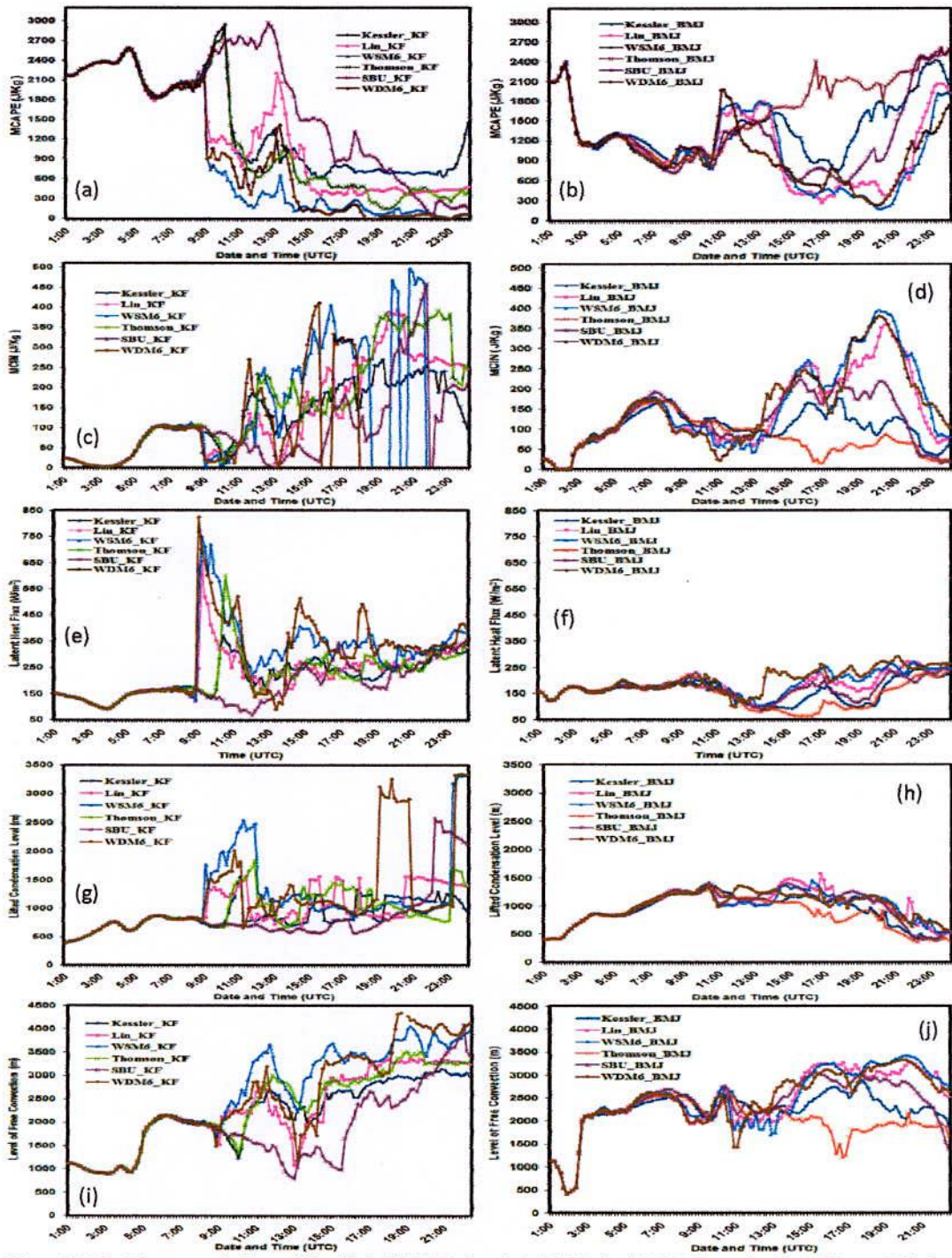


Fig. 4.1.13: Time variation of (a-b) MCAPE, (c-d) MCIN, (e-f) LH flux, (g-h) LCL and (i-j) LFC using six MP schemes coupling with KF and BMJ schemes at Chittagong on 7 April 2012.

The CAPE > 2500 J/kg is found for KS-KF, TH-KF and SBU-KF combinations from 0920 to 1000 UTC. The nor'wester occurred at 0740 UTC in Chittagong, but the CAPE is simulated after the occurrence time for all MPs in combination of KF scheme. At 0150 UTC (Fig. 4.1.13b), the CAPE > 2500 J/kg, which is extremely unstable condition and after that it has decreased (CAPE > 1000 J/kg) up to 0600 UTC, indicates weak instability for all MPs coupling with BMJ scheme. After 0820 UTC, the CAPE > 1000 J/kg is found for Lin-BMJ, WSM6-BMJ and WDM6-BMJ combinations.

Figs. 4.1.14(a-b) depict model simulated CAPE at Dhaka. The CAPE is less than 2500 J/kg (Fig. 4.1.14a) up to 0230 UTC, which is moderately unstable condition for all MPs coupling with KF scheme. After that the CAPE > 2500 J/kg up to 0520 UTC for all MPs coupling with KF scheme and the CAPE > 3200 J/kg is simulated by all MPs coupling with KF scheme at 0510 UTC, which indicates extremely unstable condition of atmosphere for the formation of nor'wester. It is found from the graph that the CAPE is simulated almost one hour later the time of occurrence of nor'wester for all MPs in combination with KF scheme. The CAPE is less than 2500 J/kg up to 0240 UTC (Fig. 4.1.14b) for all MPs coupling with BMJ scheme. At 0310 the CAPE > 2600 J/kg has been simulated by all MPs coupling with BMJ scheme, which is extremely unstable condition of atmosphere for the formation of nor'wester. Then it has significantly decreased for all MPs coupling with BMJ scheme.

4.1.13 Convective Inhibition (CIN)

CIN is the area of the sounding between the surface and to the level at which CAPE begins. CIN indicates the amount of energy that will prevent an air parcel from rising from the surface to the LFC. Model simulated time variation of CIN for six different MP coupling with KF and BMJ schemes at Chittagong is presented in Figs. 4.1.13(c-d). CIN is almost zero or less than 100 J/kg before 0420 UTC and after 0850 UTC, which indicates that the atmosphere is potentially unstable for the occurrence of nor'wester. Starting from 0420 UTC (Fig. 4.1.13c) the CIN has increased slowly and again CIN has decreased sharply after 0840 UTC by WDM6-KF, WSM6-KF and Lin-KF combination. At 0900 UTC, the CIN is zero simulated by WSM6-KF combination. From 0150 to 0220 UTC (Fig. 4.1.13d) the CIN is zero simulated by all MPs coupling with BMJ scheme. After that, it has increased slowly up to 0800 UTC and then it has decreased for by WDM6-BMJ, WSM6-BMJ and Lin-BMJ combination at 0830 UTC.

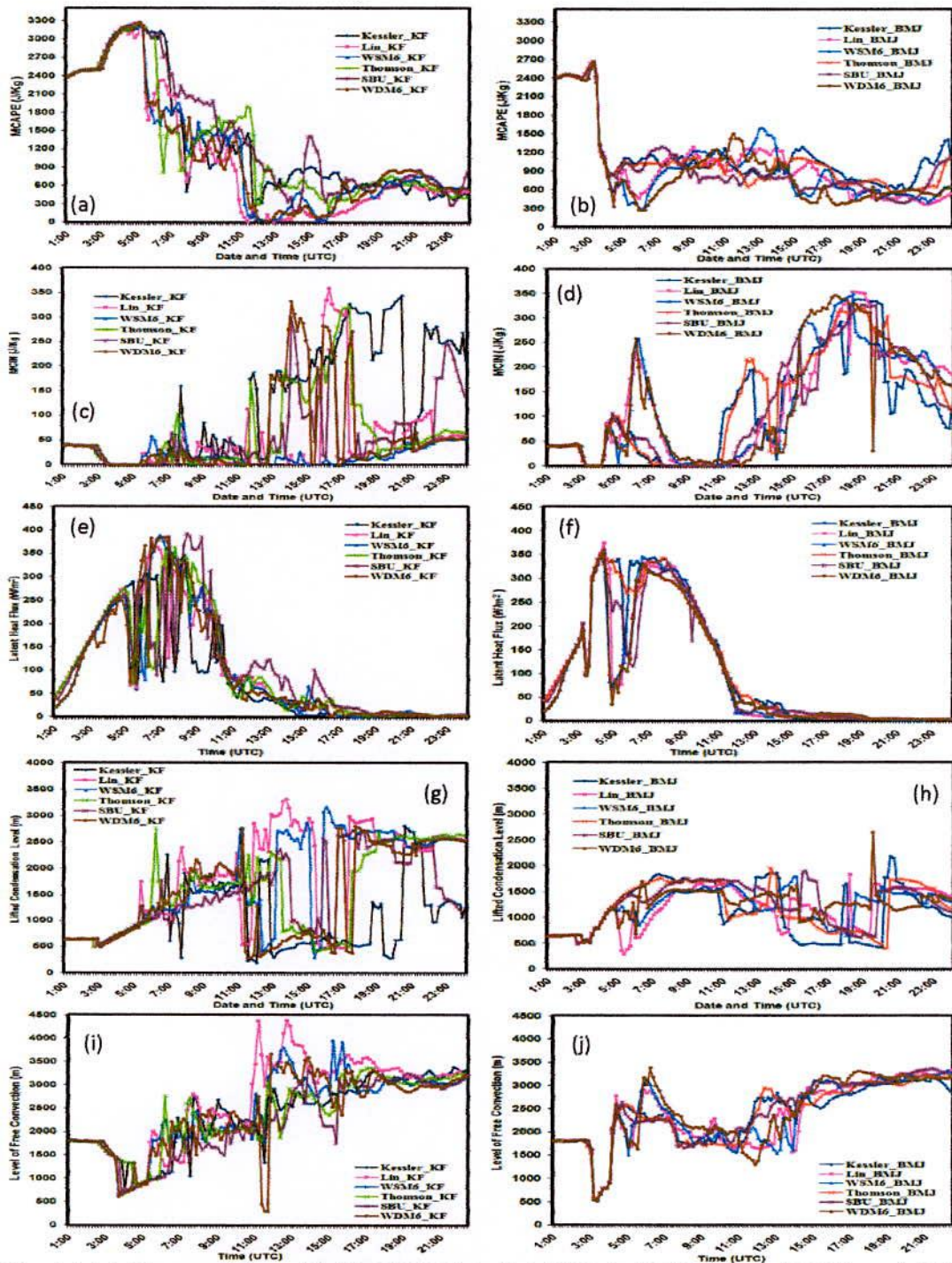


Fig. 4.1.14: Time variation of (a-b) MCAPE, (c-d) MCIN, (e-f) LH flux, (g-h) LCL and (i-j) LFC using six different MP schemes coupling with KF and BMJ schemes at Dhaka on 7 April 2012.

Up to 0450 UTC, the CIN < 100 J/kg for all MPs coupling with BMJ schemes and after 0830 UTC the CIN < 100 J/kg for Lin-BMJ and WDM6-BMJ combination, which indicates that the atmosphere is potentially unstable for the occurrence of nor'wester. At around 0730 UTC, the value of CIN is almost 175 J/kg which indicates the atmosphere is marginally stable. WRF model simulated CIN at Dhaka is given in Figs. 4.1.14(c-d). Up to 0330 UTC (Fig. 4.1.14c) the CIN < 100 J/kg and then the CIN is zero up to 0520 UTC for all MPs coupling with KF scheme. Then it has increased slowly up to 0720 UTC and the value of CIN < 100 J/kg for all MPs coupling with KF scheme. The CIN < 100 J/kg indicates that the atmosphere is potentially unstable for the occurrence of nor'wester. The simulated CIN is found minimum from 0340 to 0510 UTC for all MPs coupling with KF schemes, which is close to the observed squall at Dhaka. CIN is almost zero or less than 100 J/kg up to 0520 UTC (Fig. 4.1.14d) for all MPs coupling with BMJ scheme indicates that the atmosphere is potentially unstable for the occurrence of nor'wester. From 0310 to 0400 UTC (Fig. 4.1.14d) the CIN is zero as simulated by all MPs coupling with BMJ scheme, which is potentially unstable atmosphere for the occurrence of nor'wester and closure to the observed squall at Dhaka. After 0530 UTC, it has increased significantly for Lin-BMJ, WSM6-BMJ and WDM6-BMJ combinations and the value of CIN > 100 J/kg which is marginally stable atmosphere.

4.1.14 Latent Heat (LH) Flux

Model simulated time variation of LH flux (LHF) for six different MP coupling with KF and BMJ schemes at Chittagong is shown in Figs. 4.1.13(e-f). LHF is seen to decrease up to 0350 UTC and then it has increased slowly further (Fig. 4.1.13e) and again decreased at around 0850 UTC for all MPs coupling with KF scheme. The LHF has increased significantly at 0910 UTC to 655.3 and 752 W/m² for Lin-KF and WSM6-KF and at 0840 UTC it is 824.5 W/m² for WDM6-KF combination. In this case, the LHF released is huge in the atmosphere, which is available for the formation of severe storms. The LHF is not found any significant value (Fig. 4.1.13f) for all MPs in combination with BMJ scheme up to 0930 UTC over Chittagong.

WRF model simulated LHF at Dhaka is given in Figs. 4.1.14(e-f). Starting from 0000 UTC (Fig. 4.1.14e) the LHF is increased continuously at around 0450 UTC and then fluctuates significantly up to 0940 UTC for all MPs coupling with KF scheme. The LHF values are 275.36, 261.13, 275.5 and 263.16 W/m² for Lin-KF, WSM6-KF, TH-KF and SBU-KF at

0450 UTC, 289.66 W/m² for KS-KF at 0520 UTC and 255.93 W/m² for WDM6-KF at 0430 UTC combinations. The maximum values of LHF are 373.78, 388.48, 385.89 and 384.53 W/m² for Lin-KF, WSM6-KF, SBU-KF and WDM6-KF at 0620, 0650, 0720 and 0710 UTC respectively. Huge amount of LHF has been released in the atmosphere, which is available for the formation of severe storms. The LHF increases sharply from 0000 UTC (Fig. 4.1.14f) up to 0310 UTC and then fluctuates significantly for all MPs coupling with BMJ scheme. The maximum values LHF are found to be 348.54, 348.88 and 345 W/m² for KS-BMJ, TH-BMJ and SBU-BMJ combinations respectively at 0410 UTC and 374.38, 354.27 and 360.25 W/m² for Lin-BMJ, WSM6-BMJ and WDM6-BMJ combinations respectively at 0420 UTC.

4.1.15 Lifted Condensation Level (LCL)

Time variations of LCL for six different MP coupling with KF and BMJ schemes at Chittagong are presented in Figs. 4.1.13(g-h). Starting from 0000 UTC (Fig. 4.1.13g) the LCL is found to increase slowly up to 0350 UTC and then decrease slowly up to 0430 UTC for all MPs coupling with KF scheme. Again it has increased for all MPs except SBU coupling with KF scheme. At 0900 UTC, it has increased sharply and the maximum values of LCL are 2552.3, 2023.6 and 1573.5 m found WSM6-KF, WDM6-KF and Lin-KF combinations at 1110, 1040 and 1120 UTC respectively. From Fig. 4.1.13h, the LCL has increased slowly up to 0930 UTC for all MPs coupling with BMJ scheme. After that it is found oscillatory and decreasing for all MPs coupling with BMJ scheme.

WRF model simulated LCL for six different MP coupling with KF and BMJ schemes at Dhaka is shown in Fig. 4.1.14(g-h). At around 0300 UTC the LCL has found minimum for all MPs in combination with KF scheme (Fig. 4.1.14g) and then it has increased slowly up to 0450 UTC and after that it fluctuates for all MPs coupling with KF scheme. At 0500 UTC, it has slightly increased for all MPs coupling with KF scheme but the maximum values of LCL are found 1755, 2757 and 2266 for Lin-KF, TH-KF and KS-KF combinations at 0520, 0610 and 0650 UTC respectively. At around 0300 UTC the LCL has found minimum and then it increased sharply for all MPs coupling with BMJ scheme up to 0450 UTC (Fig. 4.1.14h) and after that it has decreased for WDM6-BMJ, Lin-BMJ and WSM6-BMJ combinations. At 0450 UTC, the LCL is found maximum and the values are 1268 and 1264 m for KS-BMJ and TH-BMJ combinations respectively.

4.1.16 Level of Free Convection (LFC)

Model simulated time variations of LFC for six different MP coupling with KF and BMJ schemes at Chittagong are presented in Figs. 4.1.13(i-j). The LFC is found minimum up to 0430 UTC (Fig. 4.1.13i), after that it has increased sharply and at around 0610 UTC, LFC is slightly high for all MPs coupling with KF scheme and then it has decreased for a short period of time for Lin-KF, WSM6-KF and WDM6-KF combination after 0850 UTC. The LFC has found minimum 1221, 1523, 1690, 1308, 866 and 1484m at 1000, 0900, 0850, 1000, 1240 and 0850 UTC for KS, Lin, WSM6, TH, SBU and WDM6 coupling with KF scheme. After that the LFC fluctuates significantly all through the simulation time. At around 0200 UTC the LFC is found minimum and LFC has increased (Fig. 4.1.13j) sharply during 0150-0240 UTC. After that it is found in an irregular pattern for all MPs coupling with BMJ scheme. It has decreased and reached minimum 2056, 1934, 2109, 2141, 2017 and 1949 m at 0920, 0830, 0850, 0930, 0940 and 0910 UTC for KS, Lin, WSM6, TH, SBU and WDM6 scheme respectively coupling with BMJ scheme.

WRF model simulated LFC at Dhaka is shown in Figs. 4.1.14(i-j). Up to 0250 UTC (Fig. 4.1.14i) the LFC is almost stable for all MPs coupling with KF scheme and then it has decreased significantly 738, 674, 631, 876, 699 and 614m at 0400, 0340, 0340, 0440, 0350 and 0340 UTC for KS, Lin, WSM6, TH, SBU and WDM6 schemes respectively in combination with KF scheme. The simulated LFC has found minimum near about the time of observation (0400 UTC) of squall line at Dhaka. After that, it has increased and fluctuates continuously for all MPs coupling with KF scheme. Up to 0230 UTC (Fig. 4.1.14j) the LFC is almost stable for all MPs coupling with BMJ scheme and then decreased significantly and reached minimum 548, 543, 515, 546, 536 and 527m at 0320 UTC respectively for KS, Lin, WSM6, TH, SBU and WDM6 schemes respectively coupling with BMJ scheme. Then it has increased slowly again from 0330 to 0400 UTC and at 0410 UTC increased sharply for all MPs coupling with BMJ scheme. Due to the sharp decrease of LFC at 0320 UTC, it may be assumed that there is a possibility of nor'wester at Dhaka.

4.1.17 Rain Water Mixing Ratio (RWMR)

The RWMR (contour, mg/kg) has been simulated along the line of maximum vertical velocity using different MPs coupling with KF and BMJ schemes and are presented in Figs. 4.1.15(a-l). Kessler scheme coupling with KF and BMJ schemes are simulated RWMR up to

100 hPa. Lin *et al.*, Thompson, SBU schemes coupling with KF and BMJ schemes have simulated RWMR up to 400 hPa. WSM6 and WDM6 coupling with KF and BMJ are simulated RWMR up to 300 hPa. The RWMR has simulated maximum at the position where the updraft and reflectivity is also maximum. The RWMR is found maximum at 500-400 hPa level for Kessler-KF and is 14 mg/kg. The maximum RWMR of 9, 9 and 8 mg/kg have also been simulated by Thompson-BMJ, WDM6-KF and WDM6-BMJ at 400, 400 and 600 hPa respectively.

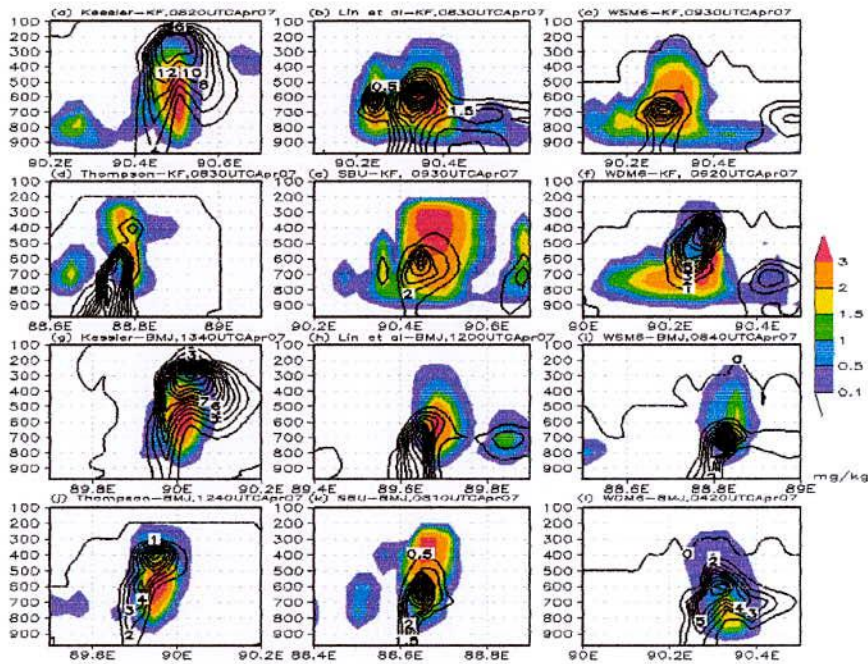


Fig. 4.1.15: WRF Model simulated CWMR (shaded) and RWMR (contour) along the line of maximum vertical velocity using Kessler, Lin *et al.*, WSM6, Thomson, SBU and WDM6 schemes coupling with (a-f) KF and (g-l) BMJ schemes on 7 April 2012.

4.1.18 Cloud Water Mixing Ratio (CWMR)

The CWMR (shaded, mg/kg) has simulated along the line of maximum vertical velocity using different MPs coupling with KF and BMJ schemes and are presented in Figs. 4.1.15(a-l). Kessler, Lin, WSM6, Thompson, SBU and WDM6 coupling with KF and BMJ have simulated CWMR up to 200 hPa. The CWMR is found maximum at 700- 400 hPa level for Kessler, Lin, WSM6, Thompson and WDM6 schemes in combination with KF and BMJ schemes and SBU coupling with KF and BMJ schemes have simulated maximum CWMR at 800-250 hPa level.

4.2 Nor'wester of 28 April 2012

The squall line is observed at Khulna (22.78°N and 89.53°E) and Chittagong (22.26°N and 91.81°E) on 28 April 2012. The observed time of squall at Khulna is 0325 UTC and Chittagong is 0640, 0647 and 0702 UTC. The squall moved at Khulna from the northwesterly direction with the maximum sustained wind speed 18m/s and moved toward southeasterly direction at Chittagong with the maximum sustained wind speed of 20, 22 and 19 m/s. On that day, the model has not simulated squall/nor'wester at Khulna but the model has simulated squall moving from northwesterly direction towards southeasterly direction. Due to the movement of squalls from central region towards southeast, the meteorological parameters for Dhaka (23.76°N and 90.38°E) and Chittagong have been analyzed. All six different MPs in combination with KF scheme have simulated squalls at 0900 UTC in the southeasterly direction and BMJ scheme has simulated squalls in the Bagerhat-Barisal region and are presented in Figs. 4.2.1(a-l). The different MP schemes have simulated squall in Dhaka region but the time and position are different than the observed time and position.

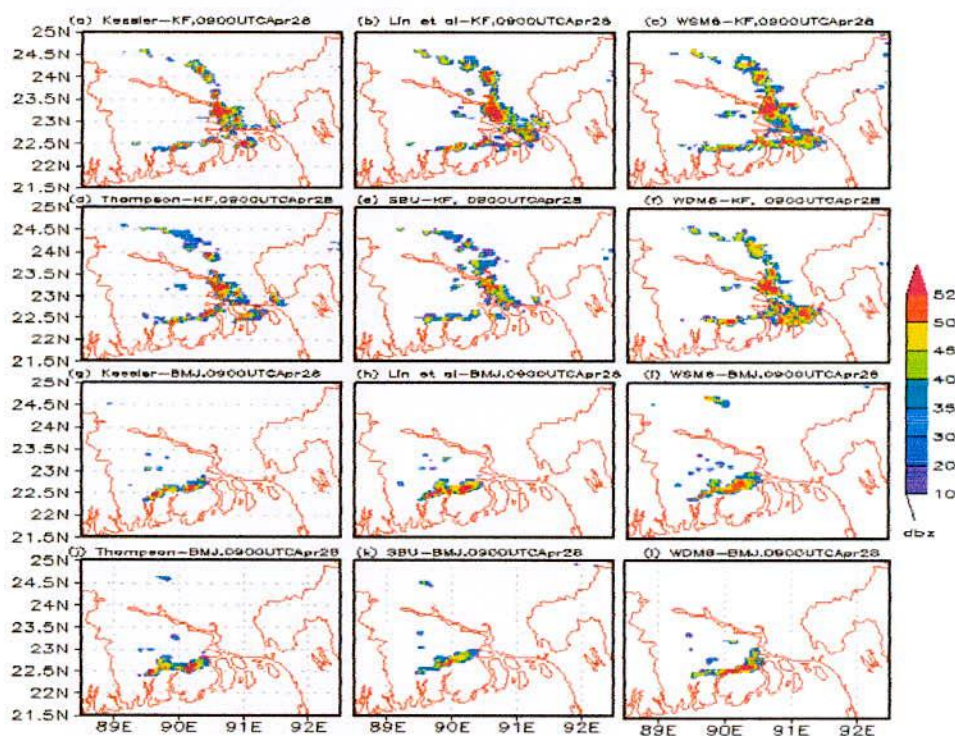


Fig. 4.2.1: Model simulated squall line/nor'wester for different MP schemes coupling with (a-f) KF and (g-l) BMJ schemes on 28 April 2012.

4.2.1 Sea Level Pressure (SLP)

Model simulated time variations of SLP for six different MP e.g. Kessler, Lin, WSM6, Thomson, SBU, WDM6 coupling with KF and BMJ schemes at Chittagong are presented in Figs. 4.2.2(a-b). The SLP has increased and fluctuates (Fig. 4.2.2a) continuously during 0100 to 0600 UTC and after that it has decreased and reached minimum at around 0930 UTC for all MPs coupling with KF scheme. The minimum SLP is found be 1004.4, 1004.2, 1003.6, 1004.5, 1003.8 and 1004.2 hPa for Kessler, Lin *et al.*, WSM6, Thompson, SBU and WDM6 in combination with KF scheme at 0910, 0930, 0940, 0930, 0940 and 0940 UTC respectively. After 0940 UTC, it has again increased and it fluctuates especially for Lin-KF, WSM6-KF and WDM6-KF combinations and reached minimum at 1200, 1250 and 1220 UTC respectively. Starting at 0310 UTC (Fig. 4.2.2b), the SLP is high and then it has decreased and fluctuates up to around 1200 UTC for all MPs coupling with BMJ scheme. The minimum values of simulated SLP are 1004.7, 1004.6, 1004.5, 1004.4, 1004.3 and 1004.6 hPa at 1300, 1230, 1220, 1210, 1220 and 1240 UTC using Kessler, Lin *et al.*, WSM6, Thompson, SBU and WDM6 in combination with BMJ scheme respectively.

Figs. 4.2.3(a-b) depict model simulated SLP at Dhaka. The SLP is oscillatory pattern up to 0300 UTC (Fig. 4.2.3a) and then has decreased sharply and reached minimum at 0800 UTC for all MPs coupling with KF scheme. The minimum SLP is found be 1001.4, 1001.4, 1001.3, 1001.4, 1001.1 and 1001.2 hPa at Dhaka for Kessler, Lin *et al.*, WSM6, Thompson, SBU and WDM6 in combination with KF scheme at 0800 UTC respectively which is almost one hour later than that of observed at Chittagong. After that, it has increased significantly and also fluctuates for all MPs coupling with KF scheme. The simulated SLP is increased and found maximum at 0410 UTC (Fig. 4.2.3b) after that it has decreased sharply and fluctuates up to around 0750 UTC for all MPs coupling with BMJ scheme. The minimum values of simulated SLP are 1003.6, 1003.4, 1003.5, 1003.4, 1003.4 and 1003.6 for hPa Kessler, Lin, WSM6, Thompson, SBU and WDM6 in combination with BMJ scheme at 0750 UTC respectively. A 2nd minimum is simulated during 0950 to 1020 UTC for all MPs in combination with BMJ scheme.

4.2.2 Maximum Wind Speed (MWS) at 10 m Level

Time variations of maximum wind speed (m/s) at 10m level simulated by six different MP schemes coupling with KF and BMJ schemes are presented in Figs. 4.2.2(c-d).

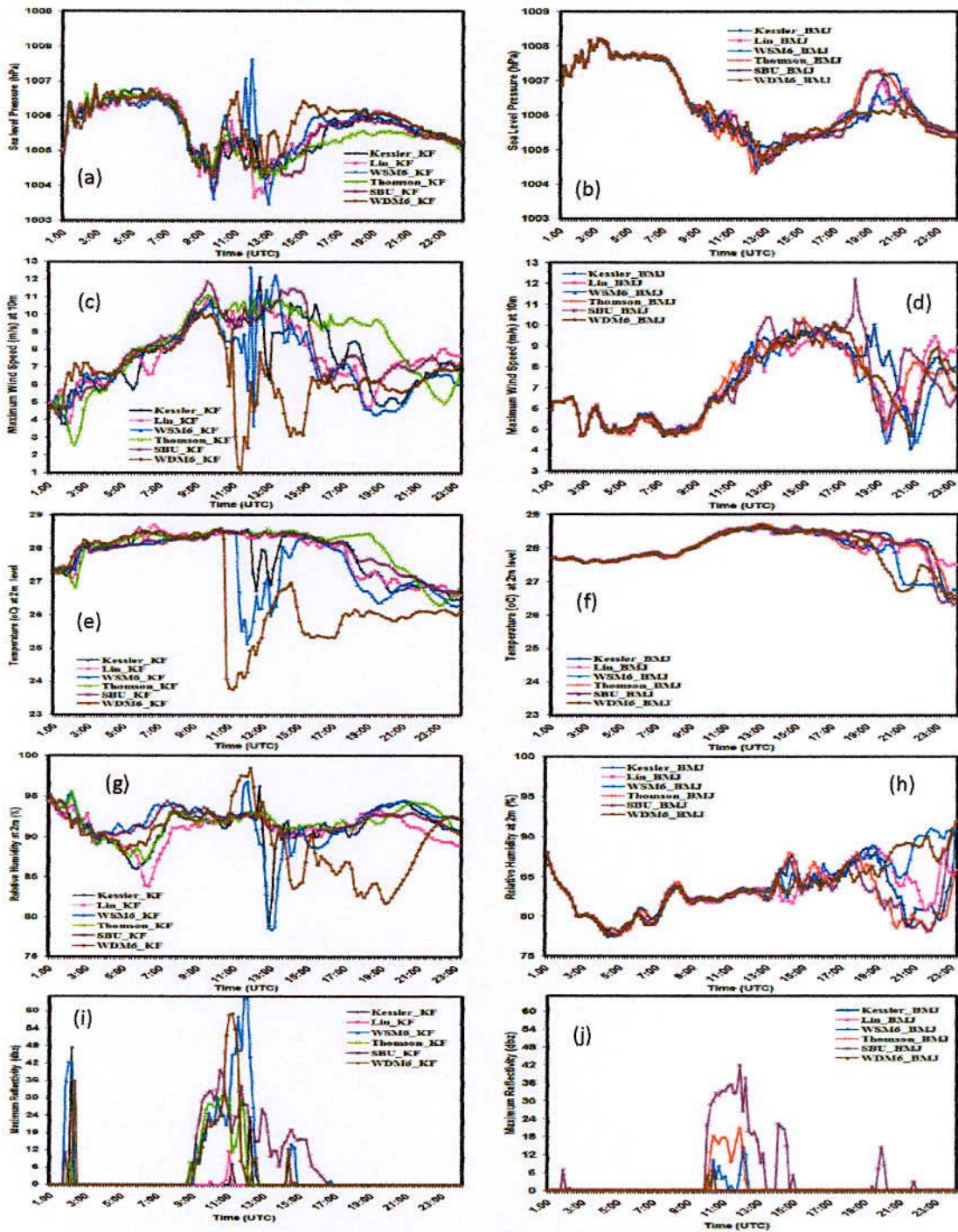


Fig. 4.2.2: Time variation of (a-b) SLP, (c-d) MWS at 10m, (e-f) Temperature at 2m, (g-h) RH at 2m and (i-j) MR using six different MP schemes coupling with KF and BMJ schemes at Chittagong on 28 April 2012.

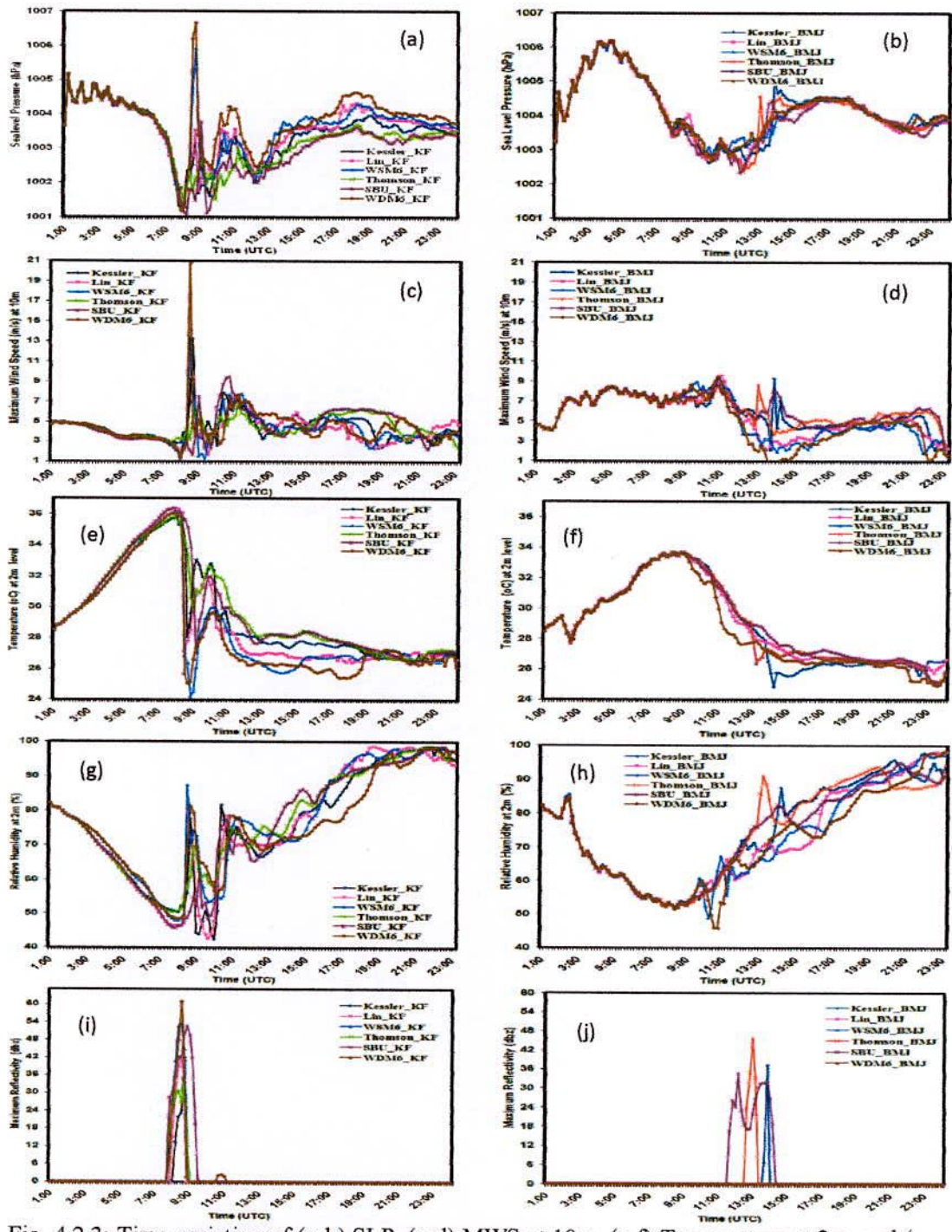


Fig. 4.2.3: Time variation of (a-b) SLP, (c-d) MWS at 10m, (e-f) Temperature at 2m, and (g-h) RH at 2m using six different MP schemes coupling with KF and BMJ schemes at Dhaka on 28 April 2012.

The wind speed has increased continuously with little exception during 0100 to 0930 UTC for all MPs coupling with KF scheme. The observed time of maximum gusty wind is 0640-0702 UTC but the model simulated MWS at around 0930 UTC by all MPs coupling with KF scheme (Fig. 4.2.2c) at Chittagong. The observed wind speed at Chittagong was 20, 22 and 19 m/s at 0640, 0647 and 0702 UTC respectively. The simulated first maximum of wind speeds of 10.9, 10.9, 10.7, 11.1, 11.9 and 10.2 m/s are found at around 0930 UTC for Kessler, Lin *et al.*, WSM6, Thompson, SBU and WDM6 schemes coupling with KF scheme. Different MPs schemes coupling with BMJ scheme (Fig. 4.2.2d) have simulated maximum wind speed after 1200 UTC at Chittagong on that day. The MWSs are found to be 9.7, 9.6, 9.1, 9.3, 10.4 and 9.1 m/s at 1440, 1540, 1200, 1230, 1300 and 1300 UTC respectively for Kessler, Lin *et al.*, WSM6, Thompson, SBU and WDM6 schemes respectively coupling with BMJ scheme and the 2nd maxima of wind speed are 12.2 and 10.1 m/s for SBU and WDM6 schemes in combination with BMJ scheme at 1740 and 1640 UTC respectively.

Figs. 4.2.3(c-d) depict model simulated MWS at 10m level at Dhaka. From Fig. 4.2.3c, the MWS of 13.3, 12.4, 13.4 and 20.8 m/s are found for KS-KF, Lin-KF, WSM6-KF and WDM6-KF combinations at 0840, 0830, 0830 and 0830 UTC respectively. Different MPs schemes coupling with BMJ scheme (Fig. 4.2.3d) have simulated less wind speed after 1040 UTC at Dhaka on that day. The simulated maximum wind speeds of 9.6, 9.5 and 9.5 m/s are found for Lin-BMJ at 1100 UTC, WSM6-BMJ at 1050 UTC and WDM6-BMJ at 1050 UTC respectively.

The model simulated maximum wind speeds at 10m level are 31.9, 32.6, 29.3, 32.3, 20.3 and 33.5 m/s at 0740, 0750, 0750, 0750, 0800 and 0750 UTC at (23.71°N & 89.83°E), (23.66°N & 89.92°E), (23.71°N & 89.91°E), (23.66°N & 89.89°E), (23.7°N & 89.86°E) and (23.71°N & 89.92°E) by Kessler, Lin, WSM6, Thompson, SBU, WDM6 schemes coupling with KF scheme and 24, 32, 23, 33, 20 and 31 m/s at 0740, 1250, 0740, 0800, 0910 and 0750 UTC at (22.98°N & 89.89°E), (24.6°N & 90.24°E), (22.97°N & 89.65°E), (22.93°N & 89.83°E), (22.68°N & 89.97°E) and (23.01°N & 89.89°E) by Kessler, Lin, WSM6, Thompson, SBU and WDM6 coupling with BMJ scheme respectively.

4.2.3 Temperature at 2m Level

Figs. 4.2.2(e-f) represent the time variations of temperature (°C) at 2m level simulated by six different MPs in combination with KF and BMJ schemes. After 0200 UTC (Fig. 4.2.2e), the

temperature at 2m Level has increased slowly and also fluctuates for all MPs in combination with KF scheme up to 1030 UTC and then it has decreased significantly at 1050 UTC for WDM6-KF and at 1140 UTC for WSM6-KF combinations. The sudden decrease of temperature has found at 1050 UTC for WDM6-KF and at 1120 UTC for WSM6-KF combinations, which indicate that the nor'wester/squall is observed at Chittagong at that time when the temperature becomes lower due to thunder showers and downdrafts of cold air. The linear trend of temperature has been observed (Fig. 4.2.2f) for all MPs in combination with BMJ scheme up to 1900 UTC at Chittagong.

WRF model simulated 2m level temperature ($^{\circ}\text{C}$) at Dhaka is presented in Figs. 4.2.3(e-f). The temperature at 2m level has increased sharply (Fig. 4.2.3e) during 0100 to 0750 UTC and reached almost 36°C for all MPs in combination with KF scheme. After that, it has decreased sharply and reached 24.2, 25.1, 27.2 and 28°C for WSM6-KF, WDM6-KF, Lin-KF and KS-KF combinations at 0850, 0840, 0830 and 0840 UTC respectively. Due to this sharp decrease of temperature at 2m level after 0830 UTC, the nor'wester/squall was observed at Dhaka at that time. From Fig. 4.2.3f, it is found that at first the temperature at 2m level sharply falls at around 0230 UTC and then increased continuously and reached maximum at 0750 UTC for all MPs combination with BMJ scheme. After that, it has been slowly decreased for all MPs in combination with BMJ scheme. This decrease in temperature may be due to the occurrence of the nor'wester.

4.2.4 Vertical Velocity

In this research at first the maximum updraft and its position are identified for all MP schemes coupling with KF and BMJ schemes. The maximum updraft for all MPs coupling with KF and BMJ schemes on 28 April 2012 is presented in Figs. 4.2.4(a-l). The times and positions of maximum updrafts simulated are different in different combinations of MPs and CP schemes. The maximum updrafts of 38, 55, 55, 46, 55 and 51 m s^{-1} are simulated at times of 0930, 0850, 0920, 1010, 1050 and 0940 UTC of 28 April by using Kessler, Lin *et al.*, WSM6, Thomson, SBU and WDM6 schemes coupling with KF scheme respectively. The maximum updrafts of 34, 45, 39, 34, 42 and 33 m s^{-1} are simulated at 1210, 1250, 0730, 1200, 0900 and 0900 UTC by using Kessler, Lin *et al.* WSM6, Thomson, SBU and WDM6 schemes coupling with BMJ scheme respectively. The maximum updraft is simulated at around 300–150 hPa by Lin-KF, WSM6-KF and at 400–250 hPa by SBU-KF combinations

on 28 April 2012. The downdraft is generally weaker but has been seen throughout the depth of the troposphere and updraft in the middle and upper troposphere. The updraft is surrounded by downdraft for all MP schemes coupling with KF and BMJ schemes. The updraft in the upper troposphere could be due to the latent heat release during glaciations and vapor deposition (Srivastava, 1985).

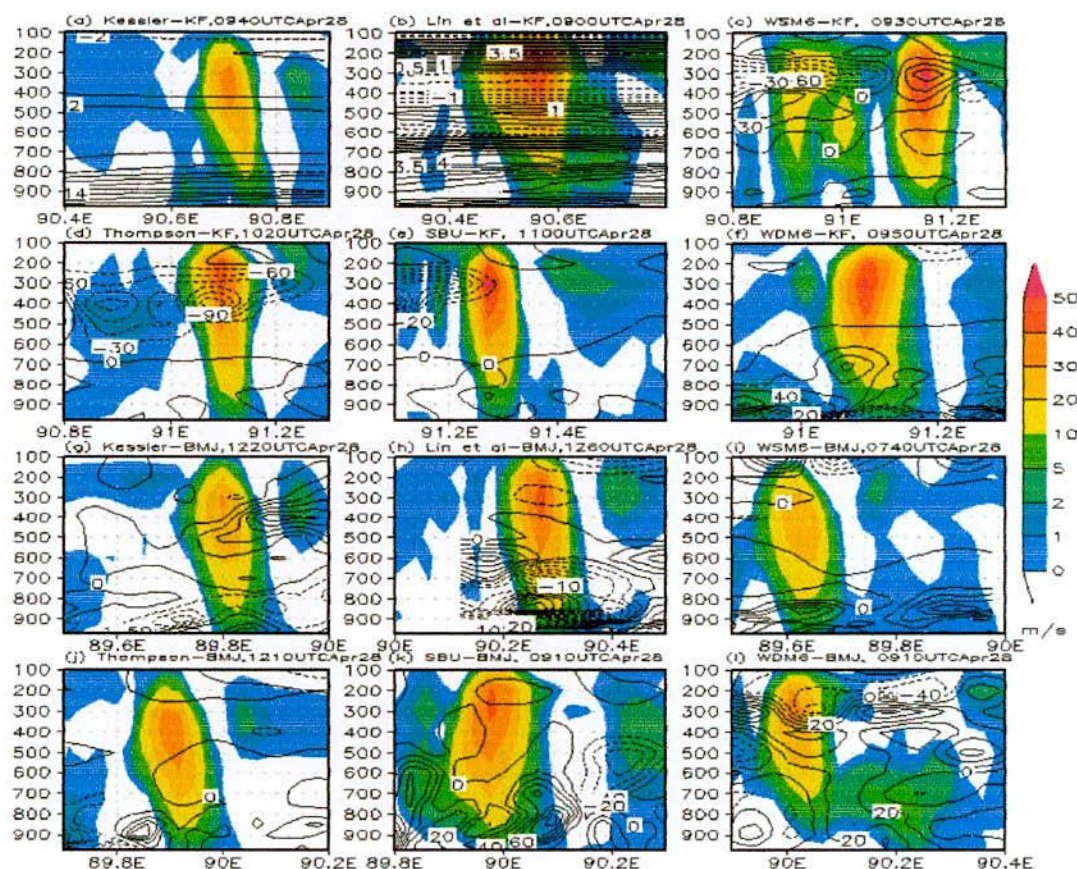


Fig. 4.2.4: WRF Model simulated maximum vertical velocity (shaded) and vorticity (contour, $\times 10^{-5}/s$) along the line of maximum vertical velocity using Kessler, Lin *et al.*, WSM6, Thomson, SBU and WDM6 schemes coupling with (a-f) KF and (g-l) BMJ schemes at 28 April 2012.

4.2.5 Vorticity

Along the line of maximum updraft, vorticity (contour $\times 10^{-5}/s$) has been simulated by different MP schemes coupling with KF and BMJ schemes on 28 April 2012 and is presented as in Figs. 4.1.4(a-l). The model has simulated positive vorticity in the lower level and negative vorticity in the upper level for all MPs in combination with KF and BMJ schemes

except WDM6-KF and Lin-BMJ combinations along the line of maximum vertical velocity. Different MP schemes in combination with KF and BMJ schemes have simulated pockets of positive and negative vorticity at different levels, which indicates cyclonic and anticyclonic circulation exist at all levels.

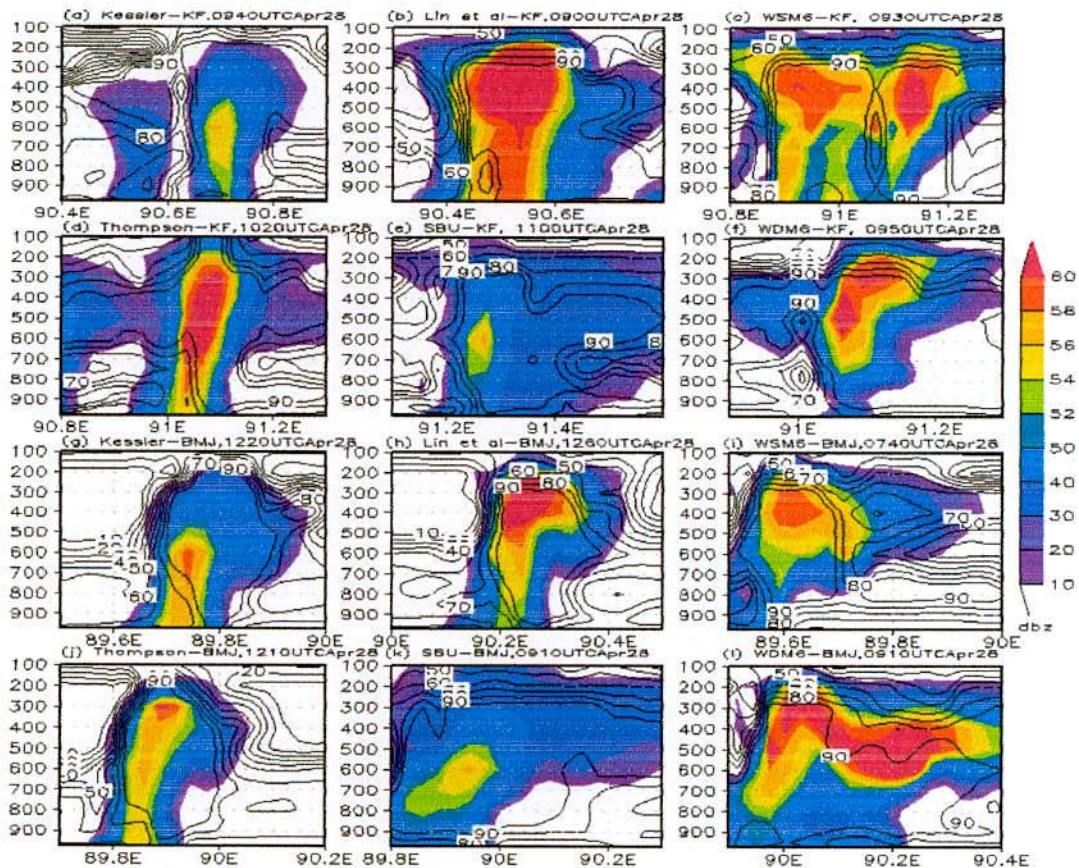


Fig. 4.2.5: WRF Model simulated reflectivity (shaded) and relative humidity (contour) along the line of maximum vertical velocity using Kessler, Lin *et al.*, WSM6, Thomson, SBU and WDM6 schemes coupling with (a-f) KF and (g-l) BMJ schemes on 28 April 2012.

4.2.6 Relative Humidity (RH) at 2m Level

The model simulated relative humidity at 2m level for six different MPs in combination with KF and BMJ schemes is presented in Figs. 4.2.2(g-h). The RH has gradually decreased (Fig.4.2.2g) and reached minimum at 0600 UTC and fluctuates for all MPs coupling with KF scheme. It has increased again and fluctuates for all MPs in combination with KF scheme and reached maximum 98.5% by WDM6-KF combination at 1150 UTC. The RH has decreased

continuously and reached minimum at 0400 UTC (Fig. 4.2.2h) and is found to increase again for all MPs in combination with BMJ scheme. After 1200 UTC, the model has simulated irregular pattern of RH for all MPs in combinations with BMJ scheme but the maximum RH has been simulated by all MPs coupling with BMJ scheme at around 0000 UTC and 2300 UTC respectively at Chittagong.

Figs. 4.2.3(g-h) depict model simulated RH at 2m level at Dhaka. The RH has decreased sharply up to around 0750 UTC (Fig.4.2.3g) and then sharply increased at around 0830 UTC for KS-KF, Lin-KF, WSM6-KF and WDM6-KF combinations. The maximum RH of 87.4% and 84% is simulated by WSM6-KF and WDM6-KF combinations at 0830 UTC and then it has decreased followed by increasing again for all MPs coupling with KF scheme. The RH is found maximum (> 84%) (Fig. 4.2.3h) at 0230 UTC then it has decreased and after 0900 UTC it has again increased significantly for all MPs coupling with BMJ scheme.

The RH (contour) has simulated along the line of maximum vertical velocity using different MPs coupling with KF and BMJ schemes and is presented in Figs. 4.2.5(a-l). All MPs coupling with KF and BMJ schemes have simulated RH up to 100 hPa. The simulated RH is > 90% for all MPs in combination with CPs up to 300 hPa level where the vertical velocity is found maximum.

4.2.7 Maximum Reflectivity (MR)

The model simulated time variations of Maximum Reflectivity (dBZ) for six different MPs coupling with KF and BMJ schemes at Chittagong are presented in Figs. 4.2.2(i-j). From Fig.4.2.2i, the reflectivity is found from 0150 to 0220 UTC and 0840 to 1300 UTC for all MPs coupling with KF scheme. The MR 47.5, 42.3 and 35.9dBZ are simulated by KS-KF, WSM6-KF and WDM6-KF combinations at 0210, 0200 and 0220 UTC. The MR 59.2 and 64.8dBZ are simulated by WDM6-KF and WSM6-KF combinations at 1110 and 1150 UTC but the observed times of squall are 0640, 0647 and 0702 UTC on that day at Chittagong. The reflectivity is simulated at 1000 to 1450 UTC (Fig.4.2.2j) for all MPs coupling with BMJ scheme. The MR 42dBZ is simulated by SBU-BMJ combination at 1150 UTC.

Figs. 4.2.3 (i-j) depict model simulated MR at Dhaka. The significant amount of reflectivity is simulated from 0750 to 0920 UTC (Fig.4.2.3i) for all MPs coupling with KF scheme. The MR 42, 41.6, 53, 35, 52.6 and 61dBZ are simulated by KS-KF, Lin-KF, WSM6-KF, TH-KF, SBU-KF and WDM6-KF combinations at 0840, 0830, 0830, 0840, 0850 and 0830 UTC.

Fig.4.2.3j shows that the reflectivity from 1140 to 1410 UTC for SBU-BMJ, 1240-1310 UTC for TH-BMJ and 1340-1350 UTC for KS-BMJ combinations. The MR simulated are 35, 46 and 37dBZ for SBU-BMJ, TH-BMJ and KS-BMJ combinations at 1210, 1300 and 1350 UTC respectively.

The reflectivity (shaded, dBZ) is simulated along the line of maximum vertical velocity using different MPs coupling with KF and BMJ schemes and are presented in Figs. 5(a-l). The reflectivity > 60dBZ has been simulated by Lin-KF and WDM6-BMJ at 600-200 hPa, at 700-300 hPa by TH-KF, at 500-200 hPa by Lin-BMJ and at 600-300 hPa level by WSM6 coupling with KF and BMJ schemes, where the up draft is found maximum.

4.2.8 Cross Total Index (CT)

The model simulated time variations of CT at Chittagong for six different MPs coupling with KF and BMJ schemes are presented in Figs. 4.2.6(a-b). The CT has been increased to > 25°C at 0200 UTC (Fig. 4.2.6a) for all MPs except Lin coupling with KF scheme. It is increased and attained > 25°C after 1020 UTC by WSM6-KF and WDM6-KF combinations, indicating strong potential for the occurrence of severe thunderstorms. The range of CT is 23 to 24°C during 0300 to 0800 UTC, which indicates moderate potential for the occurrence of severe thunderstorms at Chittagong. The CT greater than 20°C (Fig. 4.2.6b) during 0100 to 0220 UTC indicates strong potential for thunderstorms and CT greater than 19°C during 0230 to 0700 UTC indicates moderate potential for the occurrence of thunderstorms at Chittagong for all MPs in combination with BMJ scheme. After that, it is started to increase slowly and again during 0730 to 1000 UTC the CT becomes > 20°C, indicating strong potential for thunderstorms for all MPs in combination with BMJ scheme.

Figs. 4.2.7(a-b) depict model simulated CT at Dhaka. The CT is increased sharply for all MPs coupling with KF scheme during 0620 UTC to 0800 UTC (Fig. 4.2.7a) and then decreased sharply for all MPs coupling with KF scheme. The CT is simulated greater than 26°C by KS-KF, Lin-KF, WSM6-KF and WDM6-KF combinations at 0810 UTC indicates strong potential for the occurrence of severe thunderstorms at Dhaka. At 0220 UTC (Fig. 4.2.7b), the CT is maximum and found greater than 25°C for all MPs in combination with BMJ scheme. After that, it is seen to fluctuate continuously and decrease up to 0550 UTC for all MPs in combination with BMJ scheme. From 0620 to 0750 UTC, the CT is > 20°C for all MPs in combination with BMJ scheme. The CT is greater than 22°C at around 0850 UTC for

KS-BMJ, Lin-BMJ and WDM6-BMJ combinations indicates weak potential for severe thunderstorms and then it is decreased again for all MPs in combination with BMJ scheme.

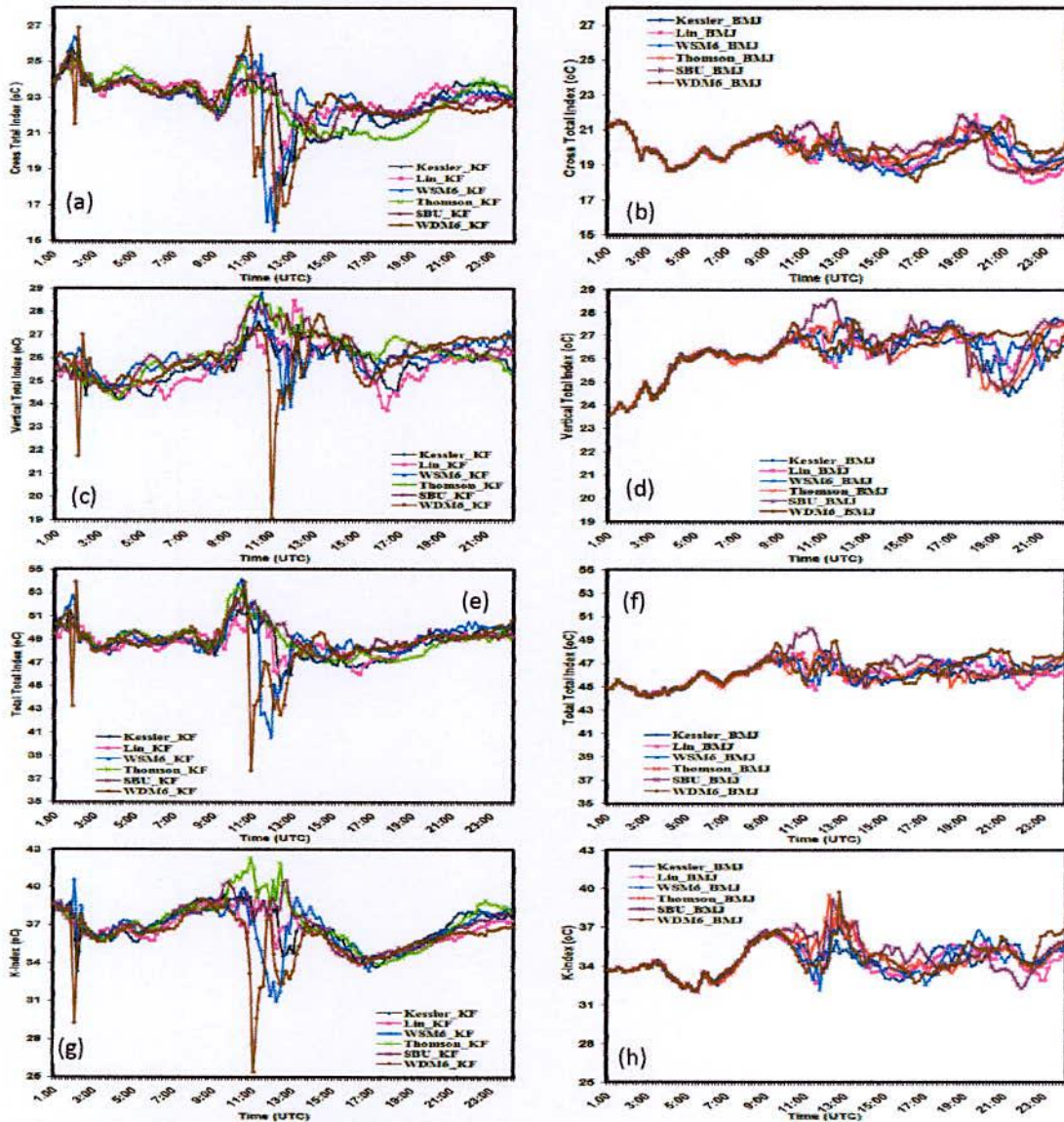


Fig. 4.2.6: Time variation of (a-b) CT, (c-d) VT, (e-f) TT and (g-h) K-Index using six different MP schemes coupling with KF and BMJ schemes at Chittagong on 28 April 2012.

4.2.9 Vertical Totals Index (VT)

The model simulated time variations of VT for six different MPs coupling with KF and BMJ schemes at Chittagong are presented in Figs. 4.2.6(c-d). The VT is simulated $> 26^{\circ}\text{C}$ (Fig.

4.2.6c) during 0100 to 0200 UTC for WSM6-KF and WDM6-KF combinations, which is favorable for the occurrence of a thunderstorm at Chittagong. After that, it has decreased for short period of time and then increased slowly and also fluctuates for all combinations. The VT is $> 26^{\circ}\text{C}$ for WSM6-KF, SBU-KF and TH-KF combinations at 0630, 0710 and 0720 UTC respectively, which is close to the observed time of squall at Chittagong.

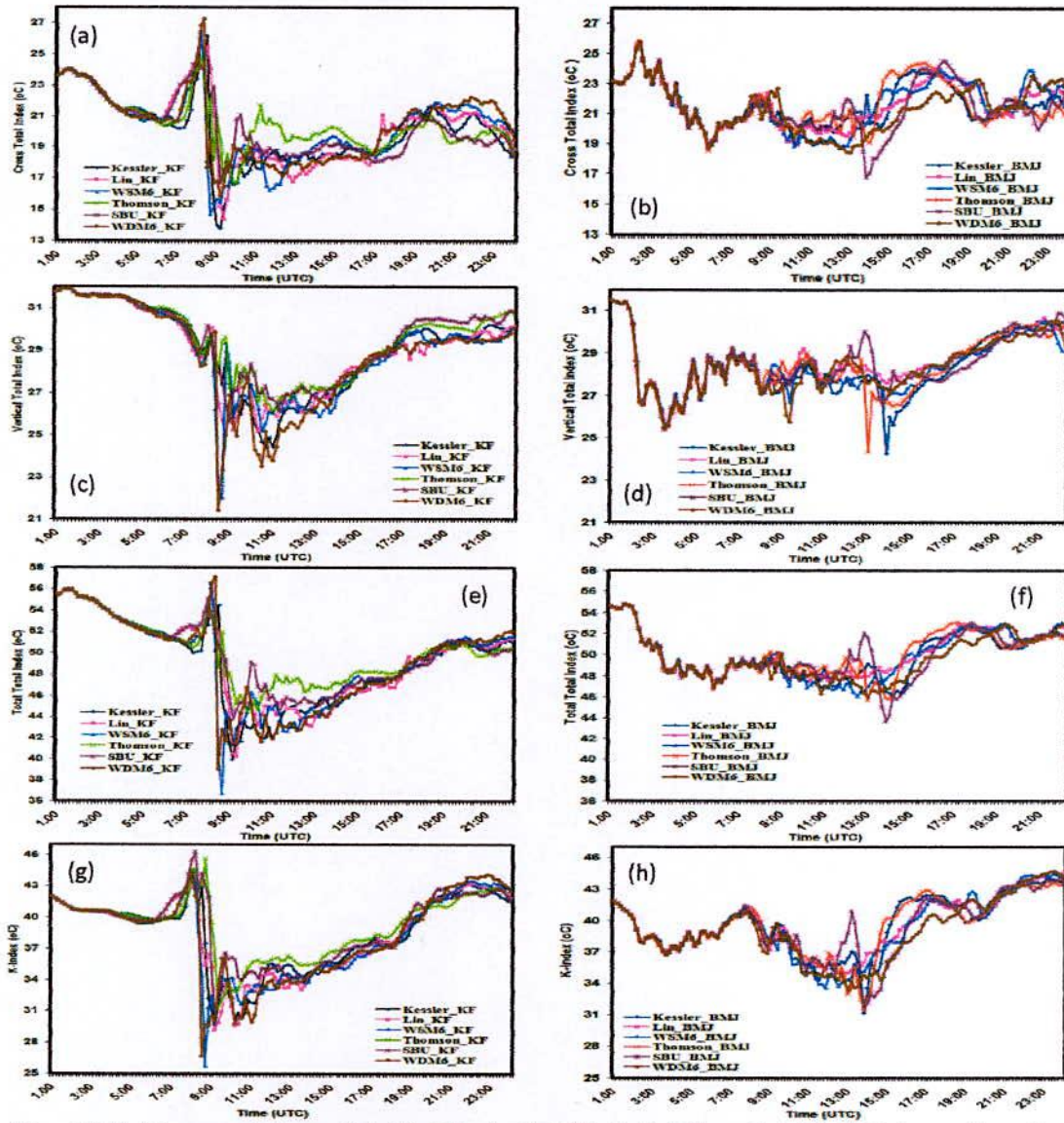


Fig. 4.2.7: Time variation of (a-b) CT, (c-d) VT, (e-f) TT and (g-h) K-Index using six different MP schemes coupling with KF and BMJ schemes at Dhaka on 28 April 2012.

The simulated VT is found $> 26^{\circ}\text{C}$ (Fig. 4.2.6d) during 0500 to 0630 UTC for all MPs coupling with BMJ scheme and it has increased again after 0700 UTC except TH-BMJ combination.

WRF model simulated VT at Dhaka are presented in Figs. 4.2.7(c-d). It is found from Fig. 4.2.7c that the VT is always greater than 28°C during 0100 to 0740 UTC indicates strong potential for the occurrence of severe thunderstorms at Dhaka for all MPs in combination with KF scheme. After that it drops significantly for all MPs but for WSM6-KF and WDM6-KF combinations it has reached around 21.5°C . Starting from 0100 UTC (Fig. 4.2.7d), the VT has gradually decreased at around 0230 UTC and then fluctuates in an irregular pattern for all MPs coupling with BMJ scheme. From 0100 to 0210 UTC the VT $> 28^{\circ}\text{C}$ indicates strong potential for the occurrence of severe thunderstorms and then after 0350 UTC the VT $> 26^{\circ}\text{C}$ indicates favorable condition for the occurrence of thunderstorm for all MPs in combination with BMJ scheme. The VT $> 28^{\circ}\text{C}$ at 0740 UTC indicates strong potential for the occurrence of severe thunderstorms for all MPs in combination with BMJ scheme.

4.2.10 Total Totals Index (TT)

The model simulated time variation of TT Index for six different MPs coupling with KF and BMJ schemes at Chittagong are shown in Figs. 4.2.6(e-f). The TT $> 51^{\circ}\text{C}$ at 0140 UTC (Fig. 4.2.6e) indicates the occurrence of isolated severe storms for KS-KF, WSM6-KF and WDM6-KF combinations. After that it shows oscillatory pattern for all MPs coupling with KF scheme and TT is 47 to 50°C indicates to the occurrence of likely thunderstorms for all MPs coupling with KF scheme up to 0930 UTC. It is increased again at around 1010 UTC and the TT is found greater than 52°C for WSM6-KF, TH-KF, SBU-KF and WDM6-KF combinations indicates the occurrence of widely scattered severe storms at Chittagong. It is found from (Fig. 4.2.6f) that the TT is increased in an oscillatory pattern and reached 44 to 48°C during 0100 to 1030 for all MPs coupling with BMJ scheme indicates the occurrence of likely thunderstorms. The maximum TT is found 50°C at 1110 UTC for SBU-BMJ combination at Chittagong.

Figs. 4.2.7(e-f) depict model simulated TT at Dhaka. The TT is found maximum $> 56^{\circ}\text{C}$ (Fig.4.2.7e) at 0130 UTC for WSM6-KF and WDM6-KF combinations and after that it has decreased gradually up to 0630 UTC for all MPs coupling with KF scheme. It has increased again for all MPs coupling with KF scheme and at 0810 UTC the TT is found maximum $>$

56°C for KS-KF, Lin-KF, WSM6-KF and WDM6-KF combinations indicates the occurrence of scattered severe thunderstorms and then sharply decrease for all MPs coupling with KF scheme. The TT is simulated maximum > 53°C during 0100 to 0210 UTC (Fig. 4.2.7f) for all MPs coupling with BMJ scheme indicates the occurrence of widely scattered severe storms and after that it has decreased and reached > 51°C at 0250 UTC indicates the occurrence of isolated severe storms at Dhaka. After that, it fluctuates in an irregular pattern and the TT lies between 45 to 50°C up to 1200 UTC for all MPs coupling with BMJ scheme, indicates the occurrence of likely thunderstorms at Dhaka.

4.2.11 K Index (KI)

The model simulated time variation of KI for six different MPs coupling with KF and BMJ schemes at Chittagong are shown in Figs. 4.2.6(g-h). The KI is found > 40.7°C (Fig.4.2.6g) at 0200 UTC for WSM6-KF combination indicates the extremely unstable atmosphere, the 100% chance for the occurrence of thunderstorm. The KI is found 36 to 40°C during 0400 to 1020 UTC, which is very unstable case for all MPs coupling with KF scheme, indicating the occurrence of thunderstorms very likely at Chittagong. At 1030 UTC, KI > 41°C is extremely unstable atmosphere for TH-KF combination, indicates maximum possibility of the occurrence of thunderstorm. The KI is changed (Fig. 4.2.6h) in an irregular pattern for all MPs coupling with BMJ scheme. The range of KI lies between 32 to 35°C up to 0810 UTC, which has the probability of numerous thunderstorms for all MPs coupling with BMJ scheme. After 0820 UTC, the KI > 36°C is very unstable atmosphere for all MPs coupling with BMJ scheme up to 1000 UTC, indicating the occurrence of very likely thunderstorms.

WRF model simulated KI at Dhaka are shown in Figs. 4.2.7(g-h). The KI has simulated > 40°C (Fig. 4.2.7g), indicates the maximum possibility of the occurrence of thunderstorm during 0100 to 0430 UTC and after 0640 to 0820 UTC for all MPs coupling with KF scheme. At 0830 UTC KI has reached minimum around 26°C for WSM6-KF and WDM6-KF combinations. The KI fluctuates (Fig. 4.2.7h) in an irregular pattern for all MPs coupling with BMJ scheme. Up to 0200 UTC and during 0700 to 0810 UTC, the KI > 40°C indicates the maximum possibility of the occurrence of thunderstorm for all MPs coupling with BMJ scheme. During 0210 to 0750 UTC, KI lies between 36 to 40°C, which is very unstable atmosphere for all MPs coupling with BMJ scheme indicates the occurrence of very likely thunderstorms.

4.2.12 Convective Available Potential Energy (CAPE)

Model simulated time variation of CAPE for six different MPs coupling with KF and BMJ schemes at Chittagong are presented in Figs. 4.2.8(a-b). The CAPE has fluctuates (Fig. 4.2.8a) in an irregular pattern for all MPs coupling with KF scheme. The CAPE > 2500 J/kg is simulated during 0100 to 1040 UTC indicates extremely unstable condition for all MPs coupling with KF scheme. After 1040 UTC the CAPE is found to decrease significantly for WDM6-KF and WSM6-KF combinations and Kessler-KF combination at around 1200 UTC. All other combinations the CAPE has decreased linearly with increase of time. CAPE provides the maximum possible kinetic energy that a statically unstable parcel can acquire. Significant decrease for WDM6-KF and WSM6-KF combinations indicates the stable atmosphere. Up to 0900 UTC (Fig. 4.2.8b) the CAPE < 1000 J/kg indicates the instability is weak for all MPs in combination with BMJ scheme. The CAPE has increased and to reach around 1800 J/kg during 1200 to 1900 UTC after that it has decreased again for all MPs in combination with BMJ scheme.

Figs. 4.2.9(a-b) depict model simulated CAPE at Dhaka. Starting from 0420 UTC (Fig. 4.2.9a) the CAPE has increased sharply up to around 0450 UTC for all MPs coupling with KF scheme and then decreased continuously and after 0820 UTC it has decreased significantly towards zero for all MPs coupling with KF scheme. The CAPE > 3000 J/kg is simulated during 0300 to 0740 UTC indicates extremely unstable condition for all MPs coupling with KF scheme. At around 0200 UTC (Fig. 4.2.9b) the CAPE > 2600 J/kg is extremely unstable condition for all MPs coupling with BMJ scheme and then sharply decreased at 0350 UTC and also fluctuates continuously for all MPs coupling with BMJ scheme. The CAPE > 1000 J/kg during 0600 to 1000 UTC indicates the moderately unstable condition for all MPs coupling with BMJ scheme.

4.2.13 Convective Inhibition (CIN)

Model simulated time variation of CIN for six different MPs coupling with KF and BMJ schemes at Chittagong is presented in Figs. 4.2.8(c-d). CIN is almost zero or less than 10 J/kg (Fig. 4.2.8c) up to 1120 UTC for all MPs coupling with KF scheme indicates the atmosphere is potentially unstable for the occurrence of nor'wester at Chittagong. After 1130 UTC, it has sharply increased (>200 J/kg) for WSM6-KF, WDM6-KF and KS-KF combinations, where the simulated CAPE is almost zero.

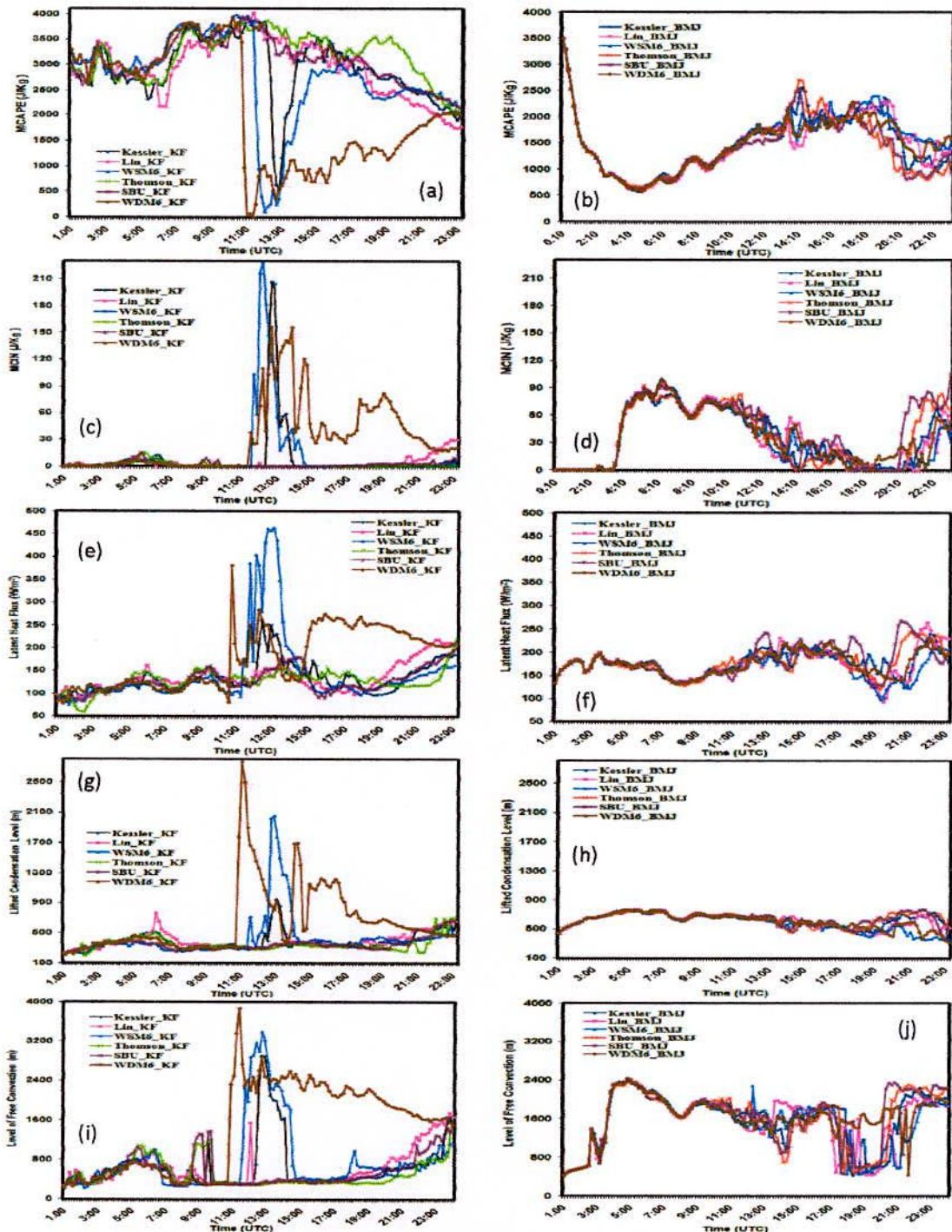


Fig. 4.2.8: Time variation of (a-b) CAPE, (c-d) CIN, (e-f) LH Flux, (g-h) LCL and (i-j) LFC using six different MP schemes coupling with KF and BMJ schemes at Chittagong on 28 April 2012.

UP to 0340 UTC (Fig. 4.2.8d) the CIN is almost zero for all MPs coupling with BMJ scheme. After that, it has sharply increased and fluctuates for all MPs in combination with BMJ scheme. At 0500 UTC the CIN has reached maximum and at that time the simulated CAPE is also found minimum. Again, the CIN is found minimum after 1810 UTC for KS-BMJ, TH-BMJ and SBU-BMJ combinations.

Figs. 4.2.9(c-d) depict model simulated CIN at Dhaka. Starting from 0100 UTC (Fig. 4.2.9c) the CIN has decreased and reached to zero indicates that the atmosphere is potentially unstable for the occurrence of nor'wester at 0820 UTC and then fluctuates significantly and reached maximum (>300 J/kg) for all MPs coupling with KF scheme. From Fig. 4.2.9d, the CIN is fluctuated in an irregular pattern for all MPs in combination with BMJ scheme. Up to 0940 UTC CIN is almost zero or less than 100 J/kg for all MPs coupling with BMJ scheme indicates that the atmosphere is potentially unstable for the occurrence of nor'wester.

4.2.14 Latent Heat (LH) Flux

Model simulated time variation of LH flux for six different MP coupling with KF and BMJ schemes at Chittagong is given in Fig. 4.2.8(e-f). LH flux fluctuates up to around (Fig. 4.2.8e) 1030 UTC for all MPs coupling with KF scheme. The LH flux has increased significantly and reached 381 and 464 W/m^2 at 1040 and 1300 UTC for WDM6-KF and WSM6-KF combinations respectively. In this case the huge amount of LH flux released in the atmosphere, which is available for the formation of severe storms. After 1200 UTC the simulated LH flux is almost zero for all MPs coupling with KF and BMJ schemes. LH flux fluctuates in an irregular pattern for all MPs coupling with BMJ scheme. LH flux is simulated minimum at around 0700 to 0900 UTC and 1830 to 2100 UTC for all MPs coupling with BMJ scheme. It is fluctuating continuously for all MPs in combination with BMJ scheme.

WRF model simulated LH flux at Dhaka is given in Figs. 4.2.9(e-f). LH flux has increased continuously up to 0630 UTC and then decrease and fluctuates up to around (Fig. 4.2.9e) 1030 UTC for all MPs coupling with KF scheme. The maximum LH flux 333, 332, 329, 333, 332 and 330 W/m^2 has been simulated for KS-KF, Lin-KF, WSM6-KF, TH-KF, SBU-KF and WDM6-KF combinations at 0620, 0640, 0640, 0620, 0630 and 0640 UTC indicates the flux released is huge in the atmosphere, which is available for the formation of severe storms at Dhaka at that time. After 1200 UTC the simulated LH flux is almost zero for all MPs coupling with KF and BMJ schemes.

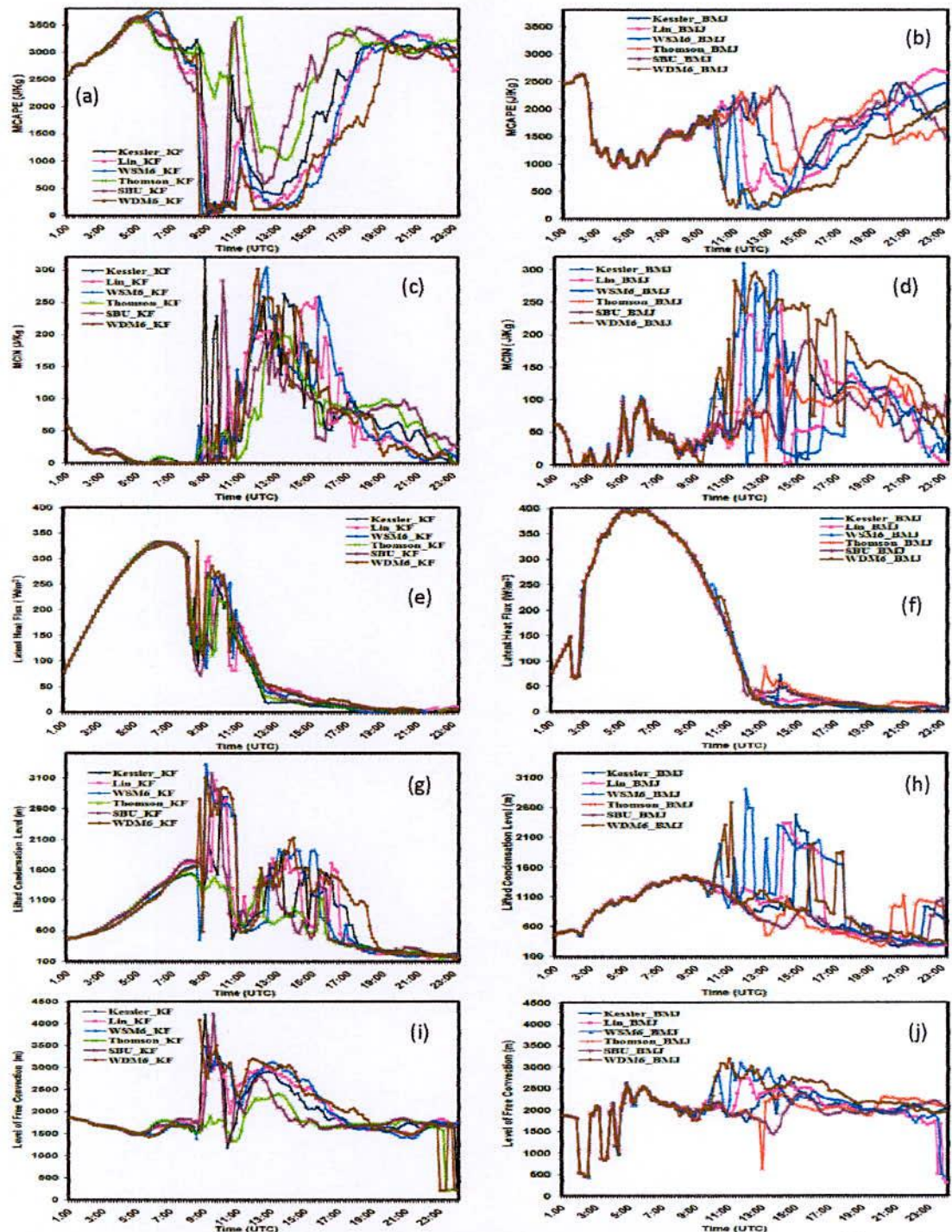


Fig. 4.2.9: Time variation of (a-b) CAPE, (c-d) CIN, (e-f) LH flux, (g-h) LCL and (i-j) LFC using six different MP schemes coupling with KF and BMJ schemes at Dhaka on 28 April 2012.

The LH flux has increased continuously up to 0630 UTC except at around 0230 UTC where sharp fall is observed (Fig. 4.2.9f) for all MPs coupling with BMJ scheme. The maximum LH flux 399, 396, 398, 398, 398 and 395 W/m² has simulated for KS-BMJ, Lin- BMJ, WSM6-BMJ, TH- BMJ, SBU- BMJ and WDM6- BMJ at 0550 UTC indicates that the LH flux released is huge in the atmosphere, which is available for the formation of severe storms.

4.2.15 Lifted Condensation Level (LCL)

Time variation of LCL for six different MPs coupling with KF and BMJ schemes at Chittagong is shown in Figs. 4.2.8(g-h). The LCL has increased up to 0630 UTC and fluctuates (Fig. 4.2.8g) all through the model run for all MPs coupling with KF scheme. At 0740, 0650, 0740, 0720 and 0750 UTC the LCL are simulated minimum 283, 270, 290, 257 and 294 m for KS-KF, WSM6-KF, TH-KF, SBU-KF and WDM6-KF combinations respectively. The LCL has increased significantly for WDM6-KF and WSM6-KF combinations at 1100 and 1250 UTC and the values are 2770 and 2060 m respectively. The LCL has increased (Fig. 4.2.8h) up to 0450 UTC and then decreased and fluctuates for all MPs coupling with BMJ scheme. The minimum LCL has found 635, 635, 612, 616, 621 and 623 m for KS-BMJ, Lin-BMJ, WSM6-BMJ, TH-BMJ, SBU-BMJ and WDM6-BMJ respectively at 0800 UTC.

WRF model simulated LCL at Dhaka is shown in Fig. 4.2.9(g-h). The LCL has gradually increased up to around 0740 UTC (Fig.4.2.9g) for all MPs coupling with KF scheme. After that, it fluctuates significantly for all MPs coupling with KF scheme. The maximum LCL 1715, 1630, 1742 and 1603 m is simulated by Lin-KF, WSM6-KF, SBU-KF and WDM6-KF combinations at 0740 UTC. The LCL has decreased sharply 457 and 586m at 0830 and 0840 UTC by WSM6-KF and WDM6-KF combinations respectively. The LCL has increased (Fig. 4.2.9h) in an oscillatory pattern for all MPs coupling with BMJ scheme during 0230 to 0820 UTC and then decrease for all MPs in combination with BMJ scheme. The maximum LCL is found 1994 and 2313 m for WSM6-BMJ and WDM6-BMJ combinations at 1020 and 1040 UTC respectively.

4.2.16 Level of Free Convection (LFC)

Model simulated time variation of LFC for six different MP coupling with KF and BMJ schemes at Chittagong is shown in Figs. 4.2.8(i-j). In the morning the LFC has found minimum (Fig.4.2.8i) and it increased in an irregular pattern up to 0600 UTC then it has

decreased and reached minimum 291, 392, 268, 309, 270 and 321m at 0740 UTC for KS, Lin, WSM6, TH, SBU and WDM6 schemes respectively coupling with KF scheme. After 0300 UTC (Fig.4.2.8j), the LFC has sharply increased and reached maximum at 0450 UTC for all MPs coupling with BMJ scheme and then it has decreased for all MPs coupling with BMJ combination. The LFC has found minimum 1655, 1652, 1621, 1611, 1638 and 1634m at 0800 UTC it has again increase for all MPs in combination with BMJ scheme.

WRF model simulated LFC at Dhaka is shown in Fig. 4.2.9(i-j). The LFC has slightly decreased (Fig. 4.2.9i) during 0000 to 0450 UTC and at around 0900 UTC it has sharply increased for all MPs coupling with KF scheme except TH-KF combination. The LFC has fluctuates (Fig. 4.2.9j) in an irregular pattern up to around 0740 UTC and then decrease at around 0850 UTC for all MPs coupling with BMJ scheme. After 0850 UTC, it has been increased again and also fluctuates continuously for all MPs in combination with BMJ scheme at Dhaka.

4.2.17 Rain Water Mixing Ratio (RWMR)

The RWMR (contour, mg/kg) has simulated along the line of maximum vertical velocity using different MPs coupling with KF and BMJ schemes and are presented in Figs. 4.1.10(a-l). Kessler scheme coupling with KF and BMJ schemes are simulated RWMR up to 100 hPa. WSM6, Lin *et al.* and SBU schemes coupling with KF and BMJ schemes are simulated RWMR up to 500 hPa. Thompson and WDM6 schemes coupling with KF and BMJ schemes have simulated RWMR up to 400 hPa. The RWMR is found maximum at the position where the updraft and reflectivity has also maximum. The RWMR is found maximum 14 mg/kg at 400-300 hPa level for KS-KF and KS-BMJ combinations. The significant amount of RWMR 13, 11, 9, 8, 8, 8, and 9 mg/kg have also been simulated by Lin-KF, WSM6-KF, TH-KF, SBU-KF, WDM6-KF, Lin-BMJ, SBU-BMJ and WDM6-BMJ combinations at 600 hPa and TH-BMJ at 400 hPa level.

4.2.18 Cloud Water Mixing Ratio (CWMR)

The CWMR (shaded, mg/kg) has simulated along the line of maximum vertical velocity using different MPs coupling with KF and BMJ schemes and are presented in Figs. 4.1.10(a-l). Kessler and SBU schemes coupling with KF and BMJ schemes are simulated CWMR up to 100 hPa. All other MPs coupling with KF and BMJ schemes are simulated CWMR up to 200 hPa. The CWMR is found maximum at 800-500 hPa level for KS-KF, WSM6-KF, TH-

KF, KS-BMJ, Lin-BMJ and TH-BMJ combinations and at 500-200 hPa level for SBU-KF and SBU-BMJ combinations.

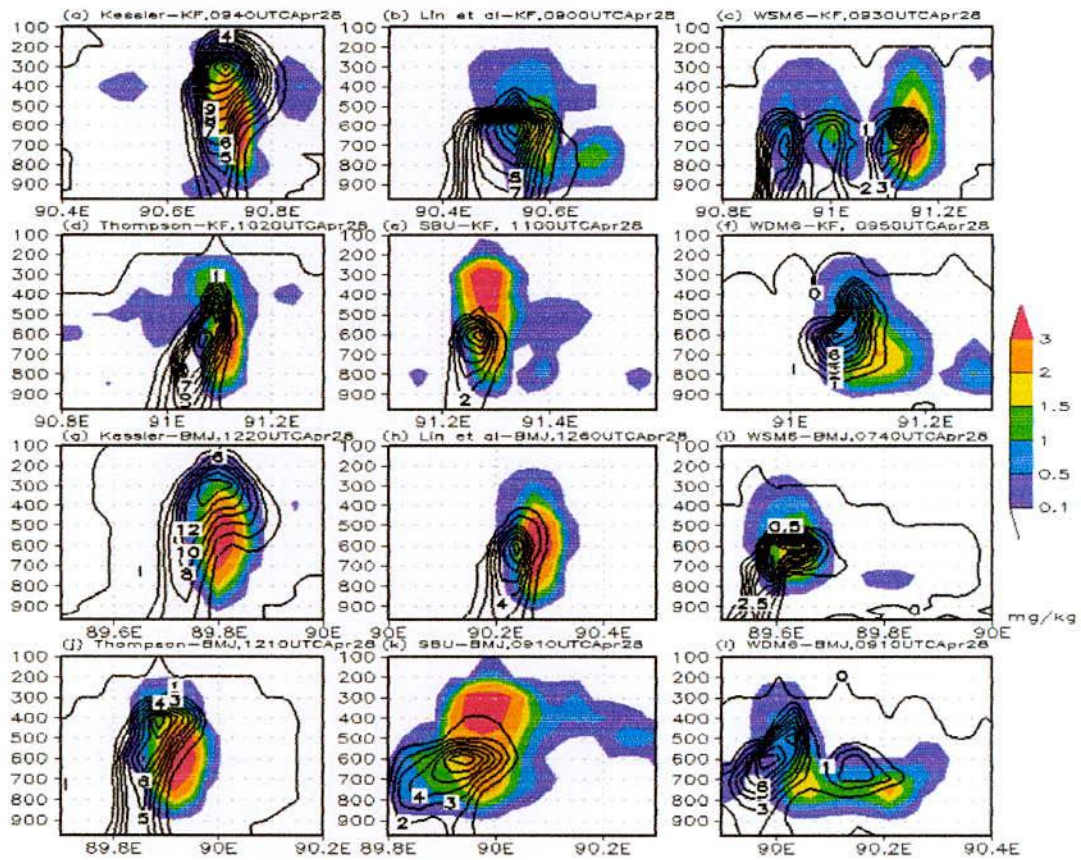


Fig. 4.2.10: WRF Model simulated CWMR (shaded) and RWMR (contour) along the line of maximum vertical velocity using Kessler, Lin *et al.*, WSM6, Thomson, SBU and WDM6 schemes coupling with (a-f) KF and (g-l) BMJ schemes at 28 April 2012.

4.3 Nor'wester of 27 April 2014

The squall line is observed at Sylhet (24.9°N and 91.83°E) and Srimangal (24.3°N and 91.73°E) on 27 April 2014. The observed time of squall at Sylhet and Srimangal is 1848-1851 and 1803-1825 UTC and moved southwesterly and westerly direction respectively with the maximum wind speed 23 m/s. On that day, the model has not simulated squall/nor'wester at Sylhet-Srimangal but it is simulated in the southwestern region of the country i.e., Khulna (22.78°N and 89.53°E). Since model has not simulated nor'wester at Sylhet-Srimangal regions we have analysed the meteorological parameters in Sylhet as well as Khulna. The different MP schemes in WRF model has simulated squall in Khulna region but the time and position is different than observed.

4.3.1 Sea Level Pressure

Model simulated time variation of SLP for six different MP schemes e.g. Kessler, Lin, WSM6, Thomson, SBU, WDM6 coupling with KF and BMJ schemes at Sylhet are presented in Figs. 4.3.1(a-b). At 1800 UTC (Fig. 4.3.1a) the SLP is greater than 1008 for KS-KF, Lin-KF, WSM6-KF and TH-KF combinations. After that, it is slowly decreased at around 1840 UTC for MPs coupling with KF scheme. The minimum SLP 1007.7 hPa is simulated by KS-KF and WSM6-KF combinations at 1840 UTC. At 1805 UTC (Fig. 4.3.1b) the SLP is greater than 1008 for KS-BMJ, Lin-BMJ, TH-BMJ and SBU-BMJ combinations. After that, it is decreased by these combinations at around 1810 UTC and the minimum SLP found 1007.79 hPa by WDM6-KF combination.

Figs. 4.3.2(a-b) depict model simulated SLP at Khulna. Starting from 0600 UTC (Fig. 4.3.2a) the SLP started to decrease sharply and reached minimum at around 0950 UTC and then increased and fluctuates for all MPs coupling with KF scheme. At 0945 UTC the SLP reached minimum 1005.45 hPa for Lin-KF combination. The SLP decreased again and minimum value 1006.2 hPa is simulated by TH-KF and SBU-KF combinations at 1220 and 1300 UTC. Starting from 0600 UTC (Fig. 4.3.2b) the SLP is decreased sharply at around 0950 and 1140 UTC for all MPs coupling with BMJ schemes. The minimum SLP 1005.49, 1005.96 and 1005.93 hPa is found at 0950, 1140 and 1200 UTC for WDM6-BMJ, TH-BMJ and SBU-BMJ combinations.

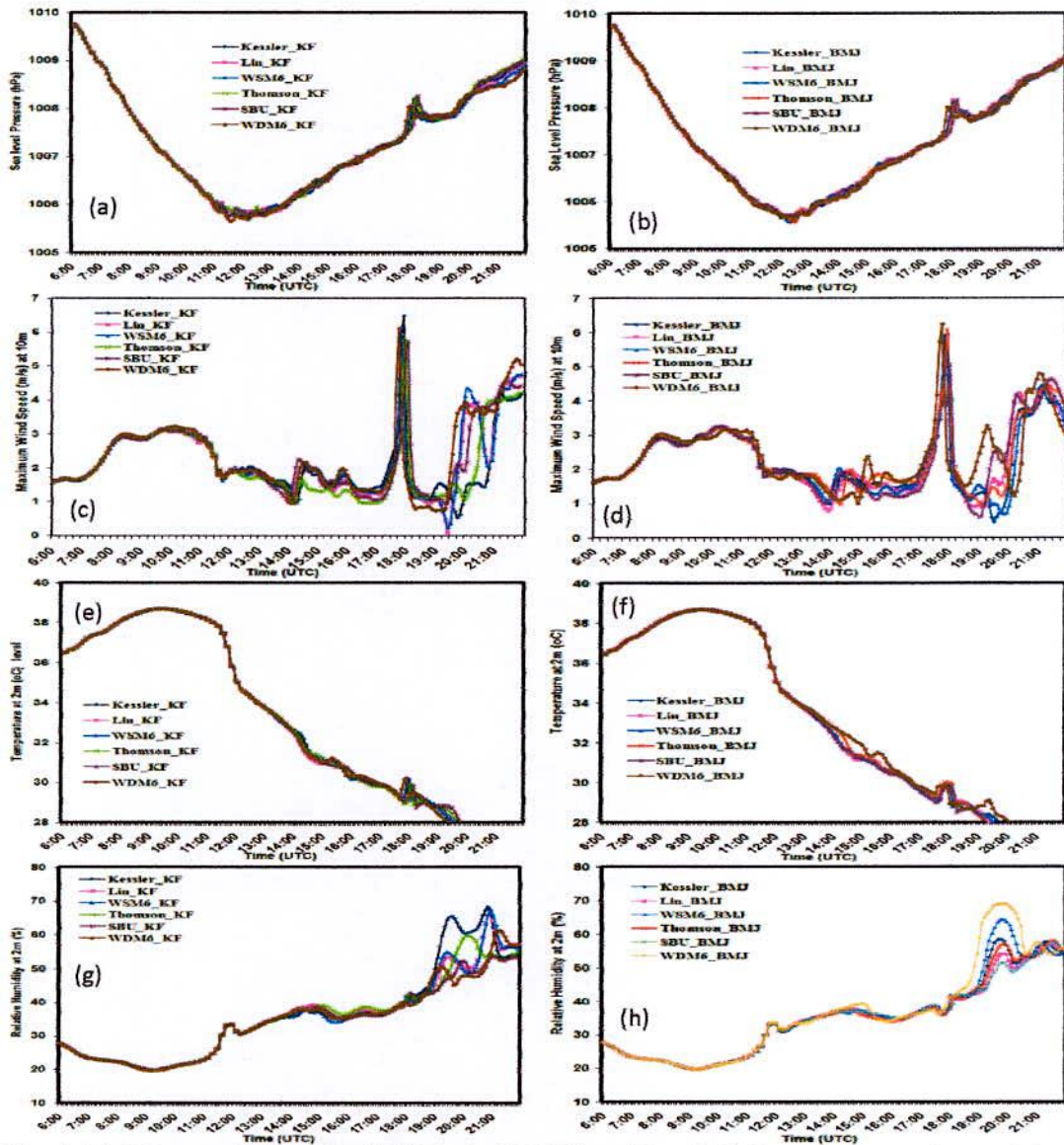


Fig. 4.3.1: Time variation of (a-b) SLP, (c-d) MWS at 10m, (e-f) Temperature at 2m, and (g-h) RH at 2m using six different MP schemes coupling with KF and BMJ schemes at Sylhet on 27 April 2014.

4.3.2 Maximum Wind Speed (MWS) at 10 m Level

Time variation of MWS at 10m level is simulated by six different MP schemes coupling with KF and BMJ schemes at Sylhet are presented in Figs. 4.3.1(c-d). The simulated first maxima of MWS 6.5, 6.2 and 6.1 m/s found at 1755, 1750 and 1745 UTC for KS, WSM6 and WDM6 schemes coupling with KF scheme (Fig. 4.3.1c).

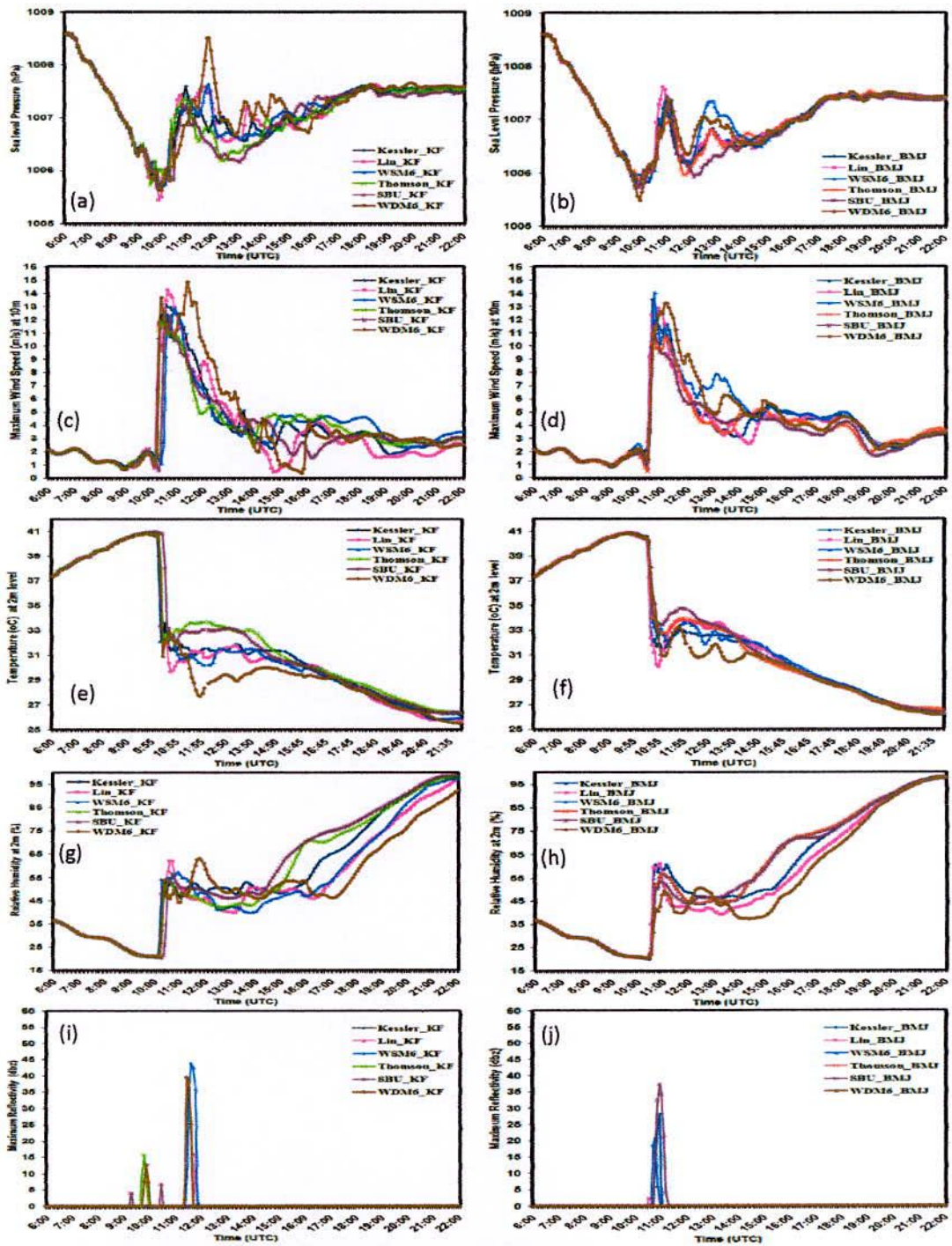


Fig. 4.3.2: Time variation of (a-b) SLP, (c-d) MWS at 10m, (e-f) Temperature at 2m, (g-h) RH at 2m and (i-j) MR using six different MP schemes coupling with KF and BMJ schemes at Khulna on 27 April 2014.

The second maxima of MWS is found 3.90, 4.35 and 3.94 m/s at 2005, 2005 and 2000 UTC by Lin *et al.*, WSM6, and WDM6 schemes coupling with KF scheme. The MWS 5.93, 5.92, 6.09 and 6.25 m/s is found at 1755, 1750, 1755 and 1745 UTC for KS, WSM6, TH and WDM6 schemes coupling with BMJ scheme (Fig. 4.3.1d). The observed wind at Sylhet was 23.05 m/s.

Figs. 4.3.2(c-d) depict model simulated MWS at Khulna. The model simulated MWS at 10m level by all MPs coupling with KF scheme at around 1030 UTC (Fig. 4.3.2c). The MWS 13.2, 14.2, and 13.7 m/s is found at 1030, 1035 and 1020 UTC for KS, Lin *et al.* and WDM6 schemes coupling with KF scheme. From Fig. 4.3.2d, the MWS is found 13.53, 14.02, and 13.25 m/s at 1035, 1040 and 1110 UTC for Kessler, WSM6 and WDM6 coupling with BMJ scheme.

The model simulated MWS at 10m level are 22.7, 24.1, 22, 21.6, 15.8 and 29.5 m/s at 1020, 1045, 1105, 0940, 1000 and 1010 UTC at (22.26°N & 89.53°E), (22.01°N & 89.53°E), (22.1°N & 89.5°E), (22.19°N & 89.33°E), (22.86°N & 89.78°E) and (22.05°N & 89.53°E) by Kessler, Lin, WSM6, Thompson, SBU, WDM6 coupling with KF scheme and 23, 21.8, 26.7, 22.7, 14.2 and 36.2 m/s at 1115, 1120, 1120, 1125, 1130 and 0935 UTC at (22.42°N & 89.09°E), (22.05°N & 89.53°E), (22.79°N & 90.45°E), (22.80°N & 90.20°E), (22.47°N & 89.09°E) and (22.77°N & 90.42°E) by Kessler, Lin, WSM6, Thompson, SBU, WDM6 coupling with BMJ scheme.

4.3.3 Temperature at 2m Level

Figs. 4.3.1(e-f) represent the time variation of temperature (°C) at 2m Level on 27 April 2014 simulated by six different MPs in combination with KF and BMJ schemes at Sylhet. It is found from Figs. 4.3.1(e-f) that the temperature is simulated significantly high during 0600-1100 UTC and maximum at 0915 UTC after that it decreased from 1100 UTC until 1800 UTC for all MPs coupling with KF and BMJ schemes. The temperature is increased slightly for KS-KF, Lin-KF and WSM6-KF at 1800 UTC and WDM6-KF at 1755 UTC, which is close to the observed time of nor'wester at Sylhet. At 1750 UTC, it increased slightly for all MPs coupling with BMJ scheme which is close to the observed time at Sylhet.

Figs. 4.3.2(e-f) depict model simulated temperature ($^{\circ}\text{C}$) at 2m Level on 27 April 2014 using six different MPs in combination with KF and BMJ schemes at Khulna. Starting from 0600 UTC (Fig. 4.3.2(e-f)) the temperature started to increase sharply and is found maximum at 1000 UTC for all MPs coupling with KF and BMJ schemes. After that, it decreased sharply and reached minimum after 1010 and 1025 UTC for all MPs coupling with KF and BMJ schemes respectively. The temperature decreased almost 10°C during 1010-1030 UTC for KF scheme and during 1025-1045 UTC for BMJ scheme. Due to this sharp decrease of temperature within short period of time for all MPs coupling with KF and BMJ schemes there is a possibility of occurring squall at Khulna during that period.

4.3.4 Vertical Velocity

The maximum updraft (shaded) are identified for the heavy rainfall event on 27 April 2014 using different MPs coupling with KF and BMJ schemes and are presented in Figs. 4.3.3(a-l). The maximum updrafts simulated times and positions are different in different combination of MPs and CP schemes (Figs. 4.3.3). The maximum updraft 28, 49, 43, 36, 37 and 34 m s^{-1} simulated by Kessler, Lin *et al.*, WSM6, Thomson, SBU and WDM6 schemes coupling with KF scheme at the times of 1020, 1045, 1105, 0940, 1000 and 1010 UTC (Fig. 4.3.3) respectively. The maximum updraft 32, 41, 46, 38, 34, and 33 m s^{-1} simulated by Kessler, Lin *et al.* WSM6, Thomson, SBU and WDM6 schemes coupling with BMJ scheme at the times of 1115, 1120, 1120, 1125, 1130 and 0935 UTC respectively. The maximum updraft is simulated at around 400–150 hPa by Lin, WSM6, Thompson and SBU schemes in combination with KF and BMJ schemes on 27 April 2014. The updraft simulated is much less by KS-KF and WDM6-KF on this day. The updraft in the middle and upper troposphere is surrounded by downdraft for all MPs coupling with KF and BMJ schemes. The updraft in the upper troposphere could be due to the latent heat release during glaciations and vapor deposition.

4.3.5 Vorticity

Along the line of maximum updraft, vorticity (contour, $\times 10^{-5}/\text{s}$) is simulated by different MP schemes coupling with KF and BMJ schemes on 27 April 2014 and are presented as in Figs. 4.3.3(a-l). The positive vorticity are simulated along the line of maximum vertical velocity by Lin-KF, WSM6-KF, KS-BMJ, Lin-BMJ, WSM6-BMJ, TH-BMJ and SBU-BMJ combinations from 900-400 hPa. The positive vorticity are also simulated by KS-KF, TH-KF,

SBU-KF, WDM6-KF and WDM6-BMJ combinations from 900-750 hPa. The negative vorticity is simulated above these levels for all combinations of MP and CP schemes, which indicates the lower atmospheric level has cyclonic circulation and upper atmospheric level has anti cyclonic circulation.

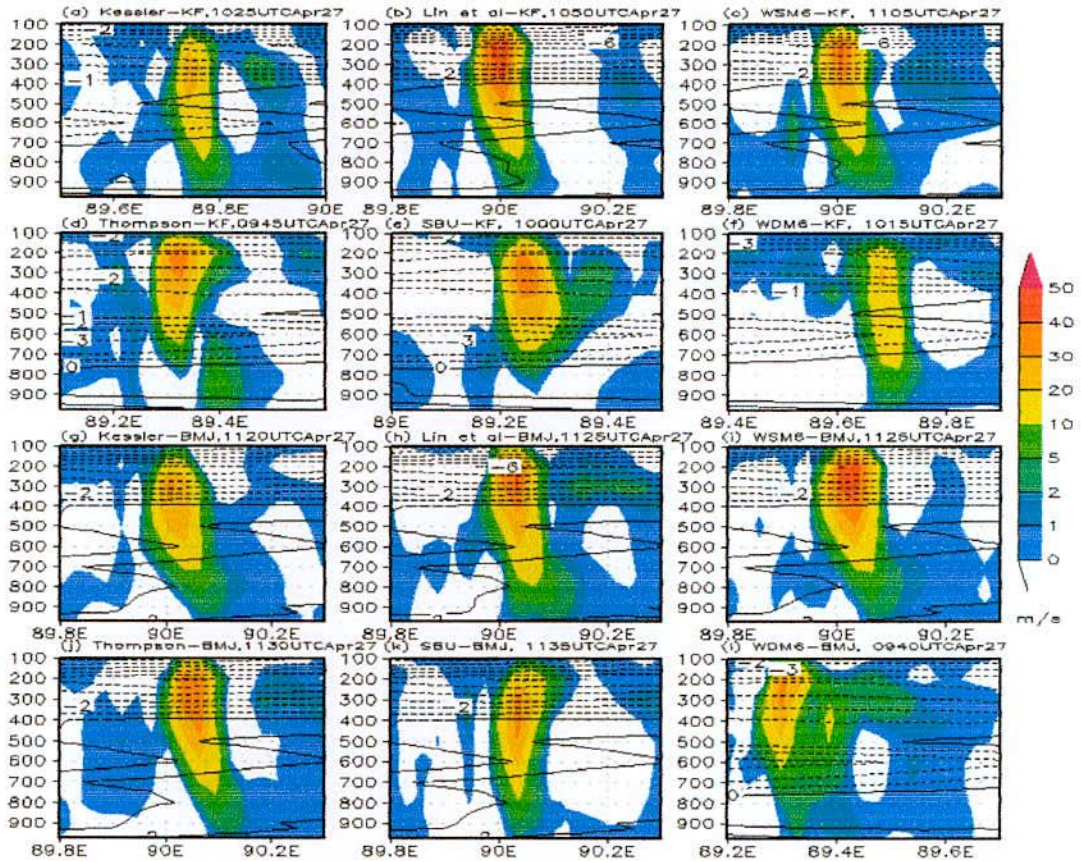


Fig. 4.3.3: WRF Model simulated maximum vertical velocity (shaded) and vorticity (contour, $\times 10^{-5}/s$) along the line of maximum vertical velocity using Kessler, Lin *et al.*, WSM6, Thomson, SBU and WDM6 schemes coupling with (a-f) KF and (g-l) BMJ schemes on 27 April 2014.

4.3.6 Relative Humidity (RH)

The model simulated time variation of RH at 2m level for six different MPs in combination with KF and BMJ schemes are presented in Figs. 4.3.1(g-h). The RH is found maximum after 1800 UTC for all MPs coupling with KF and BMJ schemes. The maximum RH is 66, 53 and 55% for KS-KF, Lin-KF and WSM6-KF at 1935, 1925 and 1925 UTC respectively. Again the RH is 68, 67 and 68 % at around 2055 UTC for KS-KF, Lin-KF and WSM6-KF

combinations respectively. The RH is increased (Fig. 4.3.1h) for Kessler-BMJ, WSM6-BMJ and WDM6-BMJ at 1940, 1945 and 1950 UTC respectively. The significant increase of RH after 1920 UTC is found positive for the occurrence of squall at Sylhet.

Figs. 4.3.2(g-h) depict model simulated RH at 2m level at Khulna. After 1015 UTC the RH is increased significantly and then it has been changed in an irregular pattern for all MPs coupling with KF (Fig. 4.3.2g) and BMJ (Fig. 4.3.2h) schemes. The maximum RH is found at 1015, 1020, 1030 and 1035 UTC for WSM6, WDM6, TH and Lin *et al.* coupling with KF schemes. The maximum RH is found at 1050 UTC for KS-BMJ and Lin-BMJ combinations. The RH decreased and it increased significantly again during 1500-2200 UTC indicates the possibility of occurrence of squall at Khulna.

The RH (contour) is simulated along the line of maximum vertical velocity using different MPs coupling with KF and BMJ schemes and is presented in Figs. 4.3.4(a-l). All MPs coupling with KF and BMJ schemes have simulated RH up to 100 hPa. The RH > 90% is simulated for all MPs in combination with KF and BMJ schemes up to 200 hPa levels where the vertical velocity and reflectivity is found maximum.

4.3.7 Maximum Reflectivity (MR)

Reflectivity (dBZ) is not simulated at Sylhet for six different MPs coupling with KF and BMJ schemes. The model simulated time variation of MR for six different MPs coupling with KF and BMJ schemes at Khulna are presented in Figs. 4.3.1(i-j). Starting from 0940 to 0955 UTC (Fig. 4.3.1i) reflectivity is found for TH-KF and WDM6-KF combinations and the MR 15.74 and 12.71dBZ is simulated by TH-KF and WDM6-KF combinations at 0945 and 0950 UTC respectively. The MR 15.89, 43.89 and 39.68dBZ are simulated by Lin-KF, WSM6-KF and WDM6-KF at 1145, 1135 and 1125 UTC respectively. The presence of maximum reflectivity (Fig. 4.3.1j) is seen after 1030 UTC for BMJ scheme coupling with MPs. The MR 28.10, 20.92 and 37.31dBZ are simulated by KS-BMJ, WSM6-BMJ and SBU-BMJ combinations at 1055, 1045 and 1055 UTC, which is positive for squall at Khulna.

The reflectivity (shaded, dBZ) is simulated along the line of maximum vertical velocity using different MPs coupling with KF and BMJ schemes and are presented in Figs. 4.3.4(a-l). Kessler and SBU schemes in combination with KF and BMJ schemes are simulated reflectivity up to 200 hPa. All other MPs coupling with KF and BMJ schemes are simulated

reflectivity up to 100 hPa. The reflectivity > 60dBZ is simulated for Lin *et al.*, WSM6, Thompson and WDM6 schemes in combination with KF and BMJ schemes where the up draft is found maximum. The reflectivity is found maximum at 500-300, 600-400, 400-300, 600-300 and 500-300 hPa level for Lin-KF, TH-KF, Lin-BMJ, TH-BMJ and WDM6-BMJ combinations respectively. WSM6-KF, WDM6-KF and WSM6-BMJ combinations are also simulated reflectivity at 550-450, 650-300 and 550-300 hPa level respectively.

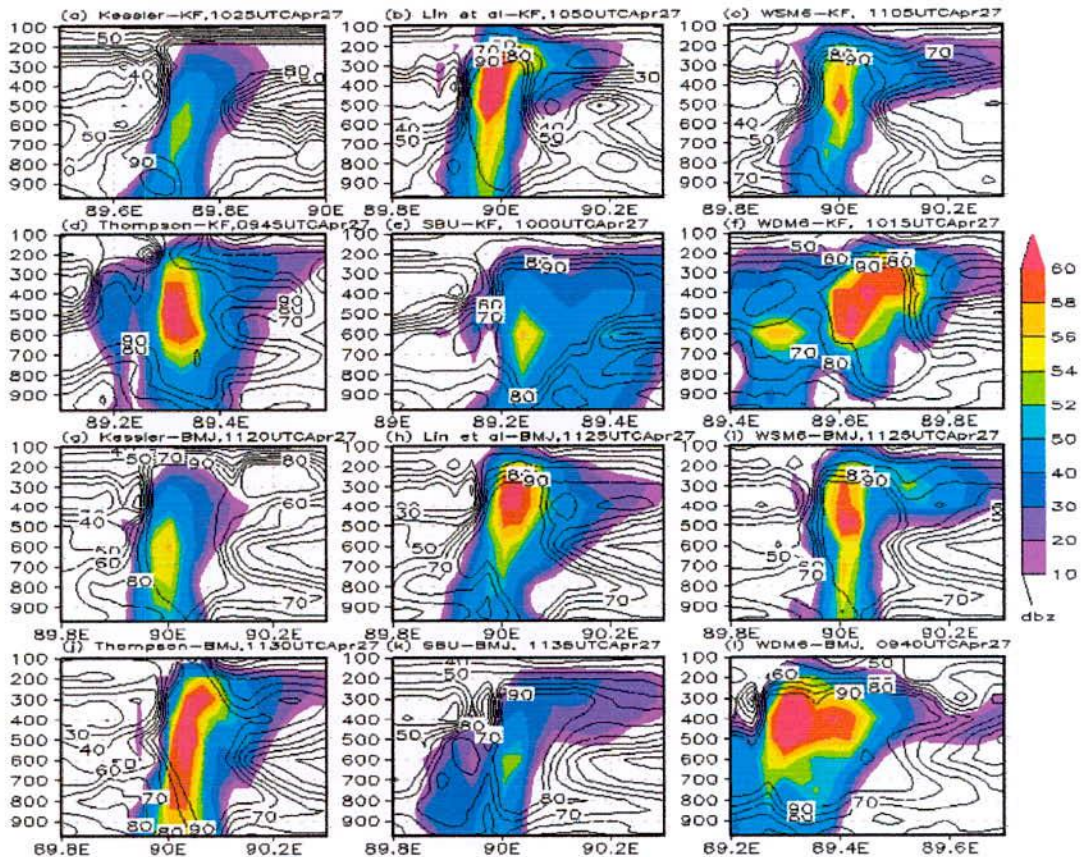


Fig. 4.3.4: WRF Model simulated reflectivity (shaded) and RH (contour) along the line of maximum vertical velocity using Kessler, Lin *et al.*, WSM6, Thomson, SBU and WDM6 schemes coupling with (a-f) KF and (g-l) BMJ schemes on 27 April 2014.

4.3.8 Cross Total Index (CT)

The model simulated time variation of CT at Sylhet for six different MPs coupling with KF and BMJ schemes are presented in Figs. 4.3.5(a-b). From 1700 to 1930 UTC (Fig. 4.3.5(a-b)) the CT lies between 20 to 21°C for all MPs coupling with KF and BMJ schemes indicates

strong potential for thunderstorms and after that it is slowly increased. Due to the increase of CT at Sylhet there is a possibility of occurrence of squall during 1700 to 1930 UTC.

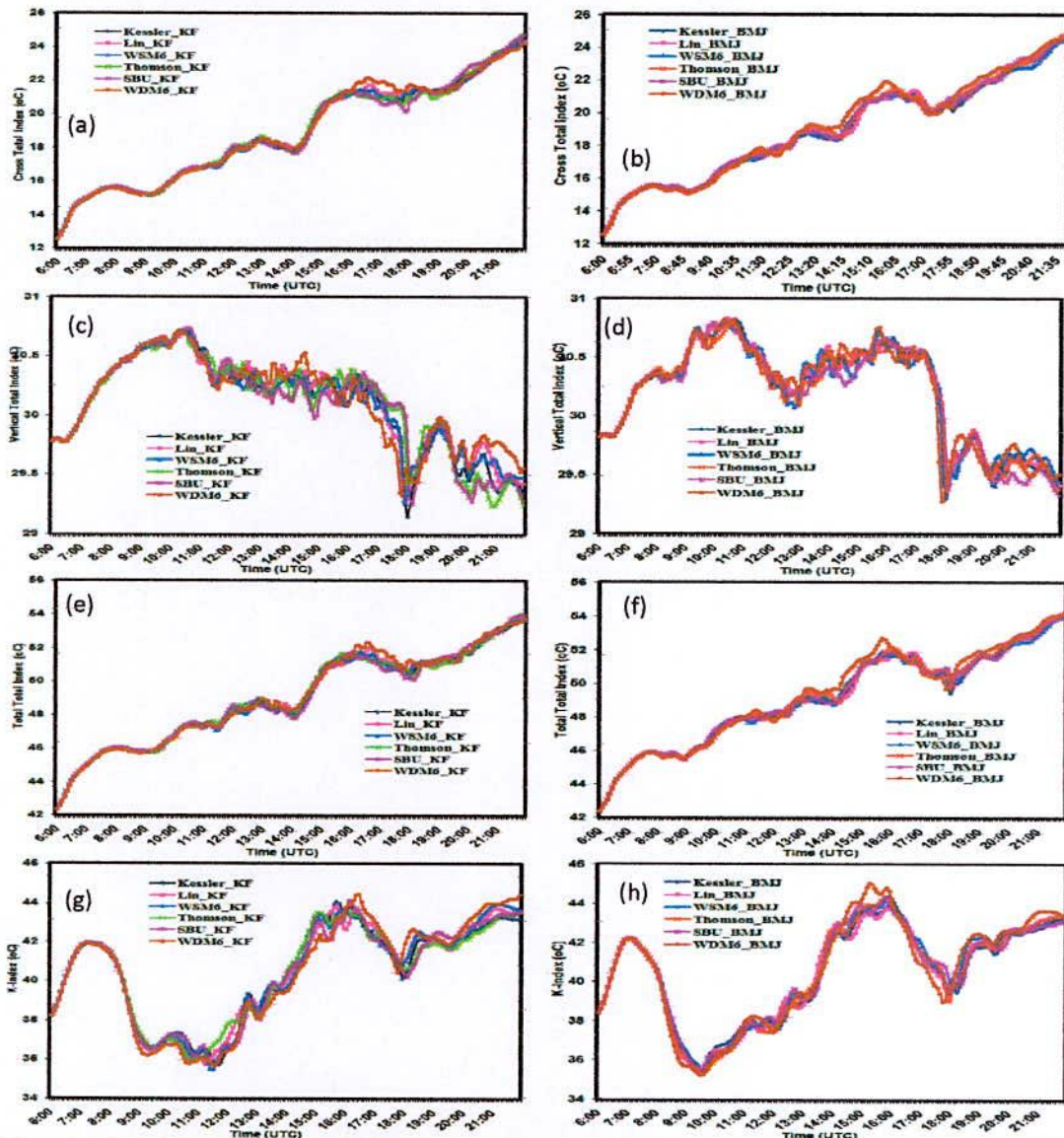


Fig. 4.3.5: Time variation of (a-b) CT, (c-d) VT, (e-f) TT and (g-h) K-Index using six different MP schemes coupling with KF and BMJ schemes at Sylhet on 27 April 2014.

Figs. 4.3.6(a-b) depict model simulated CT at Khulna. Starting from 0720 to 0820 UTC the CT > 20°C for all MPs coupling with KF and BMJ schemes indicates strong potential for thunderstorms and after that it is decreased slowly and then fluctuates continuously for all MPs coupling with KF and BMJ schemes. The maximum CT 23.21°C is simulated (Fig.

4.3.6a) at 1030 UTC by SBU-KF combination indicates weak potential for severe thunderstorms. It is found to increase CT after 1030 UTC (Fig. 4.3.6b) for all MPs coupling with BMJ scheme and CT lies between 18 to 19°C for KS-KF, Lin-KF, WSM6-KF and WDM6-KF combinations indicates moderate potential for the occurrence of thunderstorms.

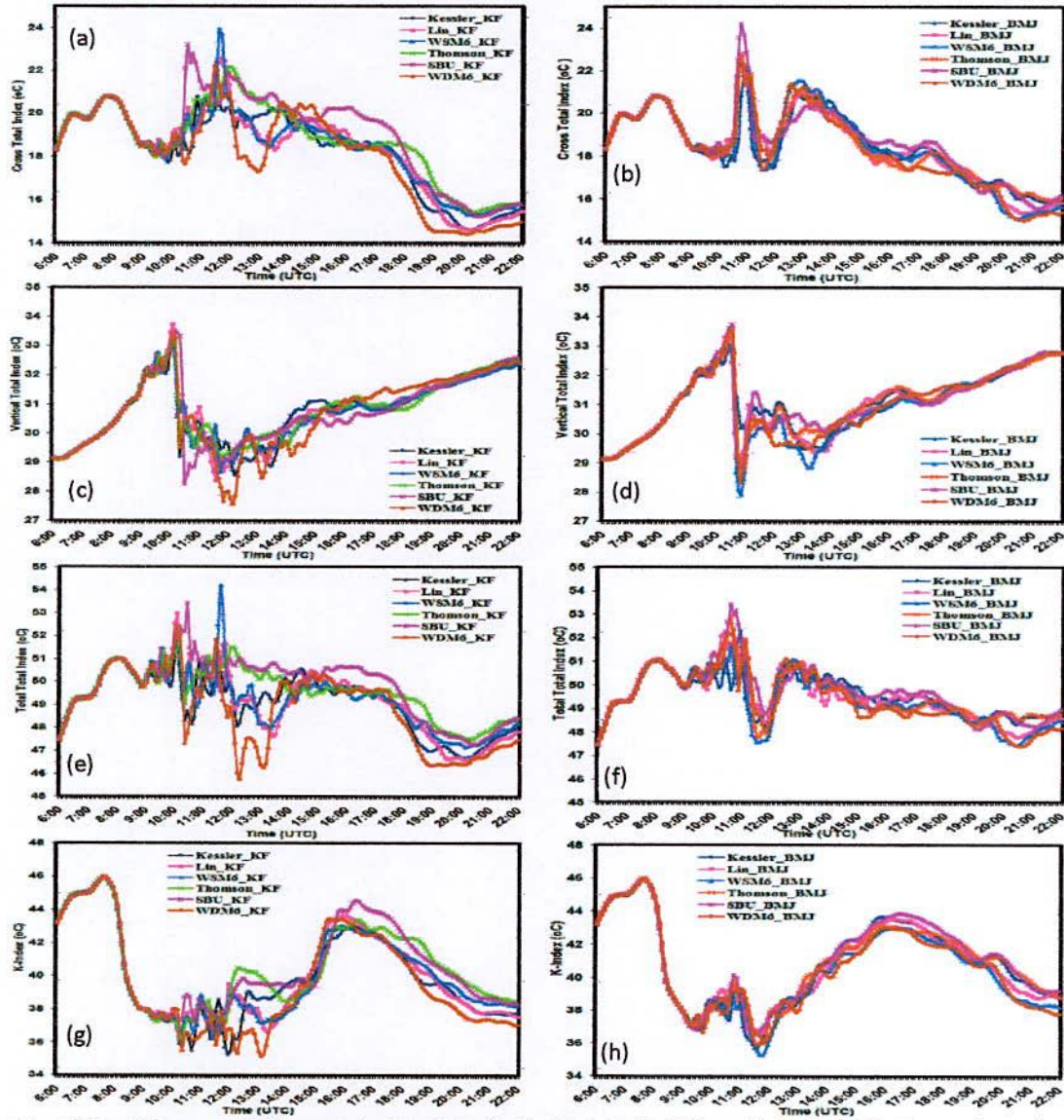


Fig.4.3.6: Time variation of (a-b) CT, (c-d) VT, (e-f) TT and (g-h) K-Index using six different MP schemes coupling with KF and BMJ schemes at Khulna on 27 April 2014.

The CT is simulated maximum 22.82, 22.54 and 22.67°C at 1045 UTC by Lin-BMJ, TH-BMJ and WDM6-BMJ combinations indicates weak potential for severe thunderstorms and

24.19°C for SBU-BMJ combinations indicates moderate potential for severe thunderstorms to occur at Khulna.

4.3.9 Vertical Totals Index (VT)

The model simulated time variation of VT for six different MPs coupling with KF and BMJ schemes at Sylhet are presented in Figs. 4.3.5(c-d). Starting from 0630 UTC (Fig. 4.3.5c) the VT has increased continuously up to 0945 UTC and then decreased for a short period and then again increased up to 1025 UTC for all MPs coupling with KF scheme. From 0705 to 1600 UTC, the VT > 30°C for all MPs coupling with KF scheme indicates strong potential for the occurrence of severe thunderstorm. The VT is found to increase in an irregular pattern (Fig. 4.3.5d) during 0600 to 1040 UTC and after that it decreased for all MPs coupling with BMJ scheme. From 0655 to 1700 UTC, the value of VT > 30°C for all MPs coupling with BMJ scheme indicates strong potential for the occurrence of severe thunderstorms.

Figs. 4.3.6(c-d) depict model simulated VT at Khulna. Starting from 0600 UTC (Fig. 4.3.6(c-d)) the VT has increased continuously up to 1005 and 1025 UTC and then decreased sharply for all MPs coupling with KF and BMJ schemes respectively. During 0600 to 1145 and 0600 to 1045 UTC the VT is simulated greater than 28°C for all MPs coupling with KF and BMJ schemes respectively indicates strong potential for the occurrence of severe thunderstorm.

4.3.10 Total Totals Index (TT)

The model simulated time variation of TT Index for six different MPs coupling with KF and BMJ schemes at Sylhet are shown in Figs. 4.3.5(e-f). The TT lies between 44 to 50°C during 0630 to 1505 UTC (Fig. 4.3.5e) for all MPs coupling with KF scheme indicates the occurrence of likely thunderstorms and then up to 2050 UTC the TT > 51°C for all MPs coupling with KF scheme indicates the occurrence of isolated severe storms and after that the TT > 53°C for all MPs coupling with KF scheme indicates the occurrence of widely scattered severe storms at Sylhet. The TT is simulated greater than 51°C (Fig. 4.3.5f) during 1500 to 1700 UTC for all MPs coupling with BMJ scheme indicates the occurrence of isolated severe storms and then up to 1830 UTC the value of TT is 49 to 50°C indicates to the occurrence of likely thunderstorms and after 1830 UTC the TT lies between 51 to 52°C for all MPs coupling with BMJ scheme indicates the occurrence of isolated severe storms at Sylhet.

Figs. 4.3.6(e-f) depict model simulated TT at Khulna on 27 April 2014. Starting from 0600 to 0750 UTC (Fig. 4.3.6e) the TT lies between 44 to 50°C for all MPs coupling with KF scheme indicates the occurrence of likely thunderstorms and at 0805 UTC the TT > 51°C for all MPs coupling with KF scheme indicates the occurrence of isolated severe storms and after up to 0950 UTC the TT lies between 44 to 50°C for all MPs coupling with KF scheme indicates the occurrence of likely thunderstorms. At around 1000 UTC for 15 minutes, the TT > 51°C for all MPs coupling with KF scheme indicates the occurrence of isolated severe storms and then TT is 48 to 50°C for all MPs coupling with KF scheme indicates the occurrence of likely thunderstorms. The maximum TT is simulated 52.99 and 53.42°C by Lin-KF and SBU-KF combinations at 1005 and 1025 UTC which indicates the occurrence of widely scattered severe storms. From Fig. 4.3.6f, the TT is increased at around 0805 UTC after that fluctuates for all MPs coupling with BMJ scheme. The maximum TT is simulated 52.88 and 53.43°C by TH-BMJ and SBU-BMJ combinations at 1035 UTC, which indicates the occurrence of widely scattered severe storms.

4.3.11 K Index (KI)

The model simulated time variation of KI for six different MPs coupling with KF and BMJ schemes at Sylhet are presented in Figs. 4.3.5(g-h). Starting from 1415 UTC (Fig. 4.3.5g) the KI has increased up to 1620 UTC and also fluctuates and after that it has decreased for all MPs coupling with KF scheme. The KI > 40°C during 1415 to 2200 UTC indicates extremely unstable atmosphere for all MPs coupling with KF scheme. Starting from 1335 UTC (Fig. 4.3.5h) the KI has increased at around 1545 UTC and after that it has decreased and also fluctuates for all MPs coupling with BMJ scheme. The KI > 40°C during 1335 to 2200 UTC indicates extremely unstable atmosphere for all MPs coupling with BMJ scheme and the maximum KI 45°C is simulated at 1515 UTC by WDM6-BMJ combination at Sylhet.

Figs. 4.3.6(g-h) depict model simulated KI at Khulna. Starting from 0615 UTC the KI has increased at around 0740 UTC for all MPs coupling with KF and BMJ schemes. After that it has decreased sharply (Fig. 4.3.6g) and reached minimum at around 1015 UTC and then fluctuates in an irregular pattern for all MPs coupling with KF scheme. From 0600 to 0820 UTC the KI > 40°C indicates extremely unstable atmosphere for all MPs coupling with KF scheme and then up to 1040 UTC the KI lies between 36 to 40°C, indicates very unstable

atmosphere for the occurrence of very likely thunderstorms for all MPs coupling with KF scheme except KS-KF and WDM6-KF combinations. At around 0745 UTC (Fig. 4.3.6h) the KI has decreased sharply up to 0925 UTC and then fluctuates for all MPs coupling with BMJ scheme. The KI > 40°C during 0600 to 0820 UTC indicates extremely unstable atmosphere for all MPs coupling with BMJ scheme. The KI > 42°C after 1600 UTC indicates very unstable case for the occurrence of very likely thunderstorms for all MPs coupling with BMJ scheme at Khulna.

4.3.12 Convective Available Potential Energy (CAPE)

The CAPE is simulated at Sylhet for six different MP schemes coupling with KF and BMJ schemes are presented in Figs. 4.3.7(a-b). The CAPE > 1000 J/kg has been simulated by KS-KF, Lin-KF, WSM6-KF and TH-KF during 1730-1740 UTC (Fig. 4.3.7a) and after that it has decreased and also fluctuates for all MPs at around 1850 UTC. From 1900 to 2125 UTC the 1000 < CAPE > 2500 J/kg has been simulated by KS-KF, Lin-KF and TH-KF, WSM6-KF, SBU-KF and WDM6-KF combinations that is moderately unstable condition for the formation of nor'wester/squall. The squall observed at 1851 UTC in Sylhet, the CAPE > 2500 J/kg is simulated by TH-KF and SBU-KF combinations at 2135 UTC which is extremely unstable condition of atmosphere for the formation of nor'wester. Starting from 1730 UTC it has decreased and then increased in an irregular pattern for all MPs coupling with BMJ scheme. The CAPE < 1000 and 1000 < CAPE > 2500 J/kg (Fig. 4.3.7b) during 1730 to 1850 UTC and 1900 to 2200 UTC respectively that is moderately unstable condition for all MPs coupling with BMJ scheme.

Figs. 4.3.8(a-b) depict model simulated CAPE at Khulna. At around 0850 (Fig. 4.3.8a) the CAPE < 1000 and has increased significantly at around 1035 UTC for all MPs coupling with KF scheme. The CAPE > 2500 J/kg has been simulated by TH-KF and SBU-KF at 1030 and 1105 UTC respectively which is extremely unstable condition of atmosphere for the formation of nor'wester. In the morning the CAPE is greater than 2100 J/kg and it has been (Fig. 4.3.8b) decreased up to 1030 UTC and attains the CAPE < 1000 J/kg for all MPs coupling with BMJ scheme. The CAPE > 2500 J/kg are simulated by Lin-BMJ, WSM6-BMJ, TH-BMJ and SBU-BMJ combinations at 1035, 1040, 1040 and 1040 UTC, which is extremely unstable condition of atmosphere for the formation of nor'wester.

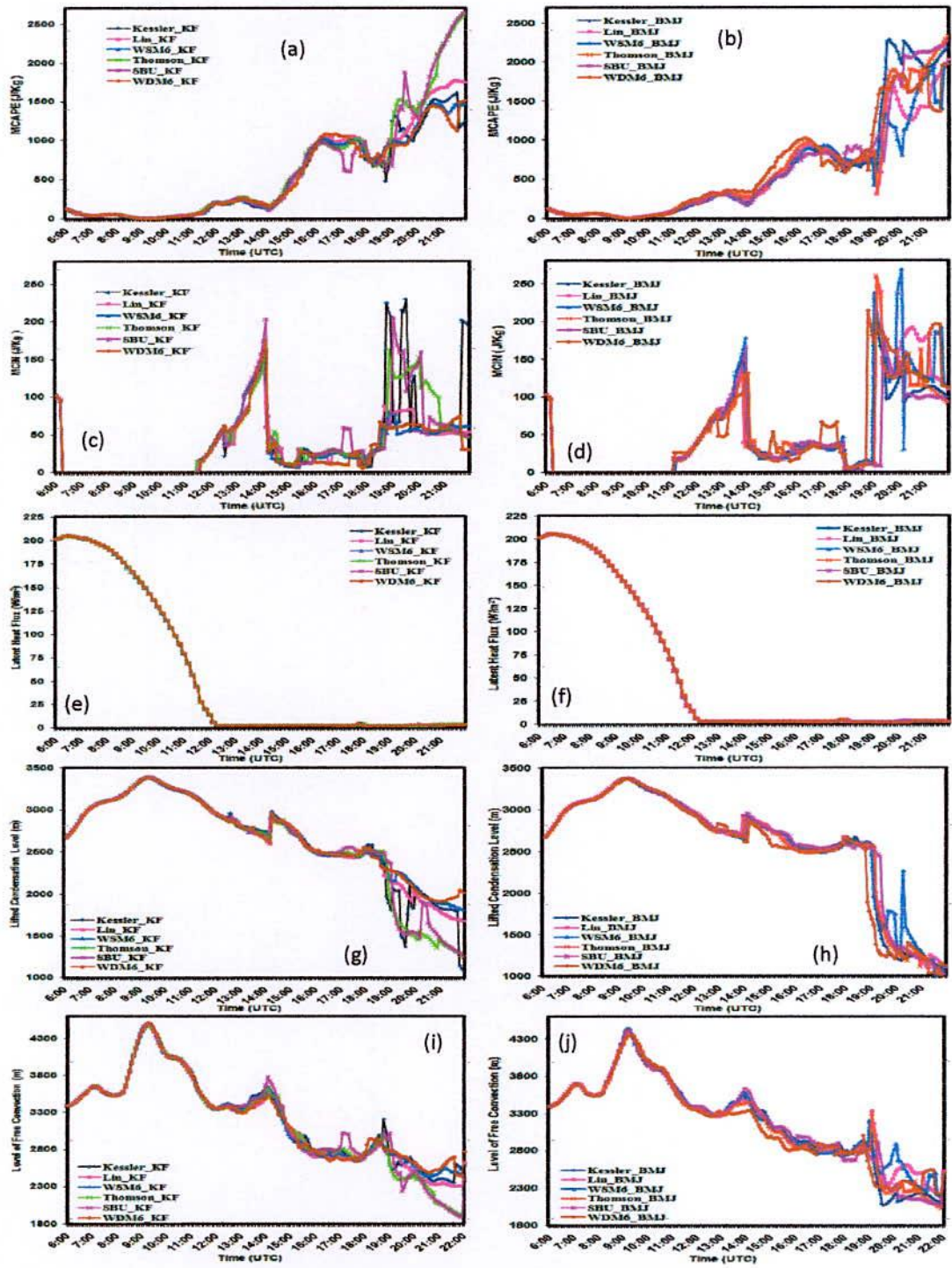


Fig. 4.3.7: Time variation of (a-b) MCAPE, (c-d) MCIN, (e-f) LH Flux, (g-h) LCL and (i-j) LFC using six different MP schemes coupling with KF and BMJ schemes at Sylhet on 27 April 2014.

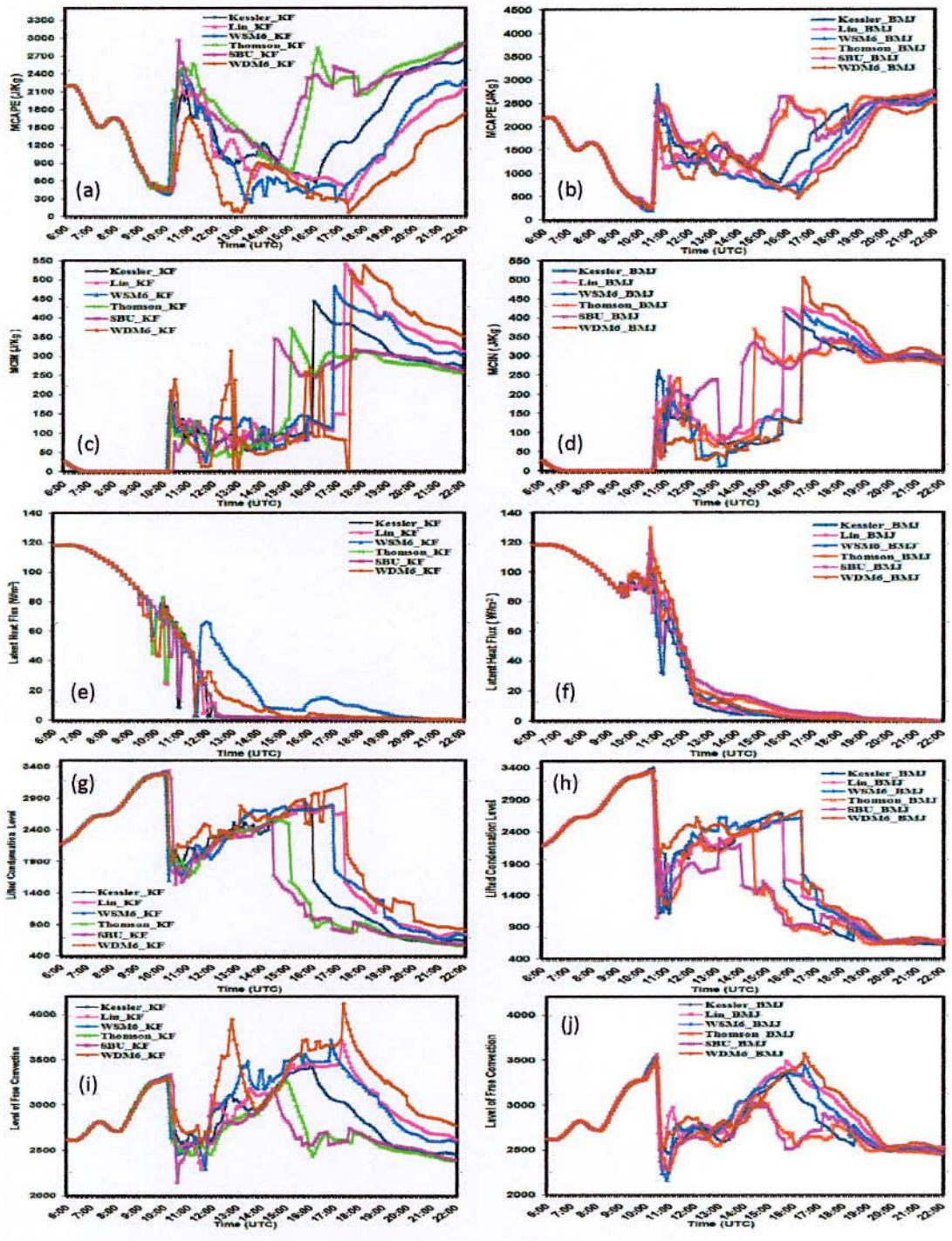


Fig. 4.3.8: Time variation of (a-b) MCAPE, (c-d) MCIN, (e-f) LH Flux, (g-h) LCL and (i-j) LFC using six different MP schemes coupling with KF and BMJ schemes at Khulna on 27 April 2014.

4.3.13 Convective Inhibition (CIN)

Model simulated time variation of CIN for six different MP coupling with KF and BMJ schemes at Sylhet is presented in Figs. 4.3.7(c-d). The simulated CIN is almost zero up to 1100 UTC after that it has increased and reached maximum at around 1405 UTC (Fig. 4.3.7(c-d)) and then sharply decreased towards zero for all MPs coupling with KF and BMJ schemes. From 1410 to 1840 UTC the CIN is seen minimum ($CIN < 50 \text{ J/kg}$) for all MPs coupling with KF and BMJ schemes, which indicates the atmosphere is potentially unstable for the occurrence of nor'wester.

At around 1350 UTC (Fig. 4.3.7d) the CIN is seen maximum which indicates that the atmosphere is marginally stable for all MPs coupling with BMJ scheme and then decreased at around 1855 UTC for all MPs coupling with BMJ scheme except WDM6-BMJ. The $CIN < 100 \text{ J/kg}$ during 1405 to 1855 UTC indicates that the atmosphere is potentially unstable for the occurrence of nor'wester. The CIN is greater than 200 J/kg for WDM6-BMJ at 1845 UTC and at 1900 UTC for KS-BMJ and WSM6-BMJ combinations.

WRF model simulated CIN at Khulna is described in Figs. 4.3.8(c-d). Starting from 0700 UTC (Fig. 4.3.8c) the CIN is 0.1 J/kg up to 1010 UTC, which indicates that the atmosphere is potentially unstable for the occurrence of nor'wester for all MPs coupling with KF schemes and then it increased significantly for all MPs coupling with KF scheme. Starting from 0700 UTC (Fig. 4.3.8d) the CIN is 0.1 J/kg up to 1025 UTC, which indicates that the atmosphere is potentially unstable for the occurrence of nor'wester for all MPs coupling with BMJ scheme. Then it is increased significantly for all MPs coupling with BMJ scheme.

4.3.14 Latent Heat (LH) Flux

Model simulated time variation of LH flux for six different MP coupling with KF and BMJ schemes at Sylhet is given in Figs. 4.3.7(e-f). The LH flux decreased sharply during 0600 to 1215 UTC and it is almost zero for all MPs coupling with KF and BMJ schemes all through the simulation time. The simulated LH flux at Khulna is given in Fig. 4.3.8(e-f). The LH flux has decreased continuously (Figs. 4.3.8(e-f)) during 0600 to 0915 UTC after that it is starting to fluctuate for different combination of MP and CP schemes at different time. The LH flux has increased again at 1000 UTC (Fig. 4.3.8e) for KS-KF, Lin-KF, WSM6-KF and TH-KF

combinations and then fluctuates for all MPs coupling with KF scheme. The huge amount of LH released at 1020 UTC in the atmosphere for Lin-KF and TH-KF combinations at Khulna. The huge amount of LH flux has been released (Fig. 4.3.8f) in the atmosphere at 1020 UTC for all MPs coupling with BMJ scheme. Then it is decreased significantly at around 1030 UTC for all MPs coupling with BMJ scheme.

4.3.15 Lifted Condensation Level (LCL)

Time variation of LCL for six different MPs coupling with KF and BMJ schemes at Sylhet is shown in Figs. 4.3.7(g-h). The LCL has decreased sharply and reached minimum 1362, 1450 and 1476m at 1930, 2000 and 2005 UTC KS-KF, TH-KF and SBU-KF combinations respectively (Fig. 4.3.7g) at Sylhet. The LCL has decreased sharply and reached minimum 1384m at 1905 by WDM6-BMJ combination and all other MPs in combination with BMJ scheme has simulated minimum one hour later than the observed squall at Sylhet. Model simulated LCL at Khulna is shown in Fig. 4.3.8(g-h). The LCL has decreased sharply and reached minimum 1856, 1706, 1611, 1838, 1543 and 1914 m at 1020, 1035, 1015, 1020, 1030 and 1020 UTC respectively for all MPs coupling with KF (Fig. 4.3.8g) scheme. The LCL has decreased sharply and reached minimum 1118, 1047, 1152, 1263, 1390 and 2020 m at 1040, 1035, 1050, 1055, 1055 and 1040 UTC respectively for all MPs coupling with BMJ (Fig. 4.3.8h) scheme at Khulna.

4.3.16 Level of Free Convection (LFC)

The LFC for six different MPs coupling with KF and BMJ schemes at Sylhet is shown in Figs. 4.3.7(i-j). The LFC has found oscillatory in nature and after 1900 UTC it has simulated minimum for all MPs coupling with KF and BMJ schemes at Sylhet. Figs. 4.3.8(i-j) depict model simulated LFC at Khulna. The LFC has increased and reached greater than 3300m at around 1005 UTC for all MPs coupling with KF and BMJ schemes at Khulna. After that it has decreased sharply and reached minimum 2540, 2511, 2455, 2440, 2149 and 2687m at 1050, 1035, 1035, 1105, 1030 and 1055 UTC for KS, Lin, WSM6, TH, SBU and WDM6 schemes coupling with KF scheme and 2418, 2373, 2158, 2267, 2280 and 2512m at 1035, 1035, 1050, 1055, 1050 and 1040 UTC for KS, Lin, WSM6, TH, SBU and WDM6 schemes respectively coupling with BMJ scheme at Khulna.

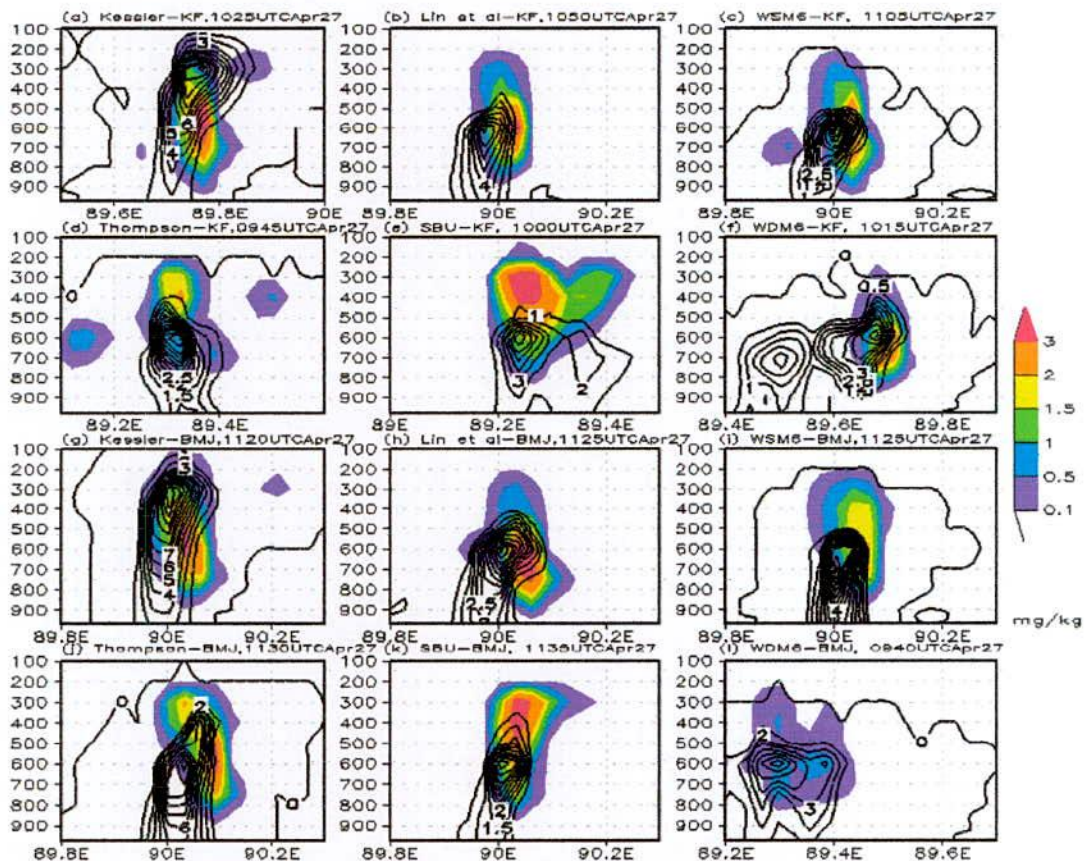


Fig. 4.3.9: Model simulated CWMR (shaded) and RWMR (contour) along the line of maximum vertical velocity using Kessler, Lin *et al.*, WSM6, Thomson, SBU and WDM6 schemes coupling with (a-f) KF and (g-l) BMJ schemes on 27 April 2014.

4.3.17 Rain Water Mixing Ratio (RWMR)

The RWMR (contour, mg/kg) has simulated along the line of maximum vertical velocity using different MPs coupling with KF and BMJ schemes and are presented in Figs. 4.3.9(a-l). Kessler scheme coupling with KF and BMJ schemes are simulated RWMR up to 100 hPa. WSM6 and TH coupling with KF and BMJ schemes are simulated RWMR up to 200 hPa. Lin *et al.*, and SBU coupling with KF and BMJ schemes are simulated RWMR up to 400 hPa. WDM6 scheme coupling with KF and BMJ schemes are simulated RWMR up to 300 hPa. The RWMR has simulated maximum at the position where the updraft and reflectivity is also maximum. The RWMR is found maximum 12 mg/kg at 400-300 hPa level for Kessler-BMJ. The maximum RWMR 11, 11, 8, 7 and 7 mg/kg have also been simulated by Kessler-

KF, Thompson-BMJ, Lin-KF, SBU-KF and WDM6-BMJ at 300, 600, 600, 600 and 600 hPa respectively.

4.3.18 Cloud Water Mixing Ratio (CWMR)

The CWMR (shaded, mg/kg) has simulated along the line of maximum vertical velocity using different MPs coupling with KF and BMJ schemes and are presented in Figs. 4.3.9(a-l). Lin-KF, WSM6-KF, TH-KF, Lin-BMJ, WSM6-BMJ, TH-BMJ, SBU-BMJ and WDM6-BMJ combinations have simulated RWMR up to 200 hPa. KS-KF, KS-BMJ and SBU-KF combinations have simulated RWMR up to 100 hPa. WDM6-KF has simulated RWMR up to 250 hPa. The CWMR is found maximum at 700-400 hPa level for Kessler, Lin, WSM6, Thompson and WDM6 schemes in combination with KF and BMJ schemes and at 800-250 hPa level for SBU scheme coupling with KF and BMJ schemes. The CWMR is found maximum at 700-500 hPa level for KS-KF, KS-BMJ and TH-BMJ combinations, at 450-250 hPa for SBU scheme and at 700-550 hPa for Lin *et al.*, scheme in combination with KF and BMJ schemes

4.4 Nor'wester of 15 May 2014

The squall line is observed at Barisal (22.75°N & 90.33°E) and Chittagong (22.26°N & 91.81°E) on 15 May 2014. The observed time of squall at Barisal was 0935 UTC and moved in the southeasterly direction with the maximum sustained wind speed 33.33 m/s. On that day the squall is also observed at Chittagong on 1200-1203 UTC moved in the northerly direction with the maximum sustained wind speed 11.66 m/s. Six different microphysics schemes e.g. Kessler, Lin *et al.*, WSM6, Thomson, SBU and WDM6 and two different cumulus parameterization e.g. KF and BMJ schemes for the simulation of squall/nor'wester over Barisal and Chittagong on 15 May 2014. All six different MPs in combination with KF and BMJ scheme is simulated squall at 1150 UTC over Bangladesh is presented in Fig. 4.4.1(a-l). The model simulated time and position of squall is different than observed.

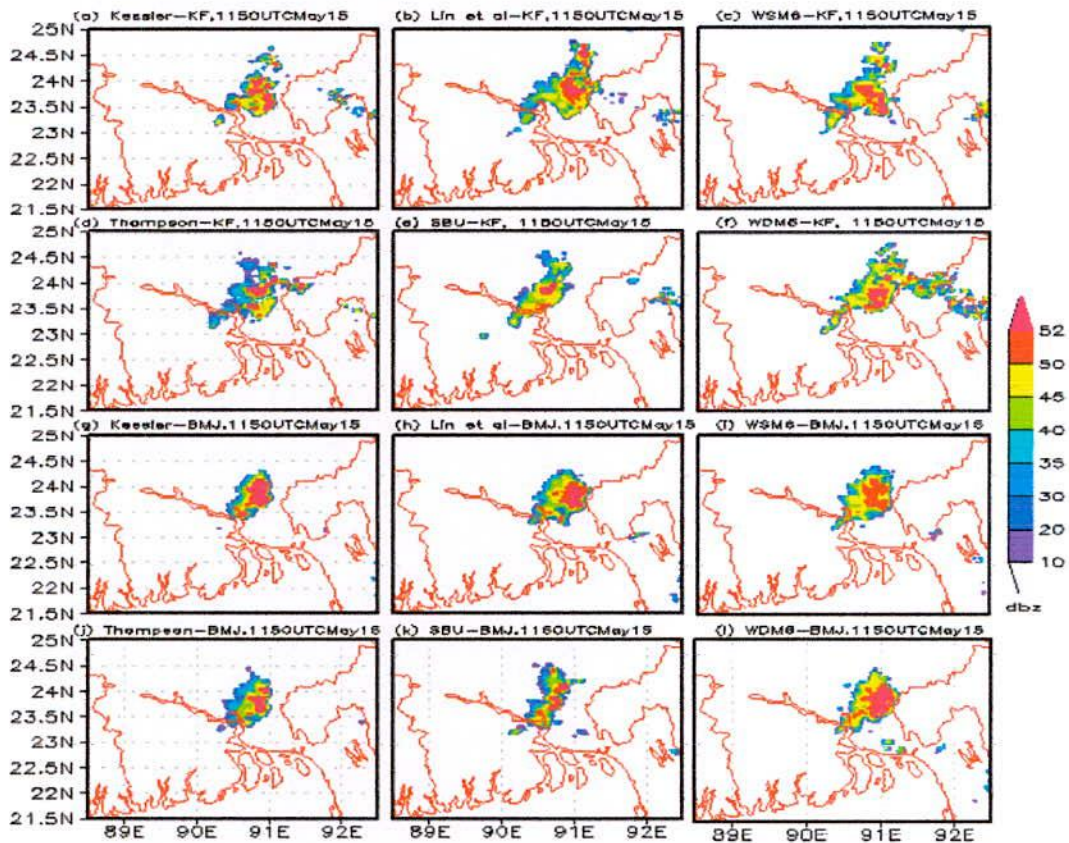


Fig. 4.4.1: Model simulated squall line for different MP schemes coupling with (a-f) KF and (g-l) BMJ schemes on 15 May 2014.

4.4.1 Sea Level Pressure (SLP)

Model simulated time variation of SLP for six different MPs coupling with KF and BMJ schemes at Barisal are presented in Figs. 4.4.2(a-b). The minimum SLP (Fig. 4.4.2a) 1001.6, 1000.9, 1001, 1001.6, 1001.4 and 1000.6 hPa are found for Kessler, Lin, WSM6, Thompson, SBU and WDM6 schemes coupling with KF scheme at 0850, 0915, 0935, 0900, 0910 and 0925 UTC respectively, which is close to the observed time (0935 UTC) of squall at Barisal. Again, the SLP is decreased significantly at around 1105 UTC and the second minima of SLP is simulated 1000.2, 999.9, 999.4, 1000.3, 1000.5 and 1000.4 hPa at around 1105 UTC by Kessler, Lin, WSM6, Thompson, SBU and WDM6 schemes in combination with KF scheme. The 1st and 2nd minima of SLP (Fig. 4.4.2b) is simulated at around 0900 and 1100 UTC respectively for all MPs coupling with BMJ scheme. The first minimum simulated SLP are 1001.5, 1001.7, 1001, 1001.8, 1001.5 and 1001.1 hPa and time at 0855 UTC by KS, Lin et al., WSM6, Thompson, SBU and WDM6 schemes in combination with BMJ scheme. The second minimum simulated SLP are 1000.2, 1000.2, 999.9, 999.75, 999.94 and 1000.4 hPa by KS, Lin et al., WSM6, Thompson, SBU and WDM6 schemes in combination with BMJ scheme and time are 1110, 1105, 1105, 1115, 1125 and 1140 UTC respectively.

Figs. 4.4.3(a-b) depict model simulated SLP at Chittagong. From Fig. 4.4.3(a-b), the SLP is decreased continuously and reached 1st minimum at around 0940 UTC and 2nd minimum at around 1140 UTC for all MPs coupling with KF and BMJ schemes. The 1st minima of SLP 1002.8, 1002.6, 1002.7, 1002.7, 1002.6 and 1002.6 hPa are simulated by Kessler, Lin, WSM6, Thompson, SBU and WDM6 schemes in combination with KF scheme at 0955, 0950, 1000, 0955, 1020 and 1000 UTC respectively. The 2nd minima of SLP is simulated 1002, 1001.7, 1002, 1001.8, 1001.4 and 1002.2 hPa by Kessler, Lin, WSM6, Thompson, SBU and WDM6 schemes in combination with KF scheme at 1135, 1140, 1140, 1140, 1155 and 1125 UTC respectively, which is close to the observed time (1200 UTC) of squall at Chittagong. The 1st minima of SLP 1002.7, 1002.7, 1002.6, 1002.7, 1002.5 and 1002.6 hPa is simulated by Kessler, Lin, WSM6, Thompson, SBU and WDM6 schemes in combination with BMJ scheme at 0940 UTC. The 2nd minim of SLP is simulated 1002.3, 1002.1, 1002.2, 1001.9, 1001.9 and 1001.4 hPa by Kessler, Lin, WSM6, Thompson, SBU and WDM6 schemes in combination with BMJ scheme at 1140, 1135, 1140, 1145, 1150 and 1150 UTC respectively which is close to the observed time (1200 UTC) of squall at Chittagong.

4.4.2 Maximum Wind Speed (MWS) at 10 m Level

Time variation of MWS (m/s) at 10m level simulated by six different MP schemes coupling with KF and BMJ schemes at Barisal is presented in Figs. 4.4.2(c-d). The MWS is simulated for all MPs coupling with KF scheme after 0900 UTC (Fig. 4.4.2c). The MWS 16.8 and 17.75 m/s is found for WDM6-KF combination at 0910 and 1005 UTC respectively, which is close to the observed time (0935 UTC) of squall at Barisal. The wind speed is simulated maximum 12.85, 18.9 and 14.2 m/s for Lin-KF, WSM6-KF and TH-KF combinations at 1020, 1020 and 1030 UTC respectively. From Fig. 4.4.2c, the first maxima of wind speed 14.1 and 11.7 m/s is found at 0910 and 0920 UTC for Lin-BMJ and WSM6-BMJ combinations. The MWS 16.2 and 16.1 m/s is simulated by Lin-BMJ and WSM6-BMJ combinations at 0945 and 0950 UTC respectively. After that, the wind speed 11.5, 13 and 13.9 m/s is found for Lin-BMJ, WSM6-BMJ and WDM6-BMJ combinations at 1205, 1210 and 1215 UTC respectively.

Figs. 4.4.3(c-d) depicts model simulated MWS at 10m level at Chittagong. From Fig. 4.4.3c, the wind speed is increased slowly up to around 1140 UTC and then fluctuates for all MPs coupling with KF scheme. The MWS 9.3, 11 and 11.6 m/s is simulated by Lin-KF, WSM6-KF and WDM6-KF combinations at 1440, 1425 and 1455 UTC. After 1400 UTC, the wind speed is simulated also maximum for Lin-KF, WSM6-KF and WDM6-KF combinations. From Fig. 4.4.3d, the wind speed is increased slowly in an oscillatory pattern up to around 1030 UTC and then decreased in an irregular pattern for all MPs coupling with BMJ scheme. Different MPs coupling with BMJ scheme is simulated very little wind at Chittagong on that day.

The model simulated MWS at 10m level were 28.5, 29.4, 27.8, 33.4, 23.3 and 35 m/s at 0455, 0510, 0510, 0705, 0655 and 0455 UTC by Kessler, Lin, WSM6, Thompson, SBU, WDM6 coupling with KF scheme and 30.5, 35.1, 34.2, 31.1, 24.4 and 33.3 m/s at 0500, 0455, 0500, 0540, 0515 and 0520 UTC by Kessler, Lin, WSM6, Thompson, SBU, WDM6 schemes coupling with BMJ scheme.

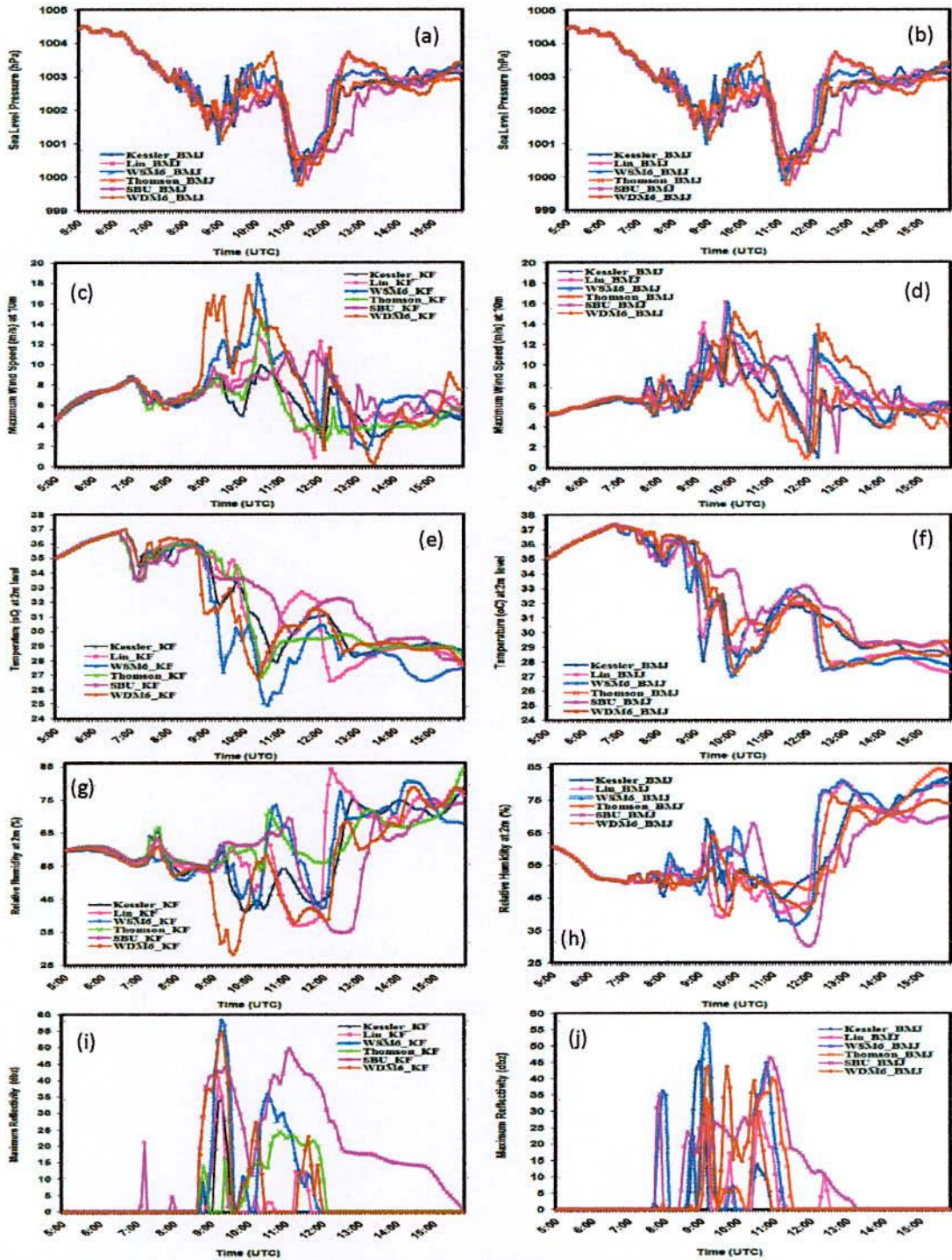


Fig. 4.4.2: Time variation of (a-b) SLP, (c-d) MWS at 10m, (e-f) Temperature at 2m, (g-h) RH at 2m and (i-j) Maximum reflectivity using six different MP schemes coupling with KF and BMJ schemes at Barisal on 15 May 2014.

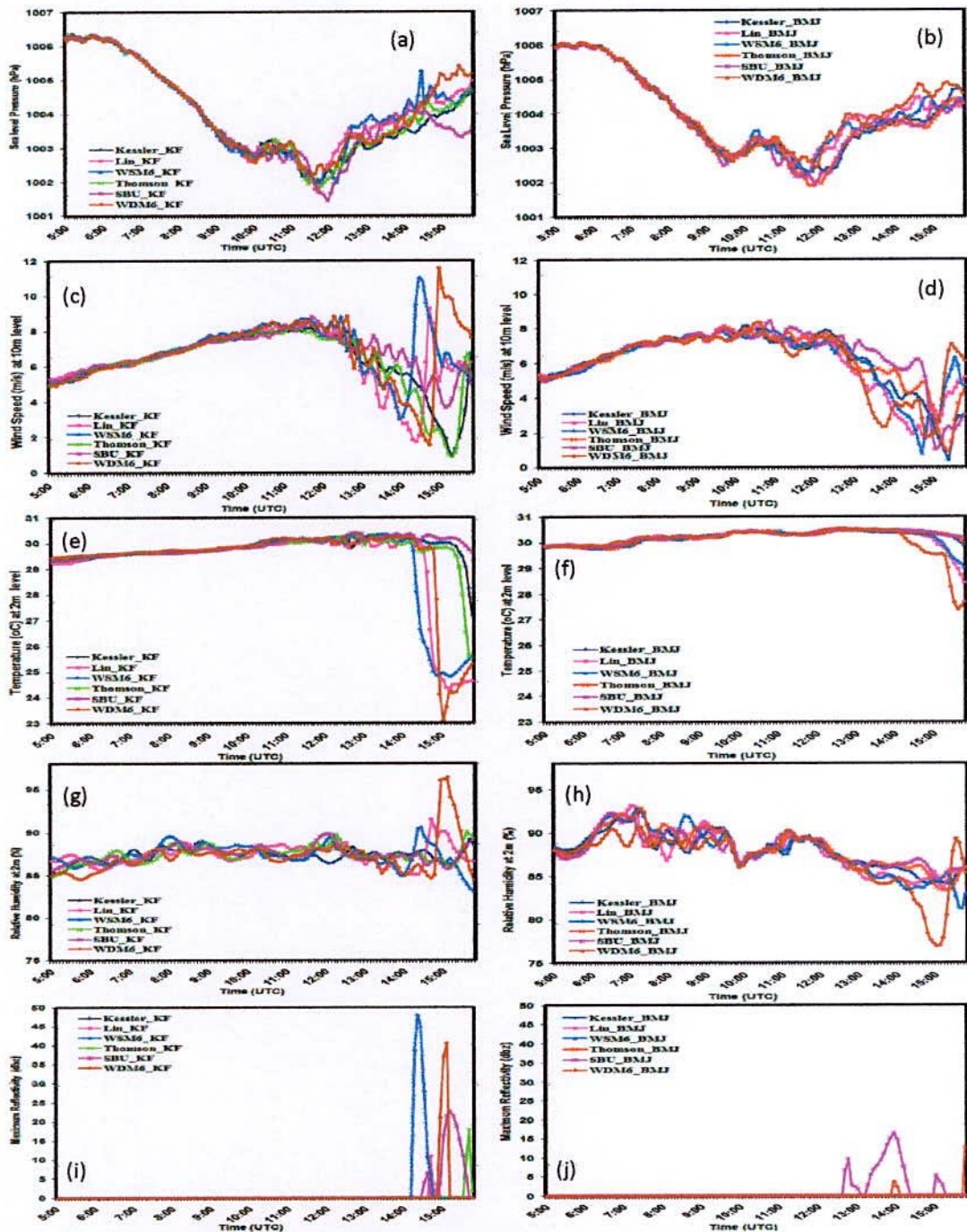


Fig. 4.4.3: Time variation of (a-b) SLP, (c-d) MWS at 10m, (e-f) Temperature at 2m, and (g-h) RH at 2m using six different MP schemes coupling with KF and BMJ schemes at Chittagong on 15 May 2014.

4.4.3 Temperature at 2m Level

Figs. 4.4.2(e-f) represent the time variation of temperature ($^{\circ}\text{C}$) at 2m Level at Barisal simulated by six different MPs in combination with KF and BMJ schemes. The temperature is increased sharply and reached maximum 37°C at 0640 UTC (Fig. 4.4.2e) after that it decreased and also fluctuates continuously for all MPs coupling with KF scheme. The temperature is decreased and reached minimum 27.6 , 24.9 , 26.8 and 26.7°C by Lin-KF, WSM6-KF, TH-KF and WDM6-KF combinations at 1025, 1035, 1025 and 1020 UTC respectively. WSM6-KF combination is also simulated much lower temperature 27.22°C at 0925 UTC, which is close to the time of observation. The temperature is increased sharply up to 0650 UTC (Fig. 4.4.2f) and reached maximum 27.3°C and then fluctuates and also decreased for all MPs in combination with BMJ scheme. The temperature is sharply decreased and reached minimum 27.05 and 27.25°C at 0955 and 1000 UTC for WSM6 and WDM6 schemes coupling with BMJ scheme.

WRF model simulated temperature ($^{\circ}\text{C}$) at 2m Level at Chittagong is presented in Figs. 4.4.3(e-f). The temperature at 2m level is increased (Fig. 4.4.3(e-f)) slowly up to 1200 UTC and then fluctuates for all MPs coupling with KF and BMJ schemes. The temperature is sharply decreased and reached minimum 24.36 , 24.82 and 23.1°C at 1510, 1510 and 1500 UTC for Lin-KF, WSM6-KF and WDM6-KF combinations respectively. After 1545 UTC the temperature decreased sharply and to reach 27.39°C for WDM6-BMJ combination.

4.1.4 Vertical Velocity

The maximum updraft for the heavy rainfall event on 15 May 2014 using different MPs coupling with KF and BMJ schemes are presented in Figs. 4.4.4(a-l). The maximum updrafts simulated times and positions are different in different combination of MPs and CP schemes (Figs. 4.4.4). The maximum updraft 32 , 40 , 40 , 37 , 43 and 38 m s^{-1} are simulated by Kessler, Lin *et al.*, WSM6, Thomson, SBU and WDM6 schemes coupling with KF scheme (Fig. 4.4.4) at the times of 1045, 1040, 0830, 1025, 1050 and 1055 UTC respectively. The maximum updraft 32 , 42 , 44 , 36 , 40 and 35 m s^{-1} simulated by Kessler, Lin *et al.* WSM6, Thomson, SBU and WDM6 schemes coupling with BMJ scheme at the times of 0645, 1100, 0650, 1100, 1130 and 0900 UTC respectively. WSM6 scheme simulated maximum updraft is earlier than that of observed squall at Barisal and Chittagong.

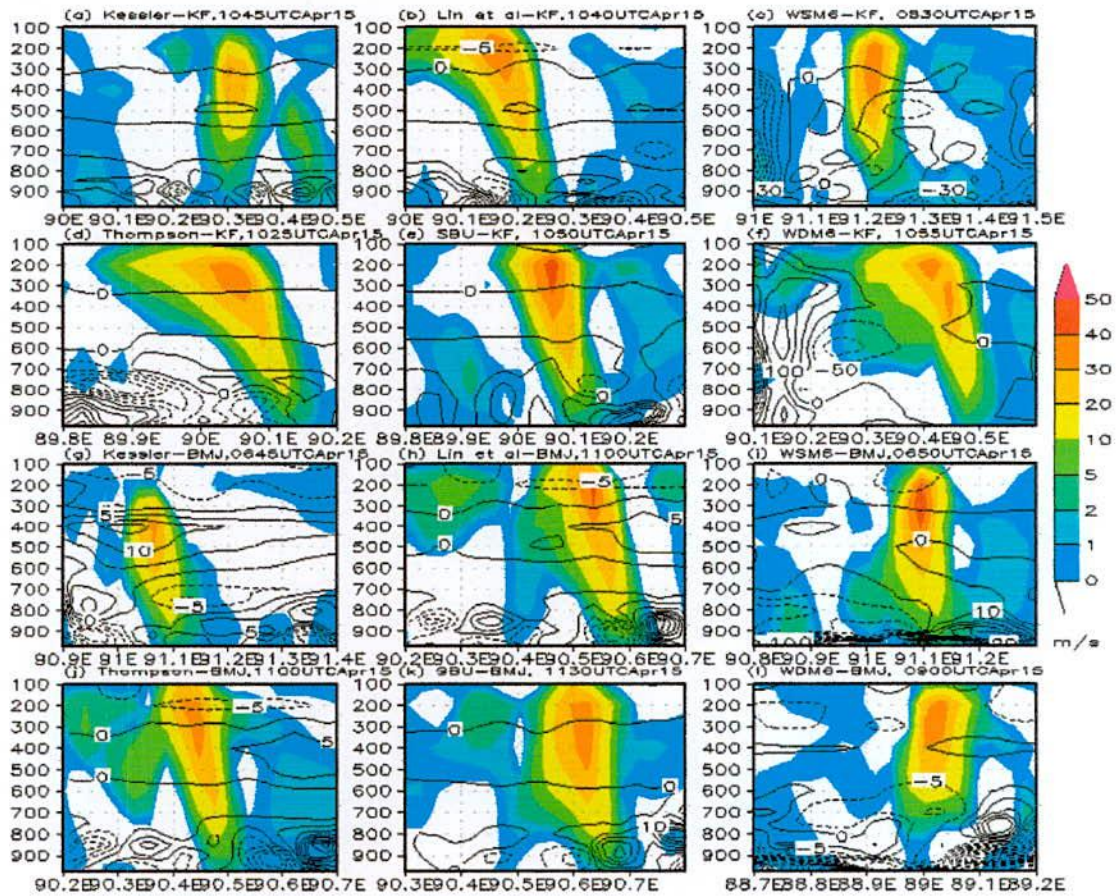


Fig. 4.4.4: WRF Model simulated maximum vertical velocity (shaded) and vorticity (contour, $\times 10^{-5}/s$) along the line of maximum vertical velocity using Kessler, Lin *et al.*, WSM6, Thomson, SBU and WDM6 schemes coupling with (a-f) KF and (g-l) BMJ schemes on 15 May 2014.

The maximum updraft is simulated at around 500–200 hPa for all MPs coupling with KF and BMJ schemes on 15 May 2014. The simulated updraft is found minimum by Kessler scheme coupling with KF and BMJ schemes on 15 May 2014.

4.4.5 Vorticity

Along the line of maximum updraft, vorticity (contour, $\times 10^{-5}/s$) is simulated by different MP schemes coupling with KF and BMJ schemes on 15 May 2014 and are presented in Figs. 4.4.4(a-l). All MPs in combination with KF and BMJ schemes are simulated positive vorticity along the vertical line, where the convection is significantly high and negative vorticity exists surroundings these high convection for all MPs in combination with KF and BMJ schemes

except TH-KF combination. Different MPs in combination with KF and BMJ schemes are simulated pockets of positive and negative vorticity at different levels, which indicates cyclonic and anticyclonic circulation exists side by side.

4.4.6 Relative Humidity (RH) at 2m Level

The model simulated time variation of RH at 2m level for six different MPs in combination with KF and BMJ schemes at Barisal have been drawn in Figs. 4.4.2(g-h). The first maxima of RH (Fig. 4.4.2g) at 2m level is found at 0730 UTC for all MPs coupling with KF scheme and fluctuates in an irregular pattern for all MPs coupling with KF scheme. The RH decreased significantly and reached minimum 28-29% during 0925-0935 UTC by WDM6-KF combination, 42% at 1010 UTC by WSM6-KF and 37-38% during 1105-1135 UTC by Lin-KF combination. Lin-KF has also been simulated maximum RH at 1210 UTC. The sharp decrease of RH is found by WDM6-KF combination at the time of observation of squall at Barisal. The maximum RH at 2m level are found 84.23 and 77.48% for Lin-BMJ and WSM6-BMJ combinations at 1210 and 1225 UTC respectively. The RH (Fig. 4.4.2h) have increased and reached maximum for Kessler-BMJ, WSM6-BMJ and TH-BMJ at 0910, 0920 and 0920 UTC respectively, which is close to the observational time (0935 UTC) of squall at Barisal. It has increased significantly after 1210 UTC for Lin-BMJ, WSM6-BMJ and WDM6-BMJ combinations.

Figs. 4.4.3(g-h) depict model simulated 2m level RH at Chittagong. From Fig. 4.4.3(g-h), the 2m level RH are simulated > 85% and also shown in an oscillatory pattern for all MPs in combination with KF and BMJ schemes. The RH has increased at around 1200 UTC for WSM6-KF, TH-KF and SBU-KF combinations, which is close to the observed time (1200 UTC) of squall at Chittagong. It has increased sharply for Lin-KF, WSM6-KF and WDM6-KF combinations after 1440 UTC. The RH are maximum (Fig. 4.4.3h) for Lin-BMJ, WSM6-BMJ and TH-BMJ combinations at 0700, 0710 and 0715 UTC respectively.

The RH (contour) are simulated along the line of maximum vertical velocity using different MPs coupling with KF and BMJ schemes and are presented in Figs. 4.4.5(a-l). All MPs coupling with KF and BMJ schemes have simulated RH up to 100 hPa. The RH have simulated > 90% for all MPs in combination with CPs up to 200 hPa level where the vertical velocity is found maximum.

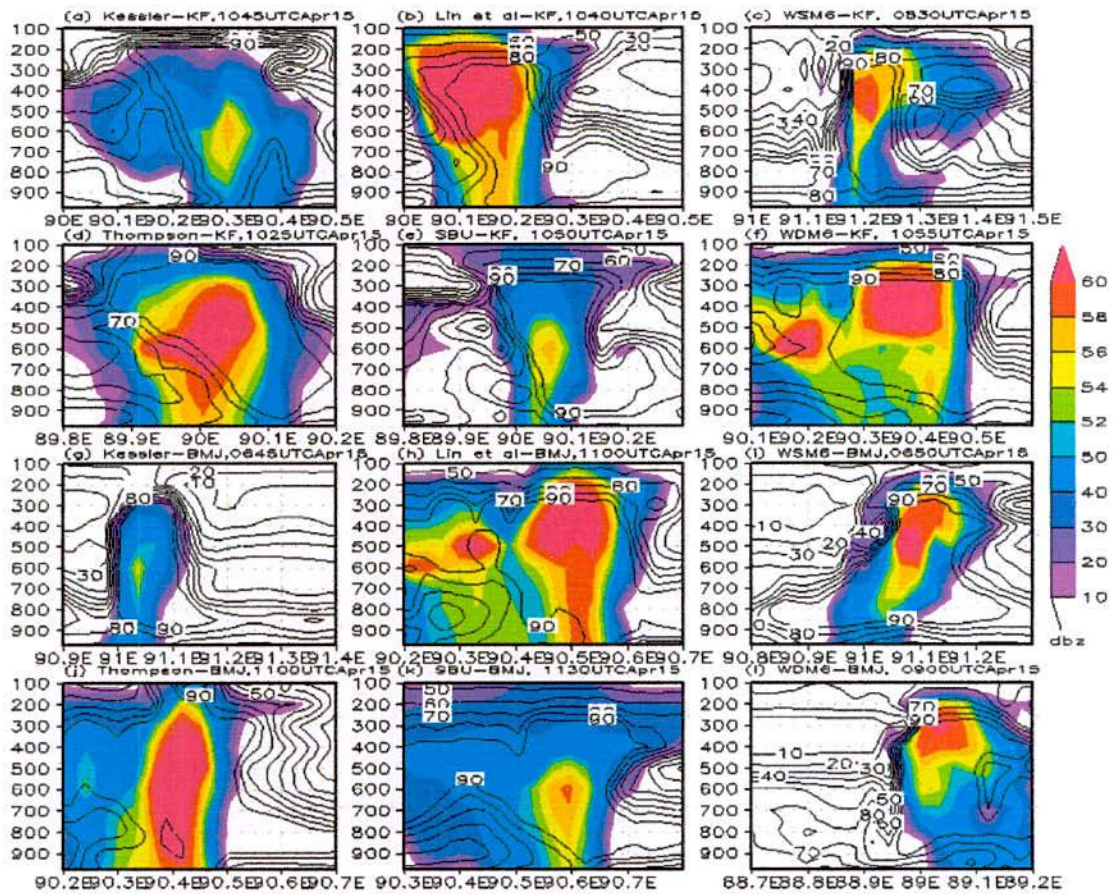


Fig. 4.4.5: WRF Model simulated reflectivity (shaded) and RH (contour) along the line of maximum vertical velocity using Kessler, Lin *et al.*, WSM6, Thomson, SBU and WDM6 schemes coupling with (a-f) KF and (g-l) BMJ schemes at 15 May 2014.

4.4.7 Maximum Reflectivity (MR)

The model simulated time variation of MR for six different MPs coupling with KF and BMJ schemes at Barisal is presented in Figs. 4.4.2(i-j). The reflectivity has been simulated (Figs. 4.4.2(i-j)) during 0800 to 1200 UTC for all MPs coupling with KF and BMJ schemes. The maximum reflectivity 58, 55 and 57 dBZ are simulated by WSM6-KF, WDM6-KF and WSM6-BMJ combinations at 0915, 0915 and 0905 UTC respectively at Barisal. All other MPs in combination with KF and BMJ schemes are not simulated significant amount of reflectivity. Figs. 4.4.3(i-j) depict model simulated MR at Chittagong. The significant reflectivity is simulated by WSM6-KF and WDM6-KF combinations after 1400 UTC and is almost zero for all MPs coupling with BMJ scheme.

The Reflectivity (shaded, dBZ) is simulated along the line of maximum vertical velocity using different MPs coupling with KF and BMJ schemes and are presented in Fig. 4.4.5(a-l). The maximum reflectivity > 60dBZ is simulated for Lin *et al.*, WSM6, TH and WDM6 coupling with KF and BMJ schemes. The Lin-KF, TH-KF, WDM6-KF, Lin-BMJ, TH-BMJ, WDM6-BMJ and WSM6 coupling with KF and BMJ schemes have been simulated maximum reflectivity at 600-200, 700-350, 600-300, 550-200, 900-300, 500-200, 600-200 and 600-300 hPa level respectively.

4.4.8 Cross Total Index (CT)

The model simulated time variation CT for six different MPs coupling with KF and BMJ schemes at Barisal are presented in Figs. 4.4.6(a-b). The CT has increased during 0500 to 0700 UTC (Fig. 4.4.6a) for all MPs coupling with KF scheme and the maximum value of CT > 26°C is found for KS-KF, WSM6-KF and WDM6-KF combinations indicates strong potential for the occurrence of severe thunderstorms at Barisal. After that, it has fluctuates in an irregular pattern for all MPs coupling with KF scheme and again the CT is reached maximum > 26°C for KS-KF and WSM6-KF combinations at 0905 and 0900 UTC indicates strong potential for severe thunderstorms.

The CT has increased (Fig. 4.4.6b) up to 0650 UTC after that it decreased for all MPs coupling with BMJ scheme. All MPs are simulated CT greater than 25°C during 0630 to 0730 UTC indicates strong potential for the occurrence of severe thunderstorms and the maximum CT is found 26.05°C by WDM6-BMJ combination at 0720 UTC. At 0900 UTC the CT > 21°C for Lin-BMJ, WSM6-BMJ and TH-BMJ combinations indicates strong potential for thunderstorms and the CT lies between 22 to 23°C for KS-BMJ, SBU-BMJ and WDM6-BMJ combinations indicates weak potential for the occurrence of severe thunderstorms at Barisal.

Figs. 4.4.7(a-b) depict model simulated CT at Chittagong. The CT has decreased up to around 1000 UTC (Fig. 4.4.7(a-b)) and then fluctuates in an irregular pattern for all MPs in combination with KF and BMJ schemes. The CT lies between 20 to 21°C during 0515 to 0720 UTC for all MPs coupling with KF and BMJ schemes and after 1230 UTC for Lin-KF, WSM6-KF, WDM6-KF, KS-BMJ, Lin-BMJ, WSM6-BMJ and WDM6-BMJ combinations indicates strong potential for the occurrence of thunderstorms at Chittagong.

4.4.9 Vertical Totals Index (VT)

The model simulated time variation of VT for six different MPs coupling with KF and BMJ schemes at Barisal are presented in Figs. 4.4.6(c-d). The VT has decreased (Fig. 4.4.6(c-d)) up to 0635 UTC and then fluctuates up to around 1220 UTC for all MPs coupling with KF and BMJ schemes. During 0820 to 0845 UTC and 0915 to 0955 UTC the VT is simulated greater than 29°C for all MPs in combination with KF scheme indicates strong potential for the occurrence of severe thunderstorms at Barisal. The maximum VT 31.7, 31.8, 31.6 and 32°C are simulated by KS-KF, Lin-KF, WSM6-KF and TH-KF combinations at 1140, 1145, 1140 and 1200 UTC. The VT > 28°C (Fig. 4.4.6d) during 0915 to 0955 UTC for all MPs in combination with BMJ scheme indicates strong potential for the occurrence of severe thunderstorms at Barisal. The maximum VT 31.19, 31.42, 31.31 and 31.52°C are simulated by KS-BMJ, Lin-BMJ, WSM6-BMJ and TH-BMJ combinations at 1130, 1150, 1200 and 1110 UTC respectively.

WRF model simulated VT at Chittagong are presented in Figs. 4.4.7(c-d). The VT has increased (Fig. 4.4.7c) up to 1125 UTC and reached greater than 28°C and then fluctuates in an irregular pattern indicates strong potential for the occurrence of squall for all MPs in combination with KF scheme. The VT found > 26°C is the favorable condition for the occurrence of thunderstorm for all MPs in combination with KF scheme at Chittagong. The VT is increased significantly (Fig. 4.4.7d) during 0500 to 1100 UTC and then fluctuates for all MPs coupling with BMJ scheme and > 28°C during 0700 to 1100 UTC for all MPs coupling with BMJ scheme indicates strong potential for the occurrence of severe thunderstorms and then up to 1230 UTC the VT > 26°C for KS-BMJ, WSM6-BMJ, TH-BMJ and SBU-BMJ combinations, which is favorable condition for the occurrence of a thunderstorm.

4.4.10 Total Totals Index (TT)

The model simulated time variation of TT for six different MPs coupling with KF and BMJ schemes at Barisal are shown in Figs. 4.4.6(e-f). The TT has increased continuously and fluctuating for all MPs coupling with KF scheme. The TT is found greater than 51°C (Fig. 4.4.6e) during 0700 to 0800 UTC indicates the occurrence of isolated severe storms and then

for short period TT is found greater than 50°C for KS-KF, WSM6-KF, SBU-KF and WDM6-KF combinations, which indicates the occurrence of likely thunderstorm at Barisal.

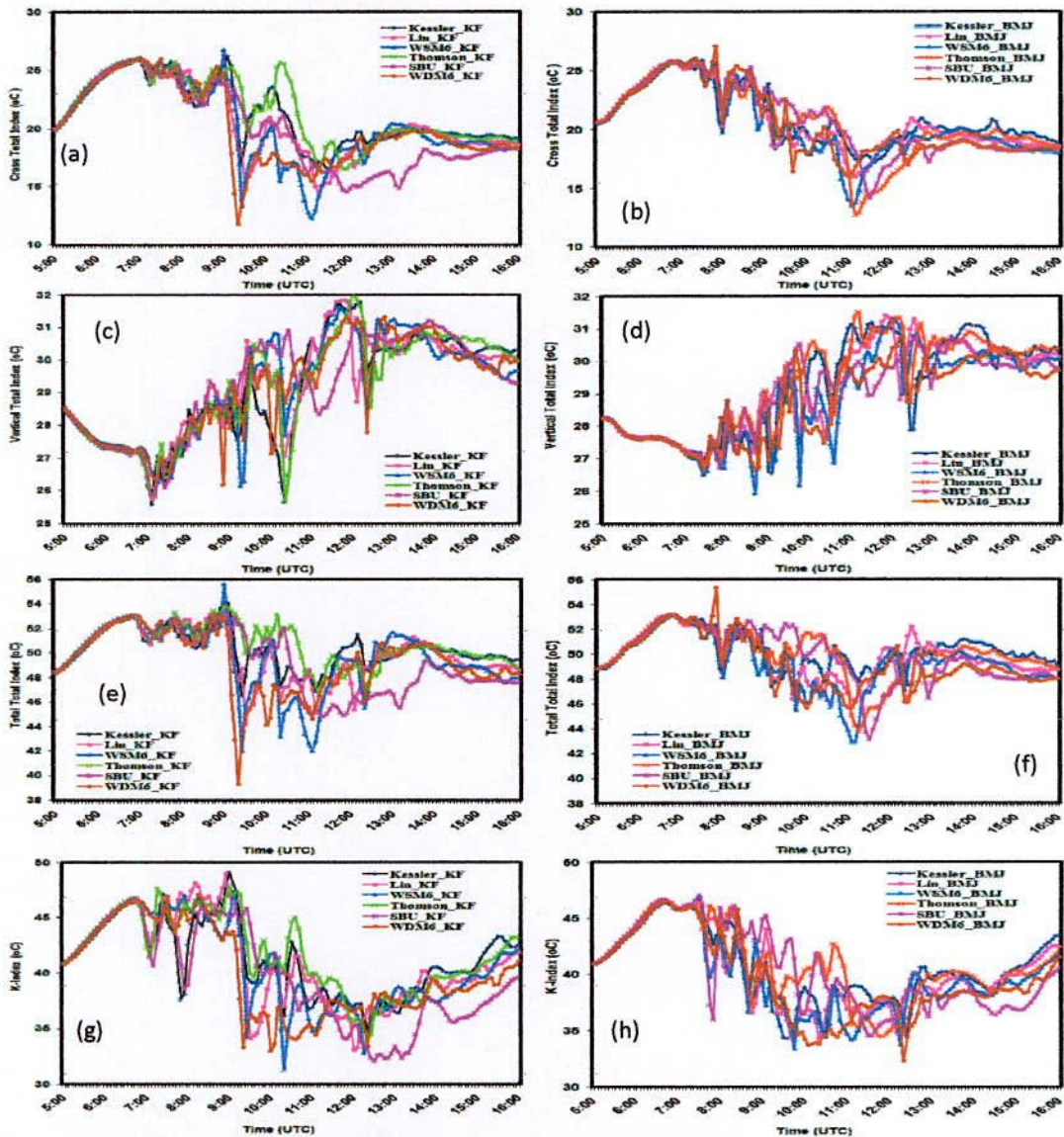


Fig. 4.4.6: Time variation of (a-b) CT, (c-d) VT, (e-f) TT and (g-h) K-Index using six different MP schemes coupling with KF and BMJ schemes at Barisal on 15 May 2014.

The maximum TT 54.1, 53.5, 55.6, 53.8, 53.1 and 53.1°C are simulated at 0905, 0900, 0900, 0900, 0905 and 0845 UTC for KS-KF, Lin-KF, WSM6-KF, TH-KF, SBU-KF and WDM6-KF combinations, indicates the occurrence of widely scattered severe storms. During 0700 to

0745 and 0805 to 0840 UTC the TT lies between 51 to 52°C (Fig. 4.4.6f) for all MPs coupling with BMJ scheme and then it also continue for SBU-BMJ combination, indicates the occurrence of isolated severe storms. The TT lies between 47 to 50°C after 0850 UTC for all MPs coupling with BMJ scheme except SBU-BMJ combination.

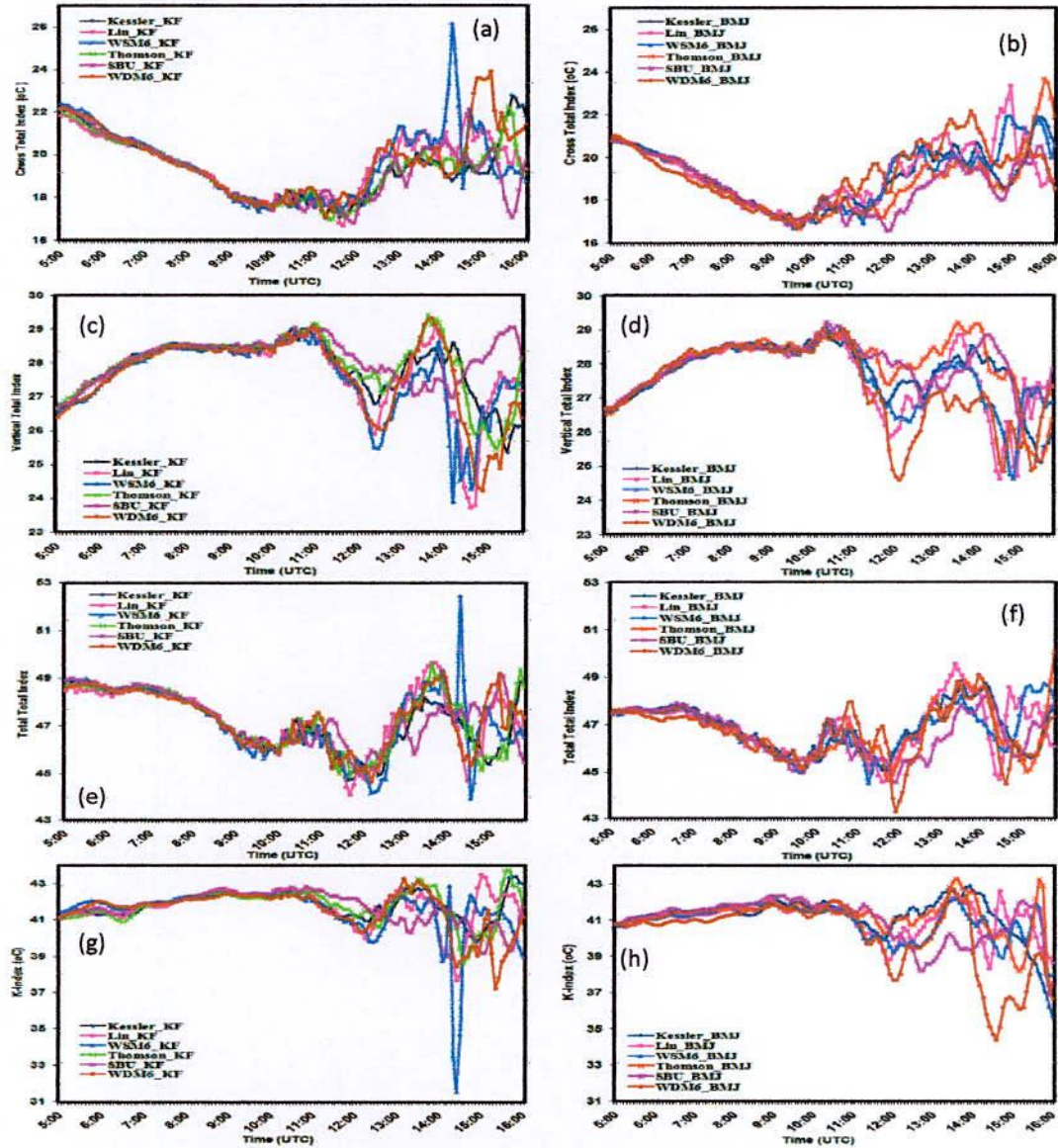


Fig. 4.4.7: Time variation of (a-b) CT, (c-d) VT, (e-f) TT and (g-h) K-Index using six different MP schemes coupling with KF and BMJ schemes at Chittagong on 15 May 2014.

WRF model simulated TT at Chittagong are presented in Figs. 4.4.7(e-f). The TT has decreased and fluctuates in an irregular pattern (Fig. 4.4.7(e-f)) up to 1200 UTC for all MPs in combination with KF and BMJ schemes. The TT lies between 44 to 49°C up to 1300 UTC for all MPs coupling with KF and BMJ schemes, indicates the occurrence of likely thunderstorms at Chittagong. The maximum TT is simulated 52.44°C (Fig. 4.4.7e) by WSM6-KF combination at 1415 UTC, indicates the occurrence of isolated severe storms and 50°C (Fig. 4.4.7f) by TH-BMJ combination at 1545UTC, indicates to the occurrence of likely thunderstorms.

4.4.11 K Index (KI)

The model simulated time variation of KI for six different MPs coupling with KF and BMJ schemes at Barisal are presented in Figs. 4.4.6(g-h). The KI has increased sharply up to 0640 UTC and then fluctuates in an irregular pattern for all MPs coupling with KF and BMJ schemes. The KI > 40°C up to 0745 and during 0800-0920 UTC (Fig. 4.4.6g) indicates extremely unstable and maximum possibility for the occurrence of thunderstorm for all MPs coupling with KF scheme. After 0920 UTC it has decreased for all MPs coupling with KF scheme. The maximum KI has found 48.95 and 49.11°C at 0855 and 0900 UTC for Lin-KF and KS-KF combinations indicates maximum possibility for the occurrence of thunderstorm at Barisal. The KI > 40°C up to 0830 UTC (Fig. 4.4.6h) indicates extremely unstable atmosphere for all MPs coupling with BMJ scheme. The KI > 40°C at 0905 UTC indicates the extremely unstable atmosphere for KS-BMJ, Lin-BMJ, TH-BMJ, SBU-BMJ and WDM6-BMJ combinations and then it continue up to 0945 UTC only for SBU-BMJ.combination, indicates maximum possibility the occurrence of thunderstorm.

Figs. 4.4.7(g-h) depict model simulated KI at Chittagong. Up to 1050 UTC (Fig. 4.4.7(g-h)) the KI is almost constant and then fluctuates for all MPs coupling with KF and BMJ schemes. The KI > 40°C during 0500 to 1210 UTC indicates extremely unstable atmosphere for all MPs coupling with KF and BMJ schemes. After that, it has decreased for Lin-KF and WSM6-KF combinations at 1215 and 1225 UTC when KI is 40 and 39.7°C, which is very unstable atmosphere, indicates the occurrence of very likely thunderstorms.

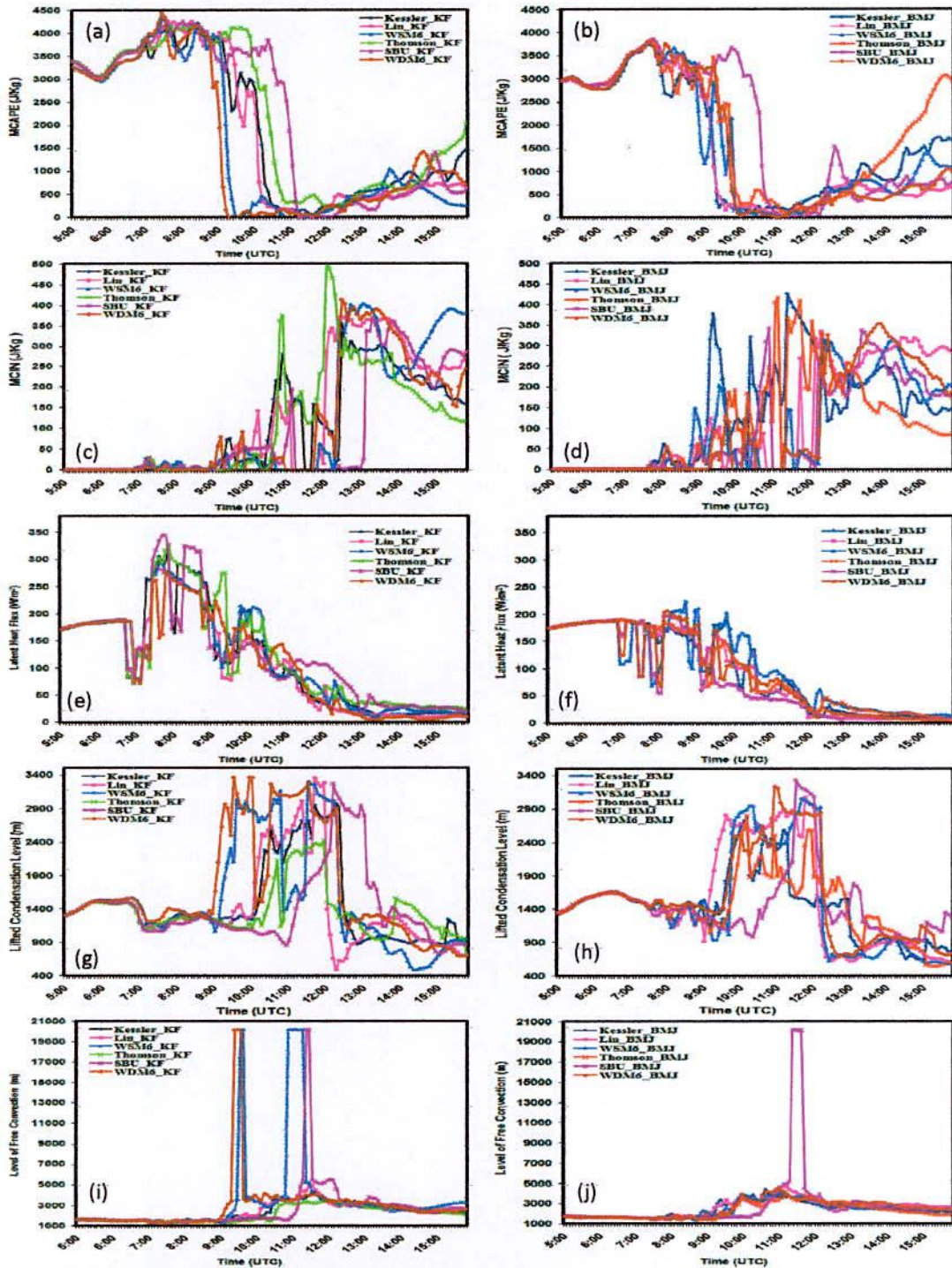


Fig. 4.4.8: Time variation of (a-b) CAPE, (c-d) CIN, (e-f) LH flux, (g-h) LCL and (i-j) LFC using six different MP schemes coupling with KF and BMJ schemes at Barisal on 15 May 2014.

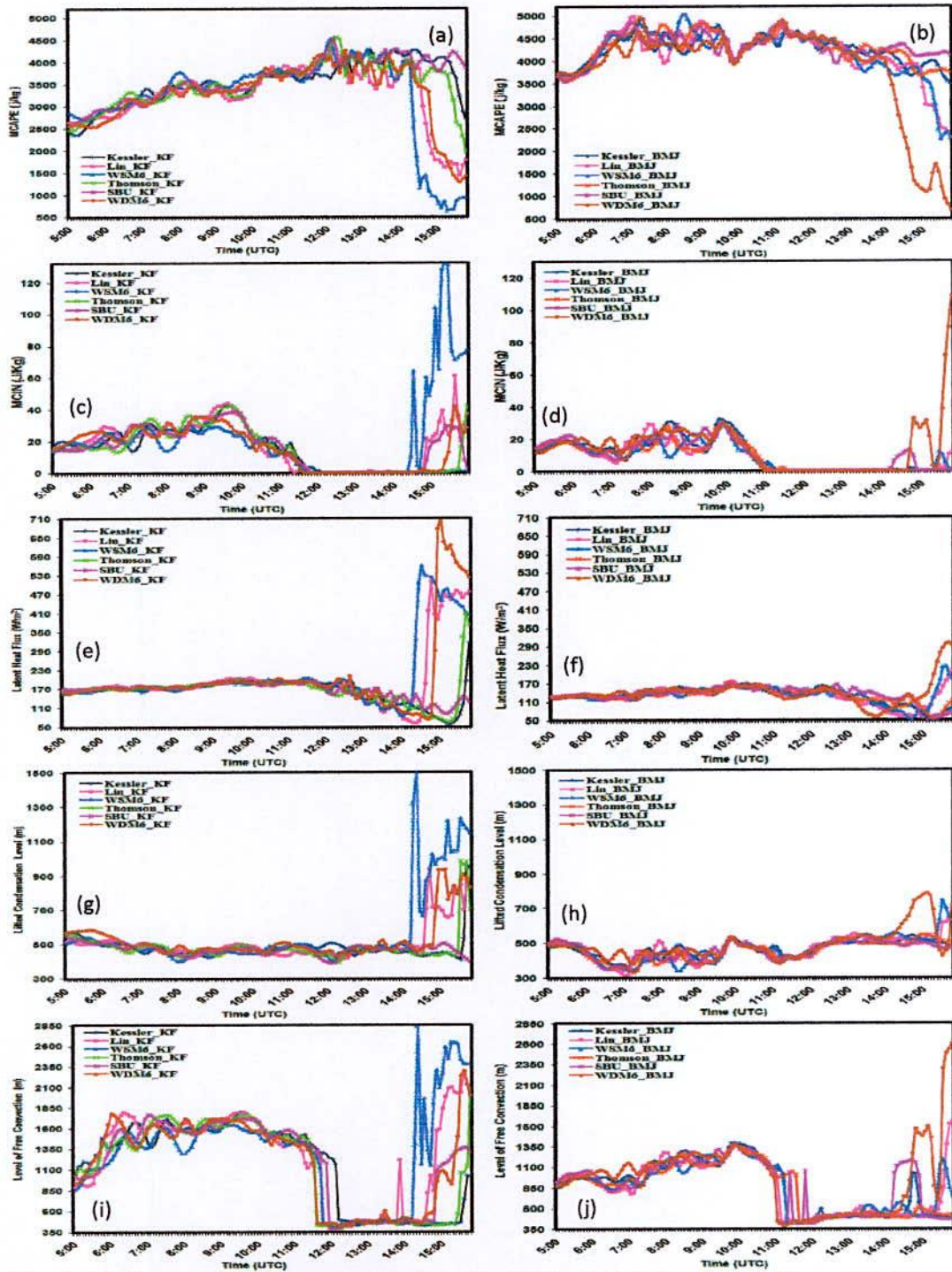


Fig. 4.4.9: Time variation of (a-b) CAPE, (c-d) CIN, (e-f) LH Flux, (g-h) LCL and (i-j) LFC using six different MP schemes coupling with KF and BMJ schemes at Chittagong on 15 May 2014.

4.4.12 Convective Available Potential Energy (CAPE)

Model simulated time variation of CAPE for six different MPs coupling with KF and BMJ schemes at Barisal are presented in Figs. 4.4.8(a-b). The CAPE is found > 3500 J/kg up to 0900 UTC (Fig. 4.4.8a) for all MPs and > 2500 J/kg up to 1000 UTC for KS-KF, Lin-KF, TH-KF and SBU-KF combinations, which is extremely unstable condition of atmosphere for the formation of nor'wester at Barisal. The CAPE has been simulated 4305 and 4454 J/kg by WSM6-KF and WDM6-KF combinations at 0725 UTC. But the CAPE has sharply decreased at 0905, 0915, 1005 and 1015 UTC for WDM6-KF, WSM6-KF, Lin-KF and KS-KF combinations and less than 1000 J/kg indicates that the instability is weak at that time. The CAPE is found > 2500 J/kg (Fig. 4.4.8b) at 0855, 0900, 0915, 0935, 1025 and 0915 UTC for Kessler, Lin, WSM6, Thompson, SBU and WDM6 schemes in combination with BMJ scheme and after that it sharply decreases to zero for all combinations. The CAPE is simulated 3851, 3836, 3831 and 3852 J/kg by KS-BMJ, Lin-BMJ, TH-BMJ and SBU-BMJ combinations at 0725 UTC, which is extremely unstable condition of atmosphere for the formation of nor'wester.

WRF model simulated CAPE at Chittagong are shown in Figs. 4.4.9(a-b). The CAPE has increased and fluctuates up to 1400 UTC and is found > 2500 J/kg for all MPs coupling with KF and BMJ schemes, which is extremely unstable condition of atmosphere for the formation of nor'wester and then it has decreased (Fig. 4.4.9a) sharply at 1425, 1445, 1450, 1540 and 1550 UTC for WSM6-KF, Lin-KF, WDM6-KF, TH-KF, KS-KF combinations. The maximum CAPE is simulated 4520, 4541 and 4573 J/kg by WSM6-KF, SBU-KF and TH-KF combinations at 1205, 1210 and 1215 UTC respectively. The CAPE is simulated 4936, 4994, 4840, 4828 and 4854 J/kg (Fig. 4.4.9b) by KS-BMJ, Lin-BMJ, WSM6-BMJ, TH-BMJ and SBU-BMJ combinations at 0720, 0715, 0705, 0900 and 0700 UTC respectively.

4.4.13 Convective Inhibition (CIN)

Model simulated time variation of CIN for six different MPs coupling with KF and BMJ schemes at Barisal is presented in Figs. 4.4.8(c-d). The CIN is zero up to 0650 UTC and < 100 J/kg up to 1025 and 0910 UTC at Barisal (Fig. 4.4.8c) and Chittagong (Fig. 4.4.8d) for all MPs coupling with KF and BMJ schemes, which indicate the atmosphere is potentially unstable for the occurrence of nor'wester at these stations. After that, it has sharply increased and found > 100 J/kg for KS-KF, Lin-KF, TH-KF and SBU-KF combinations at 1030, 1035,

1045 and 1100 UTC and for KS-BMJ, WSM6-BMJ, TH-BMJ and SBU-BMJ combinations at 0915, 0925, 0945 and 0940 UTC respectively, which indicate the atmosphere is marginally stable.

Figs. 4.4.9(c-d) depict model simulated CIN at Chittagong. Up to 1130 UTC CIN < 40 J/kg and after that CIN is zero up to 1420 UTC for all MPs coupling with KF (Fig. 4.4.9c) and BMJ (Fig. 4.4.9d) schemes indicates that the atmosphere is potentially unstable for the occurrence of nor'wester at Barisal. CIN is greater than 100 J/kg after 1505 and 1545 UTC for WSM6-KF and WDM6-BMJ combinations indicates the atmosphere is marginally stable.

4.4.14 Latent Heat (LH) Flux

Model simulated time variation of LH flux for six different MPs coupling with KF and BMJ schemes at Barisal is given in Figs. 4.4.8(e-f). LH flux increased slowly up to 0640 UTC (Fig. 4.4.8e) for all MPs coupling with KF scheme and then decreased sharply at 0645 UTC for KS-KF, Lin-KF, TH-KF and SBU-KF combinations and at 0655 UTC for WSM6-KF and WDM6-KF combinations. After that, it has fluctuates for all MPs coupling with KF scheme. The LH flux has increased significantly to 305.8, 344.8 and 324.3 W/m² at 0735, 0740 and 0750 UTC for KS-KF, SBU-KF and TH-KF combinations respectively. In this case the LH flux released is huge in the atmosphere, which is available for the formation of severe storms. LH flux increased (Fig. 4.4.8f) slowly up to 0650 UTC and then decreased for all MPs in combination with BMJ scheme except TH-BMJ combination. After 0800 UTC, it has fluctuates irregularly for all MPs coupling with BMJ scheme. The LH flux has increased significantly 196.9 and 206.4 W/m² at 0810 UTC for SBU-BMJ and WDM6-BMJ and 223.3 W/m² at 0840 UTC for WSM6-BMJ combinations. Again, the LH flux has increased 188.7, 202.8, 105.7 W/m² for KS-BMJ, WSM6-BMJ and WDM6-BMJ combinations at 0945 UTC, which is close to the observed time of squall at Barisal.

WRF model simulated LH flux at Chittagong is given in Figs. 4.4.9(e-f). The LH flux almost constant and slightly fluctuates in an oscillatory pattern for all MPs coupling with KF (Fig. 4.4.9e) and BMJ (Fig. 4.4.9f) schemes. At 1210 UTC, it has slightly increased for Lin-KF, WSM6-KF and WDM6-KF combinations but significant changes has been observed after 1400 UTC for these combinations. At around 1215 UTC, it has increased slightly for all MPs in combination with BMJ scheme and after 1500 UTC it has increased sharply for all MPs

coupling with BMJ scheme. In this case the LH flux released is huge in the atmosphere but which is too delaying to the observed time of squall at Chittagong.

4.4.15 Lifted Condensation Level (LCL)

Time variation of LCL for six different MPs coupling with KF and BMJ schemes at Barisal is shown in Figs. 4.4.8(g-h). The LCL is simulated minimum at around 0730 UTC for all MPs in combination with KF scheme. The minimum value of LCL is found at around 2 hour earlier than the observed squall at Barisal. After 0900 UTC, LCL has significantly fluctuates for all MPs in combination with KF and BMJ schemes. From Fig. 4.4.8g, the LCL has sharply increased and maximum LCL 3362 and 3038m has found for WDM6-KF and WSM6-KF combinations at 0930 and 0935 UTC. Again, it has also increased and maximum LCL 3285, 3258, 3356 and 3269m are simulated by WDM6-KF, WSM6-KF, Lin-KF and SBU-KF combinations at 1130, 1140, 1140 and 1210 UTC. From Fig. 4.4.8h, the LCL has sharply decreased to 1120, 913, 937, 1133, 1097 and 1336 m at 0910, 0900, 0920, 0930, 0940 and 0915 UTC respectively for KS, Lin, WSM6, TH, SBU and WDM6 in combination with BMJ scheme, which is close to the observed time of squall at Barisal. The maximum LCL 3233 and 3333m are simulated by WDM6-BMJ and SBU-BMJ combinations at 1055 and 1130 UTC.

Figs. 4.4.9(g-h) depict model simulated LCL at Chittagong. Up to 1400 UTC (Fig. 4.4.9g), the LCL has found in an oscillatory pattern with slightly variation for all MPs coupling with KF scheme. The LCL has found to decrease and reach minimum 430, 419, 405, 403, 391 and 432m at 1240, 1225, 1205, 1210, 1205 and 1210 UTC for KS, Lin, WSM6, TH, SBU and WDM6 respectively in combination with KF scheme. From Fig. 4.4.9h, the LCL is found minimum and fluctuates irregularly for all MPs coupling with BMJ scheme. At around 1100 UTC, it has slightly decreased for all MPs coupling with BMJ scheme.

4.4.16 Level of Free Convection (LFC)

Model simulated time variation of LFC for six different MP coupling with KF and BMJ schemes at Barisal is presented in Figs. 4.4.8(i-j). LFC has decreased slowly (Fig. 4.4.8i) and in an oscillatory pattern and reached minimum 1268, 1362, 1300, 1262, 1438 and 1377m at 0905, 0900, 0900, 0910, 0845 and 0820 UTC for KS, Lin, WSM6, TH, SBU and WDM6

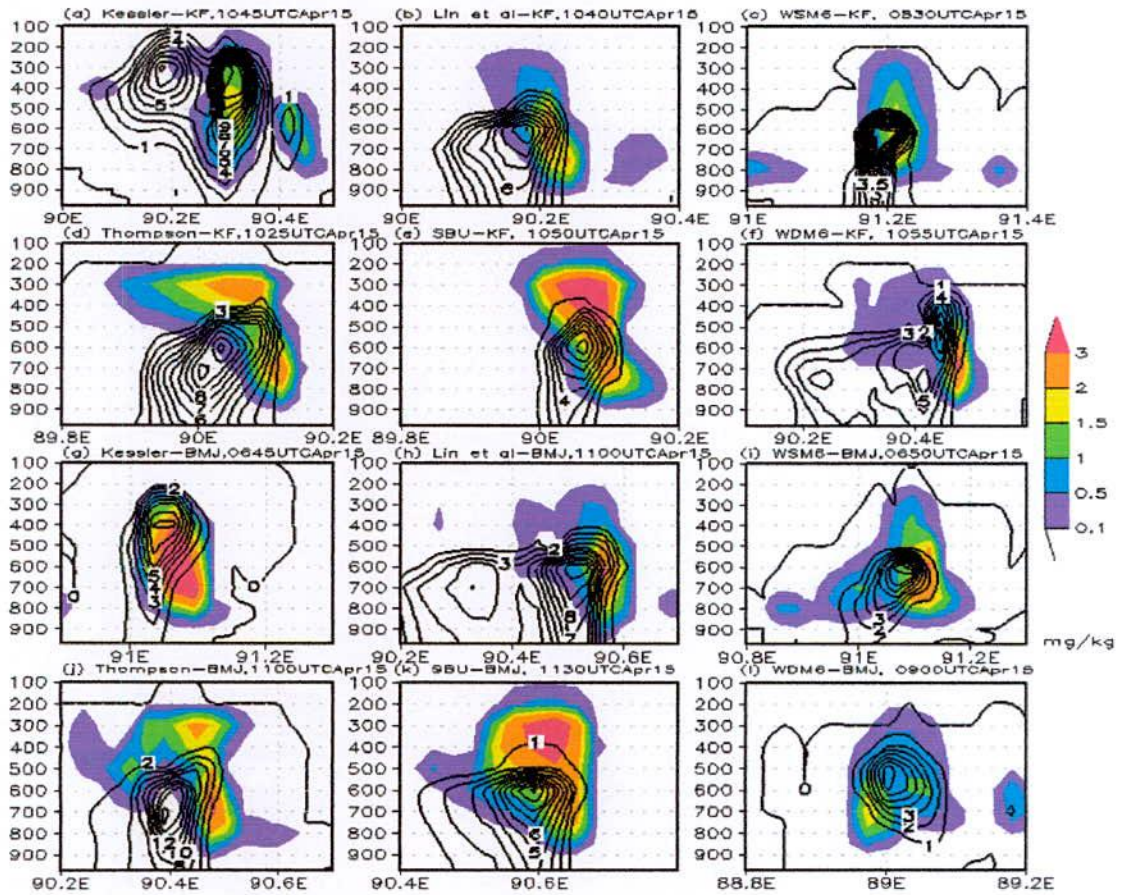


Fig. 4.4.10: WRF Model simulated CWMR (shaded) and RWMR (contour) along the line of maximum vertical velocity using Kessler, Lin *et al.*, WSM6, Thomson, SBU and WDM6 schemes coupling with (a-f) KF and (g-l) BMJ schemes on 15 May 2014.

4.4.18 Cloud Water Mixing Ratio (CWMR)

The CWMR (shaded, mg/kg) has simulated along the line of maximum vertical velocity using different MPs coupling with KF and BMJ schemes and are presented in Figs. 4.4.10(a-l). Kessler-KF combination and SBU scheme coupling with KF and BMJ schemes have simulated CWMR up to 100 hPa. All other MPs coupling with KF and BMJ schemes have simulated CWMR up to 200 hPa. The CWMR is found maximum at 500-250, 700-400 and 500-250 hPa level for SBU-KF, KS-BMJ and SBU-BMJ combinations and at 700, 600 and 700 hPa for WDM6-KF, Lin-BMJ and TH-BMJ combinations respectively.

schemes respectively in combination with KF scheme, which is close to the observed time of squall at Barisal. After that it has increased significantly and after certain time it decreased. After 0720 UTC (Fig. 4.4.8j), the LFC has started to fluctuate for all MPs coupling with BMJ scheme. The minimum value of LFC has found 1600, 1400, 1310, 1397, 1426 and 1448m at 0835, 0840, 0840, 0845, 0840 and 0900 UTC for KS, Lin, WSM6, TH, SBU and WDM6 schemes respectively in combination with BMJ scheme, which is close to the observed time at Barisal.

WRF model simulated time variation of LFC at Chittagong is described in Figs. 4.4.9 (i-j). Starting from 0500 UTC (Fig. 4.4.9i), the LFC has fluctuates irregularly and then, after 1130 UTC it has decreased significantly for all MPs coupling with KF scheme. The LFC has sharply decreased and reached minimum 430, 419, 414, 427, 390 and 432m at 1240, 1225, 1200, 1140, 1205 and 1210 UTC for KS, Lin, WSM6, TH, SBU and WDM6 schemes respectively in combination with KF scheme, which is close to the observed time of squall at Chittagong. Starting from 0500 UTC (Fig. 4.4.9j), the LFC has found oscillatory in nature and after 1050 UTC it has suddenly decreased for all MPs in combination with BMJ scheme. The LFC has found minimum 415, 399, 413, 420, 415 and 387m at 1135, 1105, 1110, 1145, 1130 and 1110 UTC for KS, Lin, WSM6, TH, SBU and WDM6 schemes respectively in combination with BMJ scheme, which is close to the observed time of squall at Chittagong.

4.4.17 Rain Water Mixing Ratio (RWMR)

The RWMR (contour, mg/kg) is simulated along the line of maximum vertical velocity using different MPs coupling with KF and BMJ schemes and are presented in Figs. 4.4.10(a-l). Kessler and Thompson schemes coupling with KF and BMJ schemes and WSM6-BMJ combination are simulated RWMR up to 100 hPa. WSM6-KF, WDM6-KF and WDM6-BMJ combinations have simulated RWMR up to 200 hPa. Lin *et al.*, and SBU schemes coupling with KF and BMJ schemes are simulated RWMR up to 400 hPa. The RWMR is simulated maximum at the position where the updraft and reflectivity has also maximum. The RWMR maximum 14 mg/kg is simulated at 400-300 hPa level for KS-KF and KS-BMJ combinations. The significant amount of RWMR 12, 11, 10, 10 and 10 mg/kg have also been simulated by KS-KF, TH-KF, Lin-KF, Lin-BMJ and SBU-BMJ combinations at 400, 600, 600, 600 and 600 hPa level respectively.

Chapter V

Conclusions

In the present study, WRF-ARW model V3.5.1 has been used to simulate the nor'westers/squall lines observed in the different stations of Bangladesh. The model has been configured in single domain, 3 km horizontal grid spacing with 173×225 grids in the east-west and north-south directions and 28 vertical levels. Time step of integration is set to 15 seconds for maintaining computational stability as the model uses third-order Runge-Kutta time integration scheme. The model has been run for 24 hours from 0000 UTC of 27 April to 0000 UTC 28 April 2014, 0000 UTC of 15 May to 0000 UTC 16 May 2014, 0000 UTC 07 April to 0000 UTC of 08 April 2012 and 0000 UTC of 28 April to 0000 UTC of 29 April 2012. In each case 2 stations are affected by nor'westers/squalls. Analyses have been made at 8 stations out of which 2 stations are not affected by nor'westers/squalls but model generated squalls on these stations. FNL data were used as the initial condition to examine the sensitivity by using Kessler, Lin *et al.*, WSM6, Thompson, SBU and WDM6 schemes and KF and BMJ schemes. The Nor'wester/Squall occurred within short period of time. The time span was not more than one hour for the formation to dissipation of the system. To study the short period events, WRF outputs have to generate every 5 minutes. The different meteorological parameters of this research under study are wind speed at 10m levels, temperature at 2m level, relative humidity at 2m level and sea level pressure. The different energies and instability indices are MCAPE, MCIN, LFC, LCL, LH, CT, VT, TT and KI, which have been calculated at the stations where squalls/nor'westers occurred. The maximum vertical velocity has also been calculated from the model output, which indicates the maximum convection. The WRF model was able to simulate many features of nor'wester/squall line events, but with some differences.

The minimum SLP is simulated by Lin-BMJ and WDM6-BMJ combinations at Dhaka and Lin-KF and WSM6-KF combinations at Chittagong on 07 April 2012. All MPs coupling with KF and BMJ schemes have simulated minimum SLP at Chittagong and Dhaka on 28 April 2012. At Sylhet, the change of SLP is insignificant and the minimum SLP is found at Khulna for Lin-KF and WDM6-BMJ combinations on 27 April 2014. At around 0930 UTC minimum SLP is found for WSM6-KF and WDM6-KF combinations which is closer to the observed time of squall at Barisal station and at around 1150 UTC for Lin-KF, SBU-KF, TH-BMJ and SBU-BMJ combinations at Chittagong, which is closer to the observed time of squall on 15 May 2014.

The MWS at 10m level is simulated by Thompson-KF and WSM6-BMJ almost half an hour later than observed time of occurrence of nor'wester at Dhaka and WSM6-KF at the time of observation at Chittagong on 07 April 2012. KS-KF, Lin -KF, WSM6-KF and WDM6-KF combinations have simulated higher wind speed at 10 m level on 28 April 2012 outside Chittagong and Dhaka stations. At Sylhet, wind speed is lower and the MWS is found at Khulna for KS-KF, Lin-KF, WDM6-KF, KS-BMJ, WSM6-BMJ and WDM6-BMJ combinations on 27 April 2014. After 0925 UTC, the simulated MWS is found closer to the observed time of squall at Barisal for WDM6-KF, WSM6-KF, Lin-BMJ and WSM6-BMJ combinations at Chittagong on 15 May 2014.

The maximum temperature at 2m level is simulated by Lin-KF, WSM6-KF and WDM6-KF combinations at the time of observation at Dhaka and at Chittagong; the temperature has suddenly decreased after the observed time occurrence of nor'westers by using Lin-KF, WSM6-KF and WDM6-KF combinations on 07 April 2012. The simulated 2m level temperature found at Dhaka is much higher than that at Chittagong at 0750 UTC after the occurrence of nor'wester at Chittagong on 28 April 2012. The maximum temperature is found for all MPs coupling with KF scheme at 0640 UTC, which is too earlier than the observation time of squall at Barisal on 15 May 2014.

The RH is found maximum for KS-BMJ, TH-BMJ and SBU-BMJ at around 0800 UTC at Chittagong and at around 0500 UTC for Lin-KF, WSM6-KF, WDM6-KF Lin-BMJ, WSM6-BMJ and WDM6-BMJ at Dhaka on 07 April 2012. The maximum RH of 98.5% is simulated by WDM6-KF at 1150 UTC, which is too much later to match with the observed time of squall at Chittagong on 28 April 2012 and 90 % RH has been simulated by all MPs in combination with CPs up to 300 hPa level, where the vertical velocity is found maximum. The RH is found maximum at around 0920 UTC for KS-BMJ, WSM6-BMJ and TH-BMJ at Barisal on 15 May 2014.

The maximum reflectivity (MR) is found after 0900 UTC for SBU-KF, WDM6-KF and WSM6-KF combinations at Chittagong and at around 0500 UTC for Lin, WSM6 and WDM6 in combination with KF and BMJ schemes at Dhaka on 07 April 2012. MR is found at Chittagong at 0900-1200 UTC, which is also much later than the actual time of observation (0640-0647 UTC) for all MPs coupling with KF scheme on 28 April 2012. At around 0910 UTC, the reflectivity is found maximum for WSM6-KF, WDM6-KF and WSM6-BMJ

combinations at Barisal, and at Chittagong it is found at about 2 hour later than that of observed time on 15 May 2014 for TH-BMJ and SBU-BMJ. The model simulated stability indices such as $CT \geq 22^{\circ}C$, $VT \geq 28^{\circ}C$, $TT \geq 56^{\circ}C$ and $KI \geq 40^{\circ}C$ are much higher than the critical values viz. $CT \geq 14^{\circ}C$, $VT \geq 24^{\circ}C$, $TT \geq 40^{\circ}C$ and $KI \geq 34^{\circ}C$ for the stations where squalls/nor'wester might had occurred.

The simulated MCAPE is greater than 2500 J/kg for all MPs coupling with KF and BMJ schemes at or before the occurrence of squalls on 7 and 28 April 2012 and 15 May 2012. The maximum CAPE (CAPE >2500 J/kg) is simulated by TH-KF and SBU-KF at 2135 UTC at Sylhet, and at Khulna it has found after 1030 UTC TH-KF, SBU-KF, Lin-BMJ, WSM6-BMJ, TH-BMJ and SBU-BMJ combinations on 27 April 2014. The CIN is found minimum around the time of observation of nor'westers at Chittagong and at Dhaka for all MPs coupling with KF and BMJ schemes on 7 and April 2012 and 15 May 2014. The huge amount of LHF is found by WSM6 and WDM6 schemes coupling with KF and BMJ schemes at different stations near about the time of observation of squalls/nor'westers under study.

The simulated LCL is found minimum near about the observation time of squall/nor'westers for WSM6-KF, WDM6-KF and Lin-BMJ combinations on 7 and 28 April 2012 and 15 May 2014. The simulated LFC is found minimum in and around the time of observation of squall/nor'westers for WDM6-KF, WSM6-KF and WDM6-BMJ combinations on 7 and 28 April 2012 and 15 May 2014.

It is found that the significant changes have been simulated for all the meteorological parameters, fluxes and energies at or near about the time of observations of squall/nor'westers where it is observed. All the combinations of MPs and CPs have simulated the events but the WSM6 and WDM6 are better than those of the other combinations.

Reference:

- Ahasan M. N., M. N. Islam and N. Ferdousi, 2008: A diagnostic study on synoptic and environmental conditions associated with Nor'westers in and around Bangladesh using MM5 model; Proceedings of the SAARC Seminar on Nor'westers and Tornadoes over the SAARC Region and their Forecasting & Preparedness, 20–21 August, 2008, Dhaka, 143–156.
- Akram, M. H. and S. Karmakar, 1998: Some meteorological aspects of the Sauria tornado, 1989-A case study, *Journal of Bangladesh Academy of Sciences*, 22, 1, 109-122.
- Akter F, Ishikawa H. 2014: Synoptic features and environmental conditions of the tornado outbreak on March 22, 2013 at Brahmanbaria in the east-central region of Bangladesh. *Nat Hazards*, 74, 1309-1326.
- Arakawa, A., and V. R. Lamb, 1977: Computational design of the basic dynamical processes of the UCLA general circulation model, *Methods of Computational Physics*, 17, New York, Academic Press, 173–265.
- Arakawa, A., and W. H. Schubert, 1974: Interaction of a cumulus cloud ensemble with the large-scale environment, Part I. *J. Atmos. Sci.*, 31, 674–701.
- Awan, N. K., H. Truhetz, and A. Gobiet, 2011: Parameterization induced error characteristics of MM5 and WRF operated in a climate mode over the Alpine region: An ensemble-based analysis. *J. Climate*, 24, 3107–3123.
- Basnayake, B. R. S. B., M. K. Das, F. F. Nessa, and M. M. Rahman, 2010: Nor'westers over Bangladesh and neighbourhood during pre-monsoon season of 2009: Observations and WRF model simulation; SAARC Meteorological Research Centre (SMRC), SMRC Scientific Report No. 36, 6.
- Bruce B. Parker, 1992: Sea level as an indicator of climate and Global Change, *Marine Technology Society Journal*, 25, 4, 13-24.
- Bukovsky, M. S., and D. J. Karoly, 2009: Precipitation simulations using WRF as a nested regional climate model. *J. Appl. Meteor. Climatol.*, 48, 2152–2159.
- Chen, G. T. J., and C. C. Yu, 1988: Study of low-level jet and extremely heavy rainfall over northern Taiwan in the mei-yu season. *Mon. Wea. Rev.*, 116, 884–891
- Chen, G. T. J., C. C. Wang, and D. T. W. Lin, 2005: Characteristics of low level jets over northern Taiwan in mei-yu season and their relationship to heavy rain events. *Mon. Wea. Rev.*, 133, 20–43.
- Chen, G. T. J., C. C. Wang, and L. F. Lin, 2006: A diagnostic study of a retreating mei-yu front and the accompanying low-level jet formation and intensification. *Mon. Wea. Rev.*, 134, 874–896.

- Chen, J. Y., Y. Sun, 2002: Hydrolysis of lignocellulosic materials for ethanol production: a review, *Biore source technology* 83, 1, 1-11.
- Chevuturi A., A. P. Dimri, U. B. Gunturu, 2014: Numerical simulation of a rare winter hailstorm event over Delhi, India, on 17 January 2013. *Nat Hazards Earth Syst. Sci.* 14, 3331-3344.
- Chowdhury, M. H. K., S. Karmakar, and A. Khatun, 1991: A diagnostic study on some aspects of tropospheric energy in relation to nor'westers over Bangladesh, *Proceedings of the SAARC Seminar on Severe Local Storms, held in Colombo, Sri Lanka, 7-11 October, 1991*, 19-33.
- Chowdhury, M. H. K., and S. Karmakar, 1986: Pre-monsoon Nor'westers in Bangladesh with case studies, *Proceeding of SAARC seminar on Local Severe Storms, Dhaka, Bangladesh*, 147-166.
- Colby, Jr., Frank P., 1984: Convective Inhibition as a predictor of Convection during AVESESAME II. *Mon. Wea. Rev.*, 112, 2239-2252.
- Das S., U. C. Mohanty, A. Tyagi, D. R. Sikka, P. V. Joseph, L. S. Rathore, A. Habib, S. K. Baidya, K. Sonam, A. Sarkar, 2014: The SAARC STORM: a coordinated field experiment on severe thunderstorm observations and regional modeling over the South Asian region. *Bull. Am. Meteorol Soc.* 95, 603-617.
- Das, M. K., M. A. M. Chowdhury, S. Das, S. K. Debsarma and S. Karmakar 2015: Assimilation of Doppler weather radar data and their impacts on the simulation of squall events during pre-monsoon season. *Nat. Hazards*, 77, 901-931.
- Das, R. C., A. A. Munim, and Q. N. Begum, 1994: A diagnostic study on some local severe storms over Bangladesh. *J. Bangladesh Acad. of Sci.*, 18, 1, 81-92.
- Das, Someshwar, B. R. S. B., Basnayake, M. K. Das, M. A. R. Akand, M. M. Rahman, and M. M. A. Sarker, 2009: Composite characteristics of Nor'westers observed by TRMM and simulated by WRF Model; SAARC Meteorological Research Centre (SMRC), SMRC Scientific Report No. 25, 47.
- Das, Someshwar, R. Ashrit and M.W. Moncrieff, 2006: Simulation of a Himalayan cloudburst event. *J. Earth System Science*, 115, 299-313.
- Davies Jones, R. P., 1982: *Thunderstorm Morphology and Dynamics*, pp.603.
- Deardorff, J. W., 1972: Parameterization of the planetary boundary layer for use in general circulation models, *Mon. Wea. Rev.*, 100, 93-106.
- Deb, S. K., C. M. Kishtawal, P. K. Pal, P. C. Joshi, 2008: Impact of TMI SST on the simulation of a heavy rainfall episode over Mumbai on 26 July 2005. *Mon Wea Rev* 136, 3714-3741

- Donner, L. J., and B. A. Colle, 2011: Parameterization of riming intensity and its impact on ice fall speed using ARM data. *Mon. Wea. Rev.*, 139, 1036–1047.
- Dudhia, J., 1989: Numerical study of convection observed during the winter monsoon experiment using mesoscale two-dimensional models, *J. Atmos. Sci.*, 46, 3077-3107.
- Ek, M. B., K. E. Mitchell, Y. Lin, E. Rogers, P. Grunmann, V. Koren, G. Gayno, and J. D. Tarpley, 2003: Implementation of Noah land surface model advances in the National Centers for Environmental Prediction operational mesoscale Eta model
- Ferrier, B. S., W.-K. Tao, and J. Simpson, 1995: A double moment multiple phase four-class bulk ice scheme, Part II: Simulations of convective storms in different large-scale environments and comparisons with other bulk parameterizations. *J. Atmos. Sci.*, 52, 1001-1033.
- Finch, J. D., and A. M. Dewan, 2003: Tornadoes in Bangladesh and East India, Available from: <http://bangladeshtornadoes.org/climo/btorcli0.htm>
- Fritsch, J. M. and C. F. Chappell, 1980: Numerical Prediction of Convective Driven Mesoscale Pressure Systems, Part I: Convective Parameterization, *J. Atmos. Sci.* 37, 1722- 1733.
- Fujita, Theodore T., 1985: The Downburst-Microburst and Macroburst, Report of projects NIMROD and JAWS, University of Chicago Press, pp. 122.
- Gallus, W. A., Jr., and J. F. Bresch, 2006: Comparison of impacts of WRF dynamic core, physics package, and initial conditions on warm season rainfall forecasts. *Mon. Wea. Rev.*, 134, 2632-2641.
- Ghose, S. K., 1986: Tornadoes and hailstorms, Proceedings of the Seminar on Local severe Storm, Bangladesh Met. Dept., held on 17-21 January 1985, 95-101.
- Gupta, H. N. and Ghosh, S. K., 1980: North Delhi tornado of 17 March 1978, *Mausam*, 31, 1, pp. 93-100.
- Holford, D., 1977: Guinness Book of Weather Facts and Feats, pp. 240.
- Hong, S. Y., Dudhia J. and Chen, S. H., 2004: A Revised Approach to Ice Microphysical Processes for the Bulk Parameterization of Clouds and Precipitation, *Mon. Wea. Rev.*, 132, 103-120.
- Hong, S.Y., and H. L. Pan, 1996: Nonlocal boundary layer vertical diffusion in a medium-range forecast model, *Mon. Weather Rev.* 124, 2322–2339.
- http://disc.gsfc.nasa.gov/hydrology/data-holdings/parameters/latent_heat_flux.shtml
- <http://spotterguides.us/advanced/advanced05.htm>
- <http://wind.mit.edu/~btangy/Home/convection.htm>

- <http://www.skystef.be/calculator-crosstotalsindex.htm>
- <http://www.skystef.be/calculator-k-index.htm>
- <http://www.theweatherprediction.com/habyhints/302>
- <http://www.skystef.be/calculator-verticaltotalsindex.htm>
- https://en.wikipedia.org/wiki/Level_of_free_convection
- https://en.wikipedia.org/wiki/Thunderstorm#/media/File:8402_STS41B_Challenger_Thunderstorms_over_Brazil.JPG
- https://en.wikipedia.org/wiki/Thunderstorm#/media/File:Chaparral_Supercell_2.JPG
- https://en.wikipedia.org/wiki/Thunderstorm#/media/File:Thunderstorm_formation.jpg
- https://upload.wikimedia.org/wikipedia/commons/8/8a/Thunderstorm_over_Wagga_Wagga.j
- Itano, T., H. Ishikawa, 2002: Effect of Negative Vorticity on the Formation of Multiple Structure of Natural Vortices. *J. Atmos. Sci.*, 59, 3254–3262.
- Janjic, Z. I., 1994: The step-mountain Eta coordinate model: Further developments of the convection, viscous sublayer, and turbulence closure schemes. *Mon. Wea. Rev.*, 122, 927–945.
- Joseph, P. V., 1982: A tentative model for Aandhi, *Mausam*, 33, 417.
- Kain, J. S., 2004: The Kain–Fritsch convective parameterization: An update; *J. Appl. Meteor.* 43 170–181.
- Kain, J. S., Fritsch, J. M., 1993: Convective parameterization for mesoscale models: the Kain-Fritsch scheme, the representation of cumulus convection in numerical models, *Meteo. Monogr*, No. 46 Amer. Meteor. Soc., 165–170.
- Kandalgaokar, S. S., M. I. R. Tinmaker, M. K. Kulkarni, and A. Nath, 2002: Thunderstorm activity and sea surface temperature over the Island stations and along the east and west coast of India, *Mausam*, 53, 245.
- Karmakar, S., 2001: Climatology of thunderstorm days over Bangladesh during the pre-monsoon season. *Bangladesh. J. Sci. and Tech.*, 3, 1, 103-112.
- Karmakar, S., and M. M. Alam, 2005: On the sensible heat energy, latent heat energy and potential energy of the troposphere over Dhaka before the occurrence of Nor'westers in Bangladesh during the pre-monsoon season, *Mausam*, 56, 671-680.
- Karmakar, S., and M. M. Alam, 2006: Instability of the troposphere associated with thunderstorms/Nor'westers over Bangladesh during the pre-monsoon season, *Mausam*, 57, 629-638.
- Karmakar, S., and M. M. Alam, 2007: Tropospheric moisture and its relationship with rainfall due to Nor'westers in Bangladesh, *Mausam*, 58, 153-160.

- Kessler, E., 1969: On the distribution and continuity of water substance on atmospheric circulation. *Meteorol. Monogr.*, 10, 32, 84.
- Kodama, Y.-M., A. Ohta, M. Katsumata, S. Mori, S. Satoh, and H. Ueda, 2005: Seasonal transition of predominant precipitation type and lightning activity over tropical monsoon areas derived from TRMM observations. *Geophys. Res. Lett.*, 32, L14710, doi: 10.1029/2005GL022986.
- Koteswaram, P. and V. Srinivasan, 1958: Thunderstorms over Gangetic West Bengal in the pre-monsoon season and the synoptic factors favourable for their formation, *Indian J. Met. Geophys.*, 9, 4, 301-312.
- Koteswaran, P., and V., 1969: Thunderstorm over Gangetic West Bengal in the pre-monsoon season and the synoptic factors favorable for their formation, *Indian J. Meteorol. Geophys.*, 9, 301.
- Krishnamurthy, V., 1969: A statistical study of thunderstorm over Poona, *Indian J. Meteorol. Geophys.*, 16, 484.
- Krishnamurti, T. N., 2003: Compendium on Tropical Meteorology for Aviation purposes, WMO-No. 930, 28-30.
- Lawrence, M. G., 2005: The relationship between relative humidity and the dew point temperature in moist air: A simple conversion and applications, *Bull. Am. Meteorol. Soc.*, 86, 225-233.
- Leung, L. R., Y.-H. Kuo, and J. Tribbia, 2006: Research needs and directions of regional climate modeling using WRF and CCSM. *Bull. Amer. Meteor. Soc.*, 87, 1747-1751.
- Lin, Y.L., Farley, R. D. and Orville, H. D., 1983: Bulk parameterization of the snow field in a cloud model, *J. Climate Appl. Meteor.*, 22, 1065-1092.
- Litta A. J., U. C. Mohanty, S. C. Bhan, 2010: Numerical simulation of a tornado over Ludhiana (India) using WRF-NMM model. *Meteorol Appl.* 17, 64-75.
- Litta A. J., U. C. Mohanty, S. Das, S. M. Idicula, 2012: Numerical simulation of severe local storms over east India using WRF_NMM mesoscale model. *Atmos Res.* 116:161-184.
- Litta, A. J., U. C. Mohanty, S. Kiran Prasad, M. Mohapatra, Ajit Tyagi, S. C. Sahu, 2012: Simulation of tornado over Orissa (India) on March 31, 2009 using WRF-NMM model, *Nat Hazards* 61, 1219-1242
- Manohar, G. K., S. S., Kandalgaokar and M. I. R. Tinmaker, 1999: Thunderstorm activity in India and Indian southwest monsoon, *J. Geophys. Res.*, 104, 4169.

- Mlawer, E. J., Taubman, S. J., Brown, P. D., Lacono, M. J. and Clough, S. A., 1997: Radiative transfer for inhomogeneous atmosphere: RRTM, a validated correlated-k model for the longwave, *J. Geophys. Res.*, 102(D14), 16663-16682.
- Mukherjee, A. K. and P. B. Bhattacharya, 1972: An early morning tornado at Diamond Harbour on March 21, 1968, *Indian J. Met. & Geophys.*, 23, 2, 223-226.
- Mukhopadhyay, P., J. Sanjay, W. R. Cotton and S. S. Singh, 2005: Impacts of surface meteorological observations on RAMS forecast of monsoon weather systems over Indian region. *Meteorol. Atmos. Phys.*, 90, 77-108.
- Nandi, J. and A. K. Mukherjee, 1966: Tornado over North-west Assam and adjoining West Bengal on 19 April, 1963, *Indian J. Met. Geophys.*, 17, 3, 421-426.
- Orlanski, I., 1975: A rational subdivision scales for atmospheric processes. *Bull. Am. Meteorol. Soc.*, 56, 527-530.
- Pleim, J., 2007: A combined local and non-local closure model for the atmospheric boundary layer. Part II: Application and evaluation in a mesoscale meteorological model, *J. Applied Meteor. Climatology*, 46, 1396-1409.
- Prasad K. 2006. Environmental and synoptic conditions associated with Nor'westers and tornadoes in Bangladesh- An appraisal on numerical weather prediction (NWP) guidance products, Dhaka, SMRC Report No. 14, 74.
- Raman, P. K., and K., Raghavan, 1961: Diurnal variation of thunderstorm in India in different seasons, *Indian J. Meteorol. Geophys.*, 12, 115.
- Rao, K. N., and P. K. Raman, 1961: Frequency of days of thunder in India. *Indian J. Meteorol. Geophys.*, 16, 103.
- Richard H. D. McRae, Jason J. Sharples, Stephen R. Wilkes, Alan Walker, 2013: An Australian pyro-tornadogenesis event, *Nat Hazards* 65, 1801-1811, DOI 10.1007/s11069-012-0443-7
- Robert A. H., W.-C. Lee and M. M. Bell, 2009: Convective Contribution to the Genesis of Hurricane Ophelia (2005). *Mon. Wea. Rev.*, 137, 2778 - 2800.
- Selvam, A. M., R. Vijaykumar, and A. S. R., Muirty, 1991: Some physical aspects of summer monsoon clouds: Comparison of cloud model results with observations. *Adv. Atmos. Sci.*, 8, 111-124
- Shin, H. H. and Hong, S. U., 2011: Inter comparison of Planetary Boundary-Layer Parametrizations in the WRF Model for a Single Day from CASES-99.
- Skamarock, W. C., J. B. Klemp, J. Dudhia, D. O. Gill, D. M. Barker, W. Wang, and J. G. Powers, 2008: A description of the Advanced Research WRF version 3, NCAR Tech. Note 4751STR, 113.

- Snyder, J. P., 1989: Album of Map Projections, United States Geological Survey Professional Paper, United States Government Printing Office, 1453.*
- Srinivasan, V., K. Ramamurthy and Y. R. Nene, 1973: Discussion of typical synoptic weather situations 2.2. Summer-Nor'westers and Andhis and large scale convective activity over Peninsula and central parts of the country, India Meteorological Department Forecasting Manual, Part III: 2.2.
- Srivastava, R. C., 1985: A simple model of evaporatively driven downdraft: Application to microburst downdraft. *J. Atmos. Sci.*, 42, 1004–1023.
- Tao, W. K., and Coauthors, 2003: Microphysics, radiation and surface processes in the Goddard Cumulus Ensemble (GEC) model. *Meteor. Atmos. Phys.*, 82, 97-137.
- Tao, W. K., J. Simpson, S. Lang, M. McCumber, R Adler and R. Penc, 1990: An algorithm to estimate the heating budget from vertical hydrometeor profiles. *J. Appl. Meteor.*, 29, 1232-1244.
- Thompson, A. M., Chatfield, R. B., Hgvan, H. G. J., Smit, 2007: Mechanisms for the intraseasonal variability of ozone during the India winter monsoon, *J. Geophys. Res.*, 112, D10303.
- Uma, K. N., and T. N. Rao, 2009: Characteristics of Vertical Velocity Cores in Different Convective Systems Observed over Gadanki, India. *Mon. Wea. Rev.*, 137, 954 – 975.
- Vaidya S. S., J. R. Kulkarni, 2007: Simulation of heavy precipitation over Santacruz, Mumbai on 26 July 2005, using Mesoscale model, *Meteorol. Atmos. Phys.* 98, 55–66.
- Vaidya, S. S., 2007: Simulation of weather systems over Indian region using mesoscale models; *Meteorol. Atmos. Phys.* 95, 15–26.
- Wu, X., W. D. Hall, W. W. Grabowski, M. W. Moncrieff, W. D. Collins, and J. T. Kiehl, 1999: Long-term behaviour of cloud systems in TOGA COARE and their interactions with radiative and surface processes. Part II: Effects of ice microphysics on cloud-radiation interaction. *J. Atmos. Sci.*, 56, 3177-3195.